# ANALYSIS OF VEHICULAR PLATOON SYSTEMS UNDER VARIOUS INFORMATION FLOW TOPOLOGIES

by

Nergiz Sermet

B.S., Mechanical Engineering, Istanbul Technical University, 2016

B.S., Management Engineering, Istanbul Technical University, 2018

Submitted to the Institute for Graduate Studies in
Science and Engineering in partial fulfillment of
the requirements for the degree of
Master of Science

Graduate Program in Electrical and Electronics Engineering

Boğaziçi University

2024

# ACKNOWLEDGEMENTS

I would like to express my deepest gratitude to my supervisor, Professor Mehmet Akar, for his invaluable guidance, support, and encouragement throughout the entire process of researching and writing of this thesis. His profound knowledge and unwavering commitment have played a crucial role in influencing the trajectory of this thesis. It has been a privilege and honor to finish my Master's study under his exceptional guidance. Without his support and direction, completing this thesis would not have been possible.

I would like to express my gratitude to my thesis committee members Professor Yağmur Denizhan and Professor Tankut Acarman for spending their valuable time and for their insightful feedback. I am truly grateful for their contributions.

My heartfelt thanks go to my beloved mother and father Sevinnas Sermet, and Servet Sermet, and my dear brothers Sedat Sermet and Engin Sermet whose love, patience, and understanding encouraged me during the challenging phases of this endeavor. Their endless support and belief in me have been a constant source of strength and motivation. Thank you all for supporting me along the way.

# ABSTRACT

## ANALYSIS OF VEHICULAR PLATOON SYSTEMS UNDER VARIOUS INFORMATION FLOW TOPOLOGIES

Intelligent transportation systems have a bright future owing to the advancements in sensing, communication, and computing technologies. Vehicles are now equipped with Advanced Driving-Assistance Systems (ADAS) such as automated parking, collision avoidance, and Adaptive Cruise Control (ACC). In addition, they also have advanced communication systems that enable them to connect to other vehicles and external systems like the Road Side Units (RSUs). As a result, vehicle platoons are becoming increasingly popular in the automotive industry. A vehicle platoon is a group of vehicles that follow each other based on an information exchange structure. Vehicle platoon systems not only promote road safety and reduce traffic congestion, but they also help to improve fuel economy.

This study explores the challenges and opportunities inherent in coordinating vehicle platoon systems under various information flow topologies. In this context, node dynamics, decentralized controllers, information flow topologies, and geometric formations are investigated. In the study, unidirectional and bidirectional information flow topologies under the spanning tree assumption are examined in detail. Furthermore, a linear P-controller and a nonlinear integral sliding mode controller are applied to a vehicle platoon system to understand the influence of the decentralized controllers. MATLAB software is utilized for testing various vehicle platoon system scenarios. The performance of the vehicle platoon system is assessed through stability analysis and convergence rate. Additionally, an analysis is conducted on an information flow topologies that lacks a spanning tree. Primary layer subgraph and secondary layer subgraph algorithms are used to understand the graph partition behavior of information flow topologies that do not include a spanning tree. It is shown that, in the case of no spanning tree, multiple platoons are formed.

# ÖZET

## ARAÇ PLATOON SİSTEMLERİNİN FARKLI İLETİŞİM TOPOLOJİLERİ ALTINDA ANALİZİ

Akıllı ulaşım sistemleri, sensör, iletişim ve bilgisayar teknolojilerindeki ilerlemeler sayesinde parlak bir gelecek vadetmektedir. Günümüzde araçlar otomatik park, çarpışma önleme ve adaptif hız sabitleme gibi gelişmiş sürüş destek sistemleri ile donatılmaktadır. Ayrıca, trafikteki diğer araçlara ve yol kenarı birimleri gibi dış sistemlere bağlanmalarını sağlayan gelişmiş iletişim sistemlerine de sahiptirler. Sonuç olarak, araç konvoy sistemleri otomotiv sektöründe öne çıkan konulardan biri haline gelmektedir. Araç konvoy sistemi, bilgi alışverişi yapısına dayalı olarak birbirini takip eden araçlar grubundan oluşmaktadır. Araç konvoy sistemleri, yol güvenliğini arttırmak ve trafik sıkışıklığını azaltmak ile kalmayarak, yakıt ekonomisinde de iyileştirme potansiyeli taşımaktadır.

Bu çalışma, farklı bilgi akışı topolojileri altında araç konvoyları koordine etmenin getirdiği zorluk ve fırsatları incelemektedir. Bu bağlamda, araç dinamikleri, merkezi olmayan kontrolörler, bilgi akış topolojileri ve geometrik formasyonlar araştırılmaktadır. Çalışmada, yayılan ağaç varsayımı altında tek ve çift yönlü bilgi akış topolojileri incelenmektedir. Ayrıca, merkezi olmayan kontrolörlerin etkisini anlamak amacıyla araç konvoy sistemlerinde doğrusal bir P-kontrolörü ve doğrusal olmayan bir integral kayan kipli kontrolör uygulanmaktadır. Çeşitli araç konvoy sistemi senaryolarını test etmek için MATLAB yazılımı kullanılmaktadır. Araç konvoy sistemi performansı, kararlılık analizi ve yakınsama süresi ile ölçülmektedir. Ek olarak, yayılan ağaç içermeyen bilgi akışı topolojileri üzerinde çalışılmaktadır. Yayılan ağaç içermeyen bilgi akış topolojileri birincil ve ikincil katman alt grafik algoritmaları kullanılarak incelenmektedir. Bu durumda birden fazla araç konvoyu oluştuğu gösterilmektedir.

# TABLE OF CONTENTS

ACKNOWLEDGEMENTS . . . . . iii
ABSTRACT . . . . . iv
ÖZET . . . . . v
LIST OF FIGURES . . . . . viii
LIST OF TABLES . . . . . xii
LIST OF SYMBOLS . . . . . xiv
LIST OF ACRONYMS/ABBREVIATIONS . . . . . xvi
1. INTRODUCTION . . . . . 1
1.1. Related Work . . . . . 2
1.1.1. Node Dynamics . . . . . 3
1.1.2. Decentralized Controllers . . . . . 3
1.1.3. Information Flow Topology . . . . . 4
1.1.4. Geometry Formation . . . . . 8
1.2. Motivation of the Thesis . . . . . 8
1.3. Contribution of the Thesis . . . . . 8
1.4. Organization of the Thesis . . . . . 9
2. VEHICULAR PLATOON SYSTEM CONTROL . . . . . 11
2.1. Graph Theory . . . . . 11
2.2. Node Dynamics . . . . . 13
2.2.1. Longitudinal Vehicle Dynamics . . . . . 13
2.3. Decentralized Controller Design . . . . . 17
2.3.1. ISMC Design . . . . . 19
2.4. Geometry Formation . . . . . 21
2.5. Vehicular Platoon Dynamics . . . . . 22
2.6. Numerical Analysis . . . . . 25
2.7. Summary of the Chapter . . . . . 34
3. ANALYSIS OF UNIDIRECTIONAL TOPOLOGIES . . . . . 35
3.1. Unidirectional Information Topologies . . . . . 35

3.2. Linear Decentralized Controller Design . . . . . 38
3.3. Stability Analysis of Unidirectional Information Flow Topologies . . . . . 41
3.4. Performance Analysis of Unidirectional Information Flow Topologies . . . 42
3.5. Numerical Analysis . . . . . 45
3.6. Summary of the Chapter . . . . . 54
4. ANALYSIS OF BIDIRECTIONAL TOPOLOGIES . . . . . 55
4.1. Bidirectional Information Topologies . . . . . 55
4.2. Stability Analysis of Bidirectional Information Flow Topologies . . . . . 56
4.3. Performance Analysis of Bidirectional Information Flow Topologies . . . . 57
4.4. Numerical Analysis . . . . . 66
4.5. Summary of the Chapter . . . . . 73
5. ANALYSIS OF TOPOLOGIES WITHOUT A SPANNING TREE . . . . . 74
5.1. Graph Partition . . . . . 74
5.2. Graph Partition Algorithms . . . . . 75
5.3. Stability Analysis of Information Flow Topologies Without a Spanning Tree 77
5.4. Numerical Analysis . . . . . 79
5.5. Summary of the Chapter . . . . . 92
6. CONCLUSION . . . . . 93
6.1. Future Work . . . . . 95
REFERENCES . . . . . 96

# LIST OF FIGURES

Figure 1.1. Components of a vehicle platoon system. . . . . 3

Figure 1.2. Common Topologies (a) Predecessor following topology, (b) Leader-Predecessor following topology, (c) Bidirectional topology, (d) Leader-Bidirectional topology. . . . . 7

Figure 2.1. Control block diagram. . . . . 18

Figure 2.2. The chattering phenomenon. . . . . 21

Figure 2.3. Geometry formation for CDG. . . . . 22

Figure 2.4. Information flow topology. . . . . 28

Figure 2.5. Position error of the observer under IFT in Figure 2.4. . . . . 29

Figure 2.6. Velocity error of the observer under IFT in Figure 2.4. . . . . 29

Figure 2.7. Acceleration error of the observer under IFT in Figure 2.4. . . . . 30

Figure 2.8. Position state of the observer under IFT in Figure 2.4. . . . . 30

Figure 2.9. Velocity state of the observer under IFT in Figure 2.4. . . . . 31

Figure 2.10. Acceleration state of the observer under IFT in Figure 2.4. . . . . 31

Figure 2.11. Position state of the vehicles under IFT in Figure 2.4. . . . . 32

Figure 2.12. Velocity state of the vehicles under IFT in Figure 2.4. . . . . 32

Figure 2.13. Acceleration state of the vehicles under IFT in Figure 2.4. . . . . 33

Figure 2.14. Control inputs under IFT in Figure 2.4. . . . . 33

Figure 3.1. Unidirectional IFTs for homogeneous vehicular platoons (a) PF, (b) PF2, (c) PF3, (d) PF4, (e) PF5, (f) PF6, (g) PLF. . . . . 37

Figure 3.2. Unidirectional IFTs for heterogeneous vehicular platoons (a) PF, (b) PF2, (c) PF3, (d) PF4, (e) PF5, (f) PF6, (g) PLF. . . . . 38

Figure 3.3. Settling time calculation algorithm. . . . . 48

Figure 3.4. Space error with linear controller for unidirectional PF IFT in Figure 3.1. 51

Figure 3.5. Space error with linear controller for unidirectional PLF IFT in Figure 3.1. . . . . 51

Figure 3.6. Space error with nonlinear controller for unidirectional PF IFT in Figure 3.2. . . . . 52

Figure 3.7. Space error with nonlinear controller for unidirectional PLF IFT in Figure 3.2. . . . . 52

Figure 3.8. Space error for vehicle 7 with linear controller for unidirectional IFTs in Figure 3.1. . . . . 53

Figure 3.9. Space error for vehicle 7 with nonlinear controller for unidirectional IFTs in Figure 3.2. . . . . 53

Figure 4.1. Bidirectional IFTs for homogeneous vehicular platoons (a) BD, (b) BD2, (c) BD3, (d) BD4, (e) BD5, (f) BD6, (g) BDL. . . . . 57

Figure 4.2. Bidirectional IFTs for heterogeneous vehicular platoons (a) BD, (b) BD2, (c) BD3, (d) BD4, (e) BD5, (f) BD6, (g) BDL. . . . . 58

Figure 4.3. Space error for vehicle 7 with linear controller under bidirectional IFTs in Figure 4.1. . . . . 70

Figure 4.4. Space error for vehicle 7 with nonlinear controller under bidirectional IFTs in Figure 4.2. . . . . 70

Figure 4.5. Space error with linear controller for bidirectional BD IFT in Figure 4.1. 71

Figure 4.6. Space error with linear controller for bidirectional BDL IFT in Figure 4.1. . . . . 71

Figure 4.7. Space error with nonlinear controller for bidirectional BD IFT in Figure 4.2. . . . . 72

Figure 4.8. Spacing error with nonlinear controller for bidirectional BDL IFT in Figure 4.2. . . . . 72

Figure 5.1. Graph partition categories (a) Vertex partitioning, (b) Edge partitioning. 75

Figure 5.2. Homogeneous platoon without a spanning tree. . . . . 79

Figure 5.3. Vehicle states of IFT in Figure 5.2 (a) Position, (b) Velocity, (c) Acceleration. . . . . 83

Figure 5.4. Two primary and two secondary layer subgraphs for IFT in Figure 5.2. 85

Figure 5.5. Space error for IFT in Figure 5.2 between consecutive vehicles with linear controller. . . . . 86

Figure 5.6. Space error for IFT in Figure 5.2 between vehicles in PLS2, SLS1, and SLS2 with linear controller. . . . . 86

Figure 5.7. Homogeneous platoon without a spanning tree. . . . . 87

Figure 5.8. Vehicle states of IFT in Figure 5.7 (a) Position, (b) Velocity, (c) Acceleration. . . . . 89

Figure 5.9. Two primary and one secondary layer subgraphs. . . . . 90

Figure 5.10. Space error for IFT in Figure 5.7 between consecutive vehicles with linear controller. . . . . 91

Figure 5.11. Space error within the primary layer subgraphs with the linear controller. 91

# LIST OF TABLES

Table 2.1. Simulation parameters. . . . . 26

Table 2.2. Vehicle parameters. . . . . 27

Table 2.3. External time-varying disturbances. . . . . 27

Table 3.1. Eigenvalues for PF and PF3 information flow topologies with $N = 4$ followers. . . . . 45

Table 3.2. Simulation parameters for the linear controller. . . . . 46

Table 3.3. Eigenvalues of the information flow topologies in Figures 3.1 and 3.2. 47

Table 3.4. Settling time in seconds for the linear controller with $1\ \%$ speed tolerance under different information flow topologies in Figure 3.1. . . . . 49

Table 3.5. Settling time in seconds for the nonlinear controller with $1\ \%$ speed tolerance under different information flow topologies in Figure 3.2. . . 49

Table 4.1. Eigenvalues for look-forward and look-backward information flow topologies with $N = 4$ followers. . . . . 65

Table 4.2. Eigenvalues for different information flow topologies in Figures 4.1 and 4.2 . . . . . 67

Table 4.3. Settling time in seconds for the linear controller with $1\ \%$ speed tolerance under different information flow topologies in Figure 4.1 . . . . . 68

Table 4.4. Settling time in seconds for the nonlinear controller with $1\ \%$ speed tolerance under different information flow topologies in Figure 4.2 . . . 68

Table 5.1. Coefficients for eigenvalues in (5.11) where $\tau = 0.5$. . . . . 80

Table 5.2. Coefficients in Table (5.1) for $k_1 = 0.4$ , $k_2 = 0.6$ and, $k_3 = 0.8$. . . . 82

Table 5.3. Validation of conditions in (5.7), (5.8) and, (5.9) for coefficients in Table 5.2. . . . . 82

# LIST OF SYMBOLS

| | |
|---|---|
| $\mathcal{A}$ | Adjacency matrix |
| $A$ | State transition matrix |
| $A^T$ | Transpose of matrix $A$ |
| $a_i$ | Acceleration of the $i^{th}$ vehicle |
| $a_{r,i}$ | Acceleration of the $i^{th}$ observer |
| A$\otimes B$ | Kronecker product of $A$ and $B$ |
| $C_{A,i}$ | Lumped aerodynamic drag coefficient of the $i^{th}$ vehicle |
| $d_{i-1,i}$ | Distance between $(i-1)^{th}$ and $i^{th}$ vehicles |
| diag$\{$x$_1, x_2, ..., x_N\}$ | Diagonal matrix formed by $x_1, x_2, ..., x_N$ |
| E | Set of edges |
| $f$ | Rolling resistance coefficient |
| $g$ | Gravitational acceleration |
| $Im(z)$ | Imaginary part of $z$ |
| $k_1$, $k_2$, $k_3$ | Linear controller gains |
| $\mathcal{L}$ | Laplacian matrix |
| $\mathcal{L}_{\mathcal{P}}$ | Information flow topology matrix |
| $m_{i,veh}$ | Mass of the $i^{th}$ vehicle |
| $m_{rp,i}$, $m_{rv,i}$, $m_{ra,i}$ | Observer gains of the $i^{th}$ vehicle |
| $n_{rp,i}$, $n_{rv,i}$, $n_{ra,i}$ | Nonlinear controller gains of the $i^{th}$ vehicle |
| $R_i$ | Tire radius of the $i^{th}$ vehicle |
| $Re(z)$ | Real part of $z$ |
| $\mathcal{P}$ | Pinning matrix |
| $p_i$ | Position of the $i^{th}$ vehicle |
| $p_{ii}$ | $\mathcal{P}(i,i)$ element of the pinning matrix |
| $p_{r,i}$ | Position of the $i^{th}$ observer |
| $s_i$ | Sliding surface of the $i^{th}$ vehicle |
| $t_s$ | Sample time |
| $T_i$ | Driving/braking torque of the $i^{th}$ vehicle |

| | |
|---|---|
| $v_i$ | Velocity of the $i^{th}$ vehicle |
| $v_{r,i}$ | Velocity of the $i^{th}$ observer |
| V | Set of vertices |
| $x_i$ | Vehicle states of the $i^{th}$ vehicle |
| $x_0$ | Leader states |
| $x_{r,i}$ | Observer states of the $i^{th}$ vehicle |
| | |
| $\sigma(A)$ | Eigenvalues of matrix $A$ |
| $\lambda_i(A)$ | $i^{th}$ eigenvalue of matrix $A$ |
| $\beta_{1,i},\ \beta_{2,i}$ | Velocity response coefficients of $i^{th}$ vehicle |
| $\varepsilon_i$ | Tracking error of the $i^{th}$ vehicle |
| $\varepsilon_{r,i}$ | Observing error of the $i^{th}$ vehicle |
| $\xi_i(t)$ | Time-varying external disturbance applying the $i^{th}$ vehicle |
| $\eta_{\tau,i}$ | Mechanical efficiency of the $i^{th}$ vehicle |
| $\tau_i$ | Internal lag of the $i^{th}$ vehicle |

# LIST OF ACRONYMS/ABBREVIATIONS

| | |
|---|---|
| ADAS | Advanced Driver Assistant Systems |
| ACC | Adaptive Cruise Control |
| BSM | Basic Safety Message |
| CAAC | Cooperative Adaptive Cruise Control |
| CAN | Controller Area Network |
| CDG | Constant Distance Gap |
| CTG | Constant Time Gap |
| CV | Connected Vehicle |
| DO | Disturbance Observer |
| DSCM | Distributed Sliding Mode Control |
| DSRC | Dedicated Short Range Communication |
| FBL | Feed-Back Linearization |
| FCC | Federal Communications Commission |
| IFM | Information Flow Matrix |
| IFT | Information Flow Topology |
| ISMC | Integral Sliding Mode Control |
| ITS | Intelligent Transport Systems |
| LTI | Linear Time Invariant |
| MAS | Multi Agent System |
| ND | Node Dynamics |
| OLHP | Open Left-Half Plane |
| PLF | Predecessor Leader Following |
| PLS | Primary layer Subgraph |
| PF | Predecessor Following |
| PPR | Packet Perception Ratio |
| SAE | Society of Automobile Engineers |
| SISO | Single Input Single Output |
| SLS | Secondary Layer Subgraph |

| | |
|---|---|
| SMC | Sliding Mode Control |
| V2G | Vehicle to Grid Communication |
| V2I | Vehicle to Infrastructure Communication |
| V2V | Vehicle to Vehicle Communication |
| V2X | Vehicle to Everything |
| VSS | Variable Structure System |
| WAVE | Wireless Access in Vehicular Environments |

# 1. INTRODUCTION

Over the years, various transportation methods including horses, oxen, bikes, automobiles, buses, and trucks, have been used to move people and goods around the roads. Road transportation not only involves tools and devices to transport and control the traffic, but a large amount of the population is also a part of this system. Nevertheless, maintaining road safety is one of the inevitable challenges faced by modern transportation infrastructures. Therefore, in order to ensure the safety of everyone involved, it is crucial to prevent human errors as much as possible.

Up until today, there have been many studies conducted on enhancing traffic efficiency, safety, and sustainability. The vehicle platoon systems have emerged as a sufficient solution to address traffic-related concerns of today's transportation systems. It would not be wrong to say that the vehicle platoon systems hold the potential to revolutionize the concept of road safety. By utilizing collective intelligence and sensor fusion, vehicle platoon systems help to prevent human error, which is the leading cause of traffic accidents.

A vehicle platoon system occupies a group of vehicles that move concurrently to maintain a predefined layout without any physical connection between its associates. Coordinated control of vehicles in a platoon system is a challenging task due to non-linear vehicle dynamics, uncertainties, external disturbances, different information topologies, and spacing policies. In the literature, numerous control methods have been proposed to govern such a system. Decentralization of vehicle control is likely to be preferred over centralized control since it can reduce expenses due to a lack of central coordination. In addition, decentralized control is more resilient against single-node failures [1].

Platooning is a technology that uses real-time communication and automated driving to enable synchronized maneuvers and collision avoidance. Unfortunately, there are still some obstacles that need to be overcome before the adaptation of the vehicle platoon systems to real life.

Technical prerequisites such as ensuring interoperability among diverse vehicle fleets, establishing protocols to regulate vehicle communication, and ensuring cybersecurity require extensive research and development efforts. Additionally, integrating platooning systems into existing transportation infrastructure demands meticulous planning and collaboration of various stakeholders for consistent deployment. Through an inclusive investigation of designated topics, this study aims to contribute to the understanding of vehicular platoon systems and their potential role in shaping the future of road transportation.

## 1.1. Related Work

This section synthesizes key findings and identifies emerging trends in platooning and its implications for future research and practice. Platooning can be considered a consensus problem at its core since it targets to achieve agreement among a group of distributed vehicles regarding a common value or decision.

A typical setup for a vehicle platoon involves a human-operated leading vehicle, called the platoon leader, which sets the pace and navigation for the convoy. The following vehicles can function autonomously, relying on sensors, communication systems, and algorithms to maintain their position and follow the lead vehicle from a safe distance [2].

Vehicle platoon systems consist of four basic components: node dynamics, decentralized controllers, information flow topology, and geometry formation as shown in Figure 1.1. In this context, vehicles within the platoon are referred to as nodes, with node dynamics describing the behavior of the vehicles. Decentralized controllers implement control algorithms for each node independently. Information Flow Topology (IFT) determines how information flows between nodes, while geometry formation focuses on the spacing between sequential nodes [3, 4].

In the next subsections, brief information will be provided about each component individually.

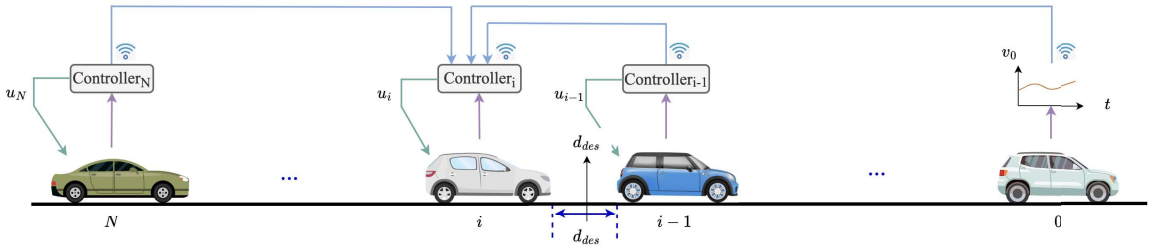


Figure 1.1. Components of a vehicle platoon system.

### 1.1.1. Node Dynamics

Node dynamics is a field of study that explains how vehicles move in various conditions. It involves the complex interactions between various components of a vehicle, such as the tires, suspension, steering, and the road surface. Understanding vehicle dynamics requires examining factors such as weight distribution, the center of gravity, aerodynamics, and the mechanical properties of the vehicle.

Commonly used vehicle dynamics models in the literature include second-order and third-order models [5]. In [6], nonlinear vehicle dynamics are simplified and then linearized using the exact linearization method. Kazemi et al. have worked on third-order vehicle dynamics for longitudinal control of the vehicles [7]. He et al. [8] are another research group that employs a third-order vehicle dynamics model in their study like Hiu and Li [9]. In previous studies of vehicle platoon systems, the main focus is on longitudinal vehicle dynamics, with lateral dynamics being neglected [5–13]. In this thesis, the same approach is adopted.

### 1.1.2. Decentralized Controllers

The controller is the next essential element of the vehicle platoon system. The controller is one of the most crucial elements for a stabilized vehicle platoon system design. Many control methods can be utilized such as Proportional Integral Derivative (PID) control, Model Predictive Control (MPC), Sliding Mode Control (SMC), etc. Nonetheless, the PID controller is the most preferred controller type used in vehicle control due to its uncomplicated implementation [7].

Huang et al. developed an Economic Distributed Model Predictive Controller (Eco-DPMC) to control a string of vehicles within a heterogeneous vehicle platoon system. In this study, the optimal cost function is determined by analyzing the variances between the desired and current trajectories. Every vehicle solves a local optimization problem. Then, the predicted state information for the next step is transmitted to or received by the related vehicles according to the information flow topology used. It is also highlighted that a vehicle platoon system with an Eco-DPMC controller responds faster than a system with a PID controller. In addition, Eco-DPMC is more advantageous in terms of fuel economy since the fuel consumption has been reduced by 19 % approximately [11].

Cheng et al. [12], discussed the growing trend of SMC-based applications in vehicle platoon systems. The chattering problem of SMC in practice is also mentioned in the same study. In order to overcome this difficulty, a saturation function is developed. However, there is a trade-off between avoiding chattering and the time taken to reach the desired system states.

In [13], string instabilities caused by factors such as external uncertainties and disturbances are eliminated by integrating a Disturbance Observer (DO), that can estimate unbounded uncertainties, with an Integral Sliding Mode Controller (ISMC). The DO contributes to the system by operating it under unconstrained disturbances. This integration enables followers to reach their desired state in less than 10 seconds. Another research that utilizes ISMC is conducted by Li et al. [5]. The ISMC controller is employed within the secondary layer of a hierarchical controller, with the first layer incorporating the state observer of the leading vehicle. The external time-varying disturbances are considered in this study. Moreover, the proposed controller makes provision against the chattering phenomena.

### 1.1.3. Information Flow Topology

All the research outlined above relies on vehicle interaction, through wireless or non-wireless communication.

Controller Area Network (CAN) is an example of a non-wireless communication method that enables communication among the different Electronic Control Units (ECUs). CAN topology determines the message packets shared between the ECUs. Furthermore, it is an economical communication method [14].

Vehicle to Vehicle (V2V) communication is a technology used in Wireless Access in Vehicular Environments (WAVE) that allows vehicles to exchange information over short distances. Vehicle to Infrastructure (V2I) communication is an additional technology that extends V2V by enabling information exchange between vehicles and infrastructure such as traffic lights and road signs. V2V and V2I communication have the potential to improve traffic safety for Intelligent Transport Systems (ITS).

In 1999, a communication protocol with a 75 MHz spectrum at a 5.9 GHz frequency band, named Dedicated Short Range Communication (DSRC), was suggested by the U.S. Federal Communications Commission (FCC) for short-range and low-latency wireless vehicle communication. DSRC protocol regulates the V2V and V2I communication. With the utilization of DSRC, vehicles transmit data to nearby vehicles. Nevertheless, the transmitting vehicle is unaware of whether there are vehicles available to receive the transmitted message or not [15, 16].

V2V communication range is approximately up to 500 meters. On the downside, V2V technology may have communication interruptions caused by wireless communication delays and packet losses, especially when numerous vehicles are simultaneously broadcasting messages on a mutual radio channel [15].

Saleh et. al performed a study involving 728 test cases to assess how various environmental factors, such as temperature and road conditions, influence communication health. Their findings suggest that variables like environmental temperature and airborne moisture minimally affect the robustness of wireless communication reliability. However, obstacles along the route, such as buildings or materials obstructing antennas like ice particles, significantly impair network health.

Furthermore, distance emerges as a critical factor adversely impacting communication success, regardless of environmental circumstances. The study concludes that irrespective of environmental variables, longer distances correlate with weaker signal strength, posing a challenge to communication success since the higher the range is, the lower the signal strength [16].

Carpenter et al. conducted extensive test cases on V2V communication in Ann Arbor, United States of America, involving 3000 vehicles. Their study highlights the variance between the theoretical expectations and the practical performance of DSRC. For instance, while a high Packet Perception Ratio (PPR), an indicator of packet receiving success, is anticipated within a 100 meter range, the actual reception of packets tends to be less reliable, particularly for distances under 125 meters. Surprisingly, contrary to common belief, PPR deteriorates further for ranges below 10 meters [17].

In summary, in the SAE J2945/1A standard titled "Vehicle Level Validation Test Procedures for V2V Safety Communications" the Society of Automotive Engineers (SAE) outlines DSRC requirements. According to this standard, DSRC communication components must transmit a message packet named Basic Safety Message (BSM) that contains the necessary information to identify the vehicle and explain its state. The core data within the broadcasted BSM should encompass the following data [18]:

1. Message Count
2. ID
3. Second Mark
4. Latitude
5. Longitude
6. Elevation
7. Positional Accuracy
8. Transmission State
9. Speed
10. Heading

11. Steering Angle
12. Acceleration Set (4 Way)
13. Brake System Status
14. Vehicle Size (Length, Width)

One aspect of data transfer is related to the technology used to share information. Another aspect is the data transfer topology, in other words, IFT. IFT defines the information transmitted within a vehicle platoon system. Earlier studies on platoon systems are predominantly based on Predecessor Following (PF) topology that can be seen in Figure 1.2 where arrows show the direction of information exchange [19]. In addition, the majority of the studies presumed a continuous communication topology either explicitly or implicitly. Therefore, issues such as communication delays and packet losses are ignored [3–5, 12, 13, 20–23]. However, this presumption is not applicable in reality. Some studies assess a switching communication topology [9, 24–26].

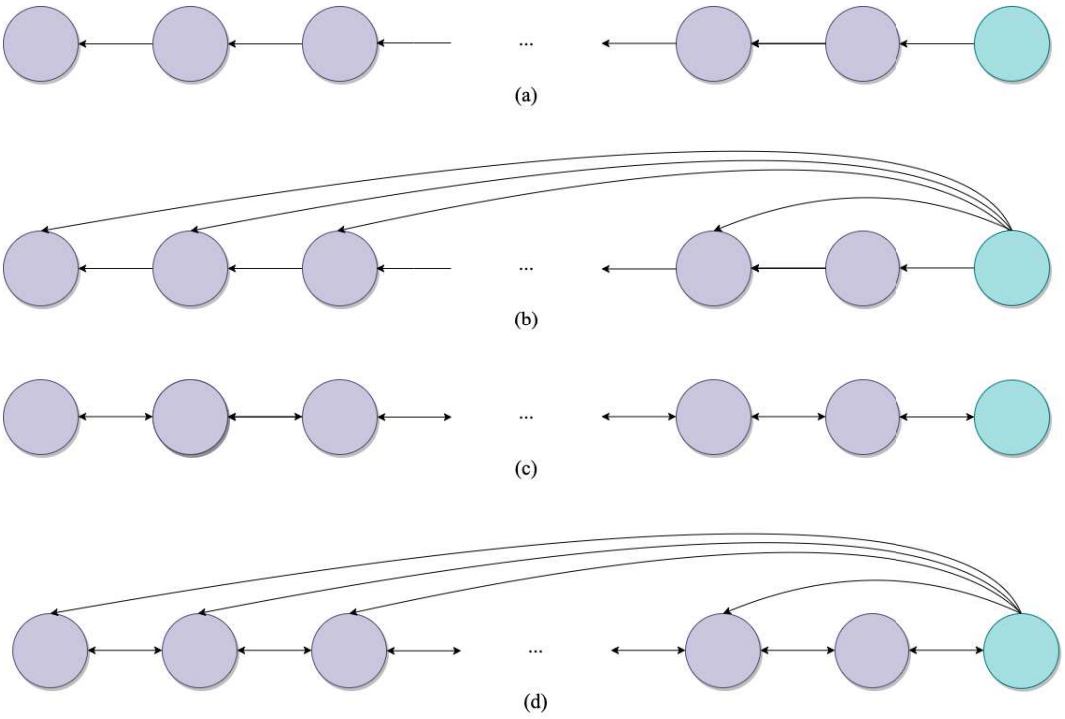


Figure 1.2. Common Topologies (a) Predecessor following topology, (b) Leader-Predecessor following topology, (c) Bidirectional topology, (d) Leader-Bidirectional topology.

The designed vehicle platoon system should react appropriately to topology changes to maintain string stability.

### 1.1.4. Geometry Formation

Lastly, it is important to mention the geometry formation, in which the spacing policy is determined since it is one of the components of the vehicle platoon system. Swaroop categorized different types of spacing policies as constant, variable, and hybrid policies [27]. The difference between the constant and variable policies is the characteristics of the distance function. Constant spacing policy has a constant function while variable spacing policies are dependent on the vehicle velocity. Hybrid spacing policies represent the geometry formation situations where vehicles can have diverse spacing policies [27].

## 1.2. Motivation of the Thesis

The advancements in autonomous vehicle technologies have brought platooning to the forefront as an opportunity to enhance efficiency and safety in road transportation. Robust control algorithms and well-designed communication layouts are essential for successful platoon implementation. This can lead to benefits such as reduced fuel consumption, improved traffic flow, and increased road safety. In this context, this thesis aims to explore control methodologies for platoon control and address key challenges such as vehicle dynamics, communication topologies, and system stability. Eventually, this study seeks to contribute to the analysis of the effect of network topology on the behavior of the vehicle platoon system.

## 1.3. Contribution of the Thesis

The main contributions of this thesis can be outlined as follows:

- The study analyzes the performance of a vehicle platoon system under various unidirectional information topologies. It utilizes eigenvalue analysis and a proposed algorithm for settling time calculation as metrics to interpret the system behavior.

The study compares results for both linear and nonlinear controllers.

- The research involves analyzing the performance of a platoon system across different bidirectional information topologies. Similar to the evaluation carried out for unidirectional IFTs, the study investigates the performance of the vehicle platoon system.
- Various unidirectional and bidirectional topologies are tested and system behavior is analyzed.
- Additionally, this study seeks to offer a new viewpoint on the analysis of vehicle platoon systems by examining information topologies without a spanning tree. Necessary and sufficient conditions conditions for the stability of these systems are examined. Moreover, the validity of the stability criteria has been tested on a specific information flow topology that lacks a spanning tree.

## 1.4. Organization of the Thesis

The remaining part of the thesis has been organized as detailed below.

Chapter 2 introduces the essential elements of a vehicle platoon system. In this chapter, graph theory is explained for an enhanced comprehension of the structure of information flow topologies. Then, the vehicle dynamics are derived under some assumptions such as rigid vehicle body, disregard of the tire slip, etc. These two sections are beneficial in revealing the vehicle platoon system dynamics. Additionally, simulation results for a nonlinear controller with a specified IFT are included. The results have been thoroughly interpreted.

Chapter 3 delves into properties of unidirectional IFTs. The matrix structure of unidirectional topologies is analyzed. Next, the eigenvalues of the IFT matrix are inspected. The effect of the unidirectional topology modification on the eigenvalues and consequently on the system behavior is explained. At the end of the chapter, the proposed results are evaluated both for linear and nonlinear controllers using MATLAB.

Chapter 4 is devoted to bidirectional IFTs, resembling Chapter 3 in structure. Initially, the chapter examines the vehicle platoon system operating with bidirectional topologies.

This is followed by an exploration of the effects of topology alterations. Consequently, the chapter provides an overview of the simulation findings.

Chapter 5 addresses the determination of essential criteria for ensuring stability in a vehicle platoon system in the absence of a spanning tree and alongside that introduces several graph partition algorithms. Additionally, an analysis of an IFT without a spanning tree is included. The subgroup establishment within the vehicle platoon system operating under specified IFT is examined. A method referred to as the primary and secondary layer subgraph, as described in existing literature, is employed to gain insights into the subgroup dynamics within the vehicle platoon system.

Chapter 6 consists of a synopsis of the study and explains the lesson learned during this research. In addition, the opportunities for future research topics are listed at the end of the chapter.

# 2. VEHICULAR PLATOON SYSTEM CONTROL

This chapter aims to review vehicle platoon system components, including information flow topology, node dynamics, decentralized controller, and geometry formation in depth. These components are fundamental for a vehicle platoon system because its performance is influenced by the design of these four components. For this reason, the upcoming sections of the chapter will deeply examine the impact of these components on the system's performance. MATLAB software will be used to test the vehicle platoon system design, and the results will be analyzed.

## 2.1. Graph Theory

The information flow topology is a critical consideration in the design of the vehicle platoon system. It specifies how the nodes, in other words, vehicles in the vehicle platoon system exchange information with each other. A node will update its state according to the information it receives. At first glance, a lack of information will be an inconvenience for the vehicle platoon system control since a node will not have a basis to perceive its state among the other vehicles.

The platoon system has a leader vehicle denoted as $\alpha_0$ and follower vehicles denoted from $\alpha_1$ to $\alpha_N$, where $N \in \mathbb{Z}^+$ corresponds to a positive integer. Information flow topology can be described by the directed graph $\mathcal{G}_N = (\mathcal{V}_N, E_N, \mathcal{A}_N)$ that consists of a vertex set $\mathcal{V}_N = \{\alpha_1, \alpha_2, \ldots, \alpha_N\}$, and an edge set $E_N \subseteq \mathcal{V}_N \times \mathcal{V}_N$ is the set of edge. If a line between the nodes has an arrow indicating the direction of the information exchange, it is a directed edge [28]. If there is an information flow from $j$ to $i$, then $(\alpha_j, \alpha_i) \in E_N$.

To represent the information flow topology, an augmented graph can be constructed as $\mathcal{G}_{N+1} = (\mathcal{V}_{N+1}, E_{N+1}, \mathcal{A}_{N+1})$ where $\mathcal{V}_{N+1} = \mathcal{V}_N \cup \{\alpha_0\}$ since a vehicle platoon system with $N$ followers has $N + 1$ vehicles when the leader vehicle is considered [5].

The graph representation of the information flow topology is associated with square matrices such as the adjacency matrix $\mathcal{A}$, the Laplacian matrix $\mathcal{L}$, and the pinning matrix $\mathcal{P}$. Next, the definitions of these matrices will be given.

**Definition 2.1** (Adjacency Matrix)**.** *$\mathcal{A} = [a_{ij}]_{N\times N}$ is the adjacency matrix that can be defined element-wise as*

$$a_{ij} = \begin{cases} 1, \ (\alpha_j, \alpha_i) \in E_N \\ 0, \ (\alpha_j, \alpha_i) \notin E_N \end{cases} . \tag{2.1}$$

**Definition 2.2** (Laplacian Matrix)**.** *$\mathcal{L} = [l_{ij}]_{N\times N}$ is the Laplacian matrix that can be defined element-wise as*

$$l_{ij} = \begin{cases} \sum_{j=1}^{N} a_{ij}, & i = j \\ -a_{ij}, & i \neq j \ and \ (\alpha_j, \alpha_i) \in E_N \\ 0, & i \neq j \ and \ (\alpha_j, \alpha_i) \notin E_N \end{cases} . \tag{2.2}$$

**Definition 2.3** (Pinning Matrix)**.** *Pinning matrix $\mathcal{P}$ is a diagonal matrix that describes the direct connectivity between the leader ($\alpha_0$) and the nodes ($\alpha_i \ for \ i = 1, \ldots, N$). It can be defined element-wise as*

$$p_{ij} = \begin{cases} 1, & i = j \ and \ (\alpha_0, \alpha_i) \in E_N \\ 0, & i \neq j \end{cases} . \tag{2.3}$$

**Definition 2.4** (Information Flow Matrix (IFM))**.** *The information flow matrix $\mathcal{L}_\mathcal{P}$ is obtained by adding the pinning matrix to the Laplacian matrix. Thus,*

$$\mathcal{L}_\mathcal{P} = \mathcal{L} + \mathcal{P}. \tag{2.4}$$

**Assumption 2.1.** *Self-loops are neglected. Hence,*

$$a_{ii} = 0, \quad \forall \quad i \in \mathbb{Z}^+ \ . \tag{2.5}$$

## 2.2. Node Dynamics

It is important to understand the nature of each vehicle to control a vehicle platoon system. Li et al. categorized the behavior of individual vehicles in the vehicle platoon system as the node dynamics [29]. Node dynamics explains the motion of the vehicle. Vehicles in the vehicle platoon system do not necessarily have the same node dynamics. A vehicle platoon system with identical node dynamics is a homogeneous platoon while a vehicle platoon system with distinct node dynamics is a heterogeneous platoon. In real-life applications, the vehicle platoon system often comprises vehicles of different dynamics, making it a heterogeneous platoon [30].

Vehicle dynamics can be classified into two categories: lateral dynamics and longitudinal dynamics. Lateral dynamics refer to the control of steering for lane keeping or lane departure. On the other hand, longitudinal dynamics refer to the control of actuators such as the throttle and brakes for the longitudinal motion of the vehicle [31].

### 2.2.1. Longitudinal Vehicle Dynamics

The longitudinal dynamics of a vehicle refer to its forward and backward movements, which are influenced by several factors. These factors can be listed as vehicle dynamics that contain aerodynamic drag force, tire force, rolling resistance force, gravitational forces, and powertrain dynamics such as the Internal Combustion Engine (ICE), torque path, and transmission system components [31].

According to the study of Yang et al., vehicle dynamics can be classified into two types of models: second-order integrator model and third-order integrator model [32]. In addition, a single integrator model and a Single Input Single Output (SISO) model mentioned by Li et al. can also come under these categories [10].

The single integrator model $\dot{p}_i = v_i$, where $p_i$ is the position and $v_i$ is the velocity of the $i^{th}$ vehicle, is not preferred as it simplifies the complex vehicle dynamics unrealistically.

Incorporating an integrator into the single integrator model can improve the performance of the model, resulting in what is known as the double integrator model [10].

The leader vehicle dynamics are expressed with a double integrator model in [5] as

$$\dot{p}_0(t) = v_0(t), \tag{2.6}$$

$$\dot{v}_0(t) = a_0(t) \tag{2.7}$$

where $x_0 = \begin{bmatrix} p_0 & v_0 & a_0 \end{bmatrix}^T$ stands for the states of the leader vehicle. Position is denoted by $p_0$, velocity is denoted by $v_0$, and the acceleration is denoted by $a_0$. The state-space representation of the leader vehicle is

$$\dot{x}_0 = A_0 x_0 \tag{2.8}$$

where

$$A_0 = \begin{bmatrix} 0 & 1 & 0 \\ 0 & 0 & 1 \\ 0 & 0 & 0 \end{bmatrix}. \tag{2.9}$$

The second-order model is not a common vehicle dynamics model. This is because it disregards inertial delays in the powertrain, which results in poor powertrain driveability in terms of tip-in or tip-out, takeoff, and gear shift capacity and quality [33]. Nonetheless, the inadequacy of the second-order model can be compensated by the addition of one more state. Then, the vehicle dynamic model becomes a third-order model. This additional state allows the consideration of driving/braking torques [5, 10].

A third-order vehicle dynamics model can be used to represent follower vehicles. To derive the longitudinal dynamics, the following assumptions are made [20–22]:

(i) The tire slip is neglected and the dynamics of the powertrain can be expressed with a first-order inertial transfer function.
(ii) The vehicle body is rigid and it is symmetric.
(iii) Lateral vehicle dynamics are neglected.
(iv) Controlled input contains driving and braking torques.

The longitudinal vehicle dynamics can be expressed as [20–22]

$$\dot{p}_i(t) = v_i(t) \tag{2.10}$$

$$\dot{v}_i(t) = \frac{1}{m_{i,veh}}\left(\eta_{T,i}\frac{T_i(t)}{R_i} - C_{A,i}v_i^2(t) - m_{i,veh}gf\right) \tag{2.11}$$

$$T_{i,des}(t) = \tau_i\dot{T}_i(t) + T_i(t) \tag{2.12}$$

where $p_i$ is the position and $v_i$ is the velocity of the $i^{th}$ node for $i = 1, 2, ..., N$. In (2.10-2.12), vehicle mass is denoted as $m_{i,veh}$, mechanical efficiency of the drivetrain is denoted as $\eta_{T,i}$, tire radius is denoted as $R_i$, the lumped aerodynamic drag coefficient is denoted as $C_{A,i}$, magnitude of the acceleration due to gravity is denoted as $g$, rolling resistance coefficient is denoted as $f$, inertial lag due to longitudinal vehicle dynamics is denoted as $\tau_i$. Actual and desired driving/braking torques are expressed as $T_i$ and $T_{i,des}$, respectively. System in (2.10-2.12) exemplify nonlinear vehicle dynamics. It can be used in further calculations of the platoon system control as in [23, 34].

Furthermore, a linear approximation can be applied to the nonlinear model. Accordingly, the nonlinear system in (2.10-2.12) is linearized using the Feed-Back Linearization (FBL) method. The application of FBL to a nonlinear system converts it into a linear and decoupled system where each input produces a single output [35].

The FBL method is operated with the selection of relative degree for the output as 3 in Zheng et al.'s study. In the same study, a control law proportional to the difference between the actual value and the reference value is applied to the controlled system [20]. The control input of the system is chosen as

$$u_i(t) = \tau_i\dot{a}_i(t) + a_i(t), \tag{2.13}$$

where $a_i$ is the acceleration of the $i^{th}$ vehicle. Hence, (2.13) can also be expressed as

$$u_i(t) = \tau_i\ddot{v}_i(t) + \dot{v}_i(t). \tag{2.14}$$

The second derivative of $v_i(t)$ can be calculated by taking derivative of $\dot{v}_i(t)$ in (2.10-2.12)

$$\ddot{v}_i(t) = \frac{1}{m_{i,veh}}\left(\eta_{T,i}\frac{\dot{T}_i(t)}{R_i} - 2C_{A,i}v_i(t)\dot{v}_i(t)\right). \tag{2.15}$$

Injecting $\ddot{v}_i(t)$ in (2.15) into (2.14) yields

$$\begin{aligned} u_i(t) =& \frac{\tau_i}{m_{i,veh}} \left( \eta_{T,i} \frac{\dot{T}_i(t)}{R_i} - 2C_{A,i} v_i(t) \dot{v}_i(t) \right) \\ &+ \frac{1}{m_{i,veh}} \left( \eta_{T,i} \frac{T_i(t)}{R_i} - C_{A,i} v_i^2(t) - m_{i,veh} g f \right) \end{aligned} \tag{2.16}$$

where $\tau_i \dot{T}_i(t)$ is defined in (2.12) as $(T_{i,des}(t) - T_i(t))$. Equation (2.16) can be rearranged as

$$\begin{aligned} u_i(t) =& \frac{1}{m_{i,veh}} \left( \eta_{T,i} \frac{T_{i,des}(t)}{R_i} - \eta_{T,i} \frac{T_i(t)}{R_i} - 2\tau_i C_{A,i} v_i(t) \dot{v}_i(t) \right) \\ &+ \frac{1}{m_{i,veh}} \left( \eta_{T,i} \frac{T_i(t)}{R_i} - C_{A,i} v_i^2(t) - m_{i,veh} g f \right) \end{aligned} \tag{2.17}$$

which can further be simplified as

$$T_{i,des}(t) = \frac{R_i}{\eta_{T,i}} (C_{A,i} v_i (2\tau_i \dot{v}_i + v_i) + m_{i,veh} g f + m_{i,veh} u_i) \tag{2.18}$$

where $u_i$ the control input. The linear state space model for each vehicle can be stated as

$$\dot{x}_i(t) = A_i x_i(t) + B_i u_i(t) \tag{2.19}$$

where

$$x_i(t) = \begin{bmatrix} p_i(t) \\ v_i(t) \\ a_i(t) \end{bmatrix}, A_i = \begin{bmatrix} 0 & 1 & 0 \\ 0 & 0 & 1 \\ 0 & 0 & -\frac{1}{\tau_i} \end{bmatrix}, B_i = \begin{bmatrix} 0 \\ 0 \\ \frac{1}{\tau_i} \end{bmatrix}. \tag{2.20}$$

When the heterogeneous platoon is considered, the vehicle model in (2.19) can represent a certain type of vehicle model named $\mathbb{T}_1$. Followers that have the $\mathbb{T}_1$ model type have desired acceleration, $u_i$, as their input. The dynamics of the $\mathbb{T}_1$ vehicle model can be simplified as

$$\begin{bmatrix} p_i(s) \\ v_i(s) \\ a_i(s) \end{bmatrix} = \begin{bmatrix} \frac{1}{s} v_i(s) \\ \frac{1}{s} a_i(s) \\ \frac{1}{\tau_i s + 1} (u_i(s) + \xi_i(s)) \end{bmatrix} \text{ for } i \in \mathbb{T}_1 \tag{2.21}$$

where $\xi_i(s)$ corresponds to external disturbances and $\tau_i \in R^+$ is the time constant related to the vehicle's powertrain characteristics. $\mathbb{T}_1$ modeled vehicles have the desired acceleration as the control input.

Defining another type of vehicle model named $\mathbb{T}_2$ is possible by taking the desired velocity as the control input. Some studies extract a second-order model from the experiment data. Using this method, Milanés et al. [36], and Tejado et al. [37] obtained the Laplace-domain transfer function

$$G(s) = \frac{K}{s^2 + 2\zeta w_n s + w_n^2} \tag{2.22}$$

where $K$ is the gain, $\zeta$ is the damping ratio, and $w_n$ is the natural frequency. Li et al. [5] reformulate this transfer function as

$$p_i(s) = \frac{1}{s} v_i(s) \tag{2.23}$$

$$v_i(s) = \frac{1}{\beta_{1,i} s^2 + \beta_{2,i} s + 1} (u_i(s) + \xi_i(s)) \tag{2.24}$$

where external disturbances denoted by $\xi_i(s)$ and $\beta_{1,i}, \beta_{2,i} \in R^+$ are the velocity response coefficients for $i \in \mathbb{T}_2$. The state-space equation is given by

$$\dot{x}_i(t) = A_{2,i} x_i(t) + B_{2,i} u_i(t), \; i \in \mathcal{N} \tag{2.25}$$

where

$$x_i(t) = \begin{bmatrix} p_i(t) \\ v_i(t) \\ a_i(t) \end{bmatrix}, A_{2,i} = \begin{bmatrix} 0 & 1 & 0 \\ 0 & 0 & 1 \\ 0 & -1/\beta_{1,i} & -\beta_{1,i}/\beta_{2,i} \end{bmatrix}, B_{2,i} = \begin{bmatrix} 0 \\ 0 \\ 1/\beta_{1,i} \end{bmatrix}. \tag{2.26}$$

In order to test more realistic scenarios, external disturbances should be considered. However, the absolute value of these disturbances that affect each vehicle is considered to be smaller than a non-negative constant [38].

## 2.3. Decentralized Controller Design

Various types of controller designs can be used to address the platoon control problem. One of these control designs is the centralized controller. In the centralized approach, all control decisions are made by a central authority, which could be a network supervisor responsible for the entire vehicle platoon system [39]. In contrast, the decentralized control approach requires each vehicle to make its own control decisions [1].

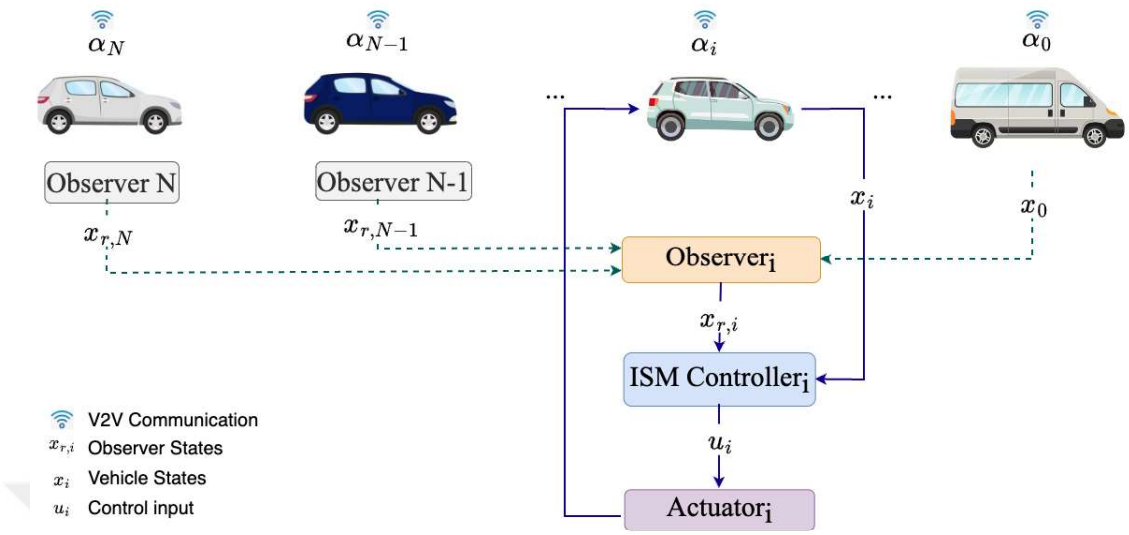


Figure 2.1. Control block diagram.

It is worth noting that the centralized control approach has a higher computational complexity than the decentralized controller [39].

In this chapter, a hierarchical controller proposed by Li et al. [5] will be used in the vehicle platoon system. The hierarchical controller contains two layers: the upper layer and the lower layer. On the upper layer, there is an observer to estimate the current state of the leading vehicle. The lower level uses state estimation in the ISMC to generate a control input signal. Figure 2.1 illustrates the control scheme of the $i^{th}$ vehicle. Vehicles are communicating via V2V technology, and the information from the other vehicles is represented as dashed lines (- - - -).

In [5] an observer has been proposed to estimate the observer states $x_{r,i}$ for the $i^{th}$ vehicle as

$$\dot{x}_{r,i} = \begin{bmatrix} \dot{p}_{r,i} \\ \dot{v}_{r,i} \\ \dot{a}_{r,i} \end{bmatrix} = \begin{bmatrix} v_{r,i} + m_{rp,i}p_{ii}(p_0 - p_{r,i}) + m_{rp,i}\Sigma_{j=1}^{N} a_{ij}(p_{r,i} - p_{r,i}) \\ a_{r,i} + m_{rv,i}p_{ii}(v_0 - v_{r,i}) + m_{rv,i}\Sigma_{j=1}^{N} a_{ij}(v_{r,j} - v_{r,i}) \\ m_{ra,i}p_{ii}(a_0 - a_{r,i}) + m_{ra}\Sigma_{j=1}^{N} a_{ij}(a_{r,j} - a_{r,i}) \end{bmatrix}. \tag{2.27}$$

In (2.27), $p_{r,i}, q_{r,i}, a_{r,i}$ represent position, velocity and acceleration, respectively for the $i^{th}$ vehicle. $p_{ii}$ is the $\mathcal{P}(i,i)$ element of the pinning matrix. Furthermore, $m_{rp,i}, m_{rv,i}, m_{ra,i} \in R$ are the design parameters of the observer.

### 2.3.1. ISMC Design

SMC, as a Variable Structure System (VSS) method, can adeptly control a system even when uncertainties and disturbances are present. The sliding surface should be determined to apply the SMC to a system. The system moves along this sliding surface and the goal is to confine the system's motion onto this surface. Then control actions are taken to steer the system towards the desired state.

Generally, the control process in SMC can be divided into two main phases: the reaching phase and the sliding phase. The reaching phase is where the system states reach the sliding surface in finite time. The sliding phase is where the system dynamics are constrained to move along the sliding surface. Pan et al. noted that the system is vulnerable to external factors such as disturbances during the reaching phase [40]. Therefore, factors such as uncertainties and the chattering phenomena have a negative impact on robust performance, meaning the invariance property, of SMC [41]. The invariance of SMC can be secured by removing the reaching phase with the use of ISMC. Distinguishing characteristics of the sliding surface in ISMC is the part with the integral term. It also has a part that is a linear combination of the system dynamics like SMC [42].

To cancel out the undesirable system reaction to the external disturbances, Li et al. proposed to use the ISMC approach in their study. The proposed ISMC consists of two parts: a traditional part related to tracking control and an additional part for compensating external time-varying disturbances [5].

In case of no external time-varying disturbance, $\xi_i(t) = 0$, tracking control of the vehicle model $\mathbb{T}_1$ is managed in [5] as

$$\begin{aligned} u_i^{nom}(t) =& n_{p,i}(p_{r,i}(t) - i \cdot l_0 - p_i(t)) + n_{v,i}(v_{r,i}(t) - v_i(t)) \\ &+ n_{a,i}(a_{r,i}(t) - a_i(t)) + a_{r,i}(t) \end{aligned} \tag{2.28}$$

where $n_{p,i}, n_{v,i}, n_{a,i} \in R$ are controller parameters for the $i^{th}$ vehicle.

If the vehicle model type is $\mathbb{T}_2$, tracking control of the vehicle is calculated in [5] as

$$\begin{aligned} u_i^{nom}(t) =& n_{p,i}(p_{r,i}(t) - i \cdot l_0 - p_i(t)) + n_{v,i}(v_{r,i}(t) - v_i(t)) \\ &+ n_{a,i}(a_{r,i}(t) - a_i(t)) + \beta_{2,i} a_{r,i}(t) + v_{r,i}(t) \end{aligned} \tag{2.29}$$

To eliminate the effect on external time-varying disturbances, $\xi_i(t) \neq 0$, in [5] the sliding surface is designed as

$$s_i(t) = \int_0^t (\tau_i \dot{a}_i(\theta) + a_i(\theta) - u_i^{nom}(\theta))\, d\theta \qquad i \in \mathbf{T}_1 \tag{2.30}$$

$$s_i(t) = \int_0^t (\beta_{1,i} \ddot{v}_i(\theta) + \beta_{2,i} \dot{v}_i(\theta) + v_i(\theta) - u_i^{nom}(\theta))\, d\theta \quad i \in \mathbf{T}_2. \tag{2.31}$$

The next step is to saturate the outputs coming from (2.30) and (2.31)

$$u_i^{sli}(t) = -\delta sgn(s_i(t)) \tag{2.32}$$

where $\delta$ is the control gain. The control input is the total of the nominal input and ISMC input. It can be expressed as [5]

$$u_i(t) = u_i^{nom}(t) + u_i^{sli}(t). \tag{2.33}$$

In practical applications of ISMC, difficulties in switching (e.g. delayed switching), and control feedback continuities can conduce to undesirable oscillations, as shown in Figure 2.2, that are called the chattering phenomenon [43]. Chattering is defined as oscillations that have finite frequency and amplitude [15]. Chattering not only degrades the performance of the system but also corrodes the materials.

To prevent the chattering phenomena, Li et al. [5] adopted a saturation function

$$sat(s_i(t)) = \begin{cases} 1, & s_i(t) > \gamma, \\ \frac{s_i(t)}{\gamma}, & |s_i(t)| \leq \gamma, \\ -1, & s_i(t) < -\gamma \end{cases} \tag{2.34}$$

where $\gamma$ is the boundary layer and $i \in \mathbf{Z}^+$. The sign function in (2.32) is replaced with the saturation function in (2.34) to minimize the negative effects of the chattering phenomenon.

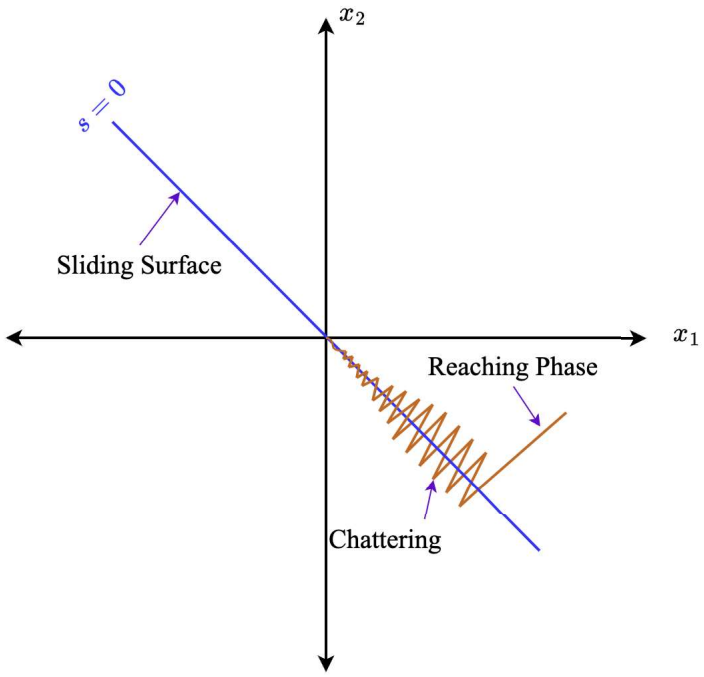


Figure 2.2. The chattering phenomenon.

## 2.4. Geometry Formation

Geometry formation refers to the spacing policy between the adjacent vehicles in the vehicle platoon system. To maintain a safe inter-vehicle space within the vehicle platoon system is essential to avoid collisions.

In the literature, two types of spacing policies, Constant Spacing Policy (CSP) and variable spacing policies, are introduced. As the spacing policy type naming implies, CSP has constant inter-vehicle space while variable spacing policies regulate the inter-vehicle space as a function of vehicle speed. The most common variable spacing policy is the Constant Time Gap (CTG) [4].

The CTG spacing policy adjusts the distance between vehicles based on their velocity, while the Constant Distance Gap (CDG) spacing policy maintains a constant inter-vehicle distance. The CTG approach is considered safer because it aims for a longer distance between vehicles as the vehicle speed increases. However, this can result in inefficiencies such as communication loss due to the longer distances maintained between vehicles [44].

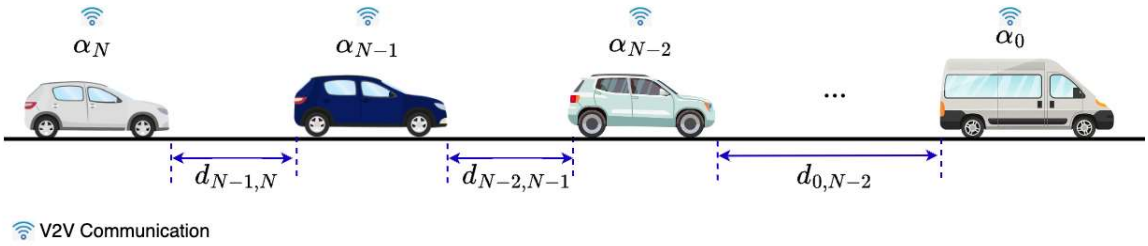


Figure 2.3. Geometry formation for CDG.

This study goes forward with the CDG spacing policy shown in Figure 2.3. In consequence, the distance between consecutive vehicles is constant. CDG is applied as

$$d_{i-1,i} = p_{i-1}(t) - p_i(t) \tag{2.35}$$

where desired distance between the $i^{th}$ vehicle and its neighbor $i-1$ is denoted by $d_{i-1,i}$.

## 2.5. Vehicular Platoon Dynamics

The vehicular platoon is designed as a heterogeneous system in the proposal of Li et al., meaning the vehicles in the platoon might have distinct dynamics [5]. The assumption of the constant spacing policy was made like the previous linearly controlled vehicular platoon design. To ensure all vehicles in the vehicular platoon will receive the leader vehicle information, either directly or indirectly, Assumption 2.2 is accepted.

**Assumption 2.2.** *Vehicular platoon set $V_{N+1}$ forms a directed spanning tree where node $\alpha_0$, in other words, the leading vehicle plays the role of a root node.*

**Lemma 2.1** ([5,20])**.** *A vehicle platoon system with $\mathcal{G}_{N+1} = (V_{N+1}, E_{N+1})$ augmented graph is asymptotically stable if all eigenvalues of the information flow matrix $\mathcal{L}_{\mathcal{P}}$ are on the Open Left-Half Plane (OLHP), $Re(\lambda_i(\mathcal{L}_{\mathcal{P}})) > 0$ for all $i \in \mathbb{Z}^+$, under Assumption 2.2.*

Lemma 2.1 emphasizes an important point in ensuring the stability of the vehicle platoon system since it explains that under Assumption 2.2 eigenvalues of the IFT will be real numbers. In addition, for stability analysis, it is necessary to analyze the observer and tracking errors separately due to the hierarchical structure of the control system.

The observer error can be defined as the difference between the observer's estimation of the leader vehicle's states calculated in (2.27) and the actual states of the leader vehicle coming from (2.8). The observer error can be written as

$$\dot{x}_{r,i}(t) = A_0 x_{r,i}(t) + M_r \sum_{j=1}^{N} a_{ij}(\varepsilon_{r,j}(t) - \varepsilon_{r,i}(t)) - M_r p_i \varepsilon_{r,i}(t) \tag{2.36}$$

where $M_r$ is the block diagonal matrix of the observer parameters in (2.27). The observer error matrix is denoted by $\varepsilon_{r,i}(t)$ and, can be computed as

$$\dot{\varepsilon}_{r,i}(t) = A_0 \varepsilon_{r,i}(t) + M_r \sum_{j=1}^{N} a_{ij}(\varepsilon_{r,j}(t) - \varepsilon_{r,i}(t)) - M_r p_i \varepsilon_{r,i}(t) \tag{2.37}$$

where $\varepsilon_{r,i}(t) = \begin{bmatrix} \varepsilon_{pr,i}(t) & \varepsilon_{vr,i}(t) & \varepsilon_{ar,i}(t) \end{bmatrix}^T = x_{r,i}(t) - x_0(t)$ [5]. By collecting observer errors as $\varepsilon_r(t) = \begin{bmatrix} \varepsilon_{r,1}(t)^T & \varepsilon_{r,2}(t)^T & \dots & \varepsilon_{r,N}(t)^T \end{bmatrix}^T$, its state space representation can be attained as

$$\dot{\varepsilon}_r(t) = \big(I_N \otimes A - \mathcal{L}_{\mathcal{P}} \otimes M_r\big)\varepsilon_r(t) \tag{2.38}$$

where $\otimes$ denotes the Kronecker product.

All in all, the control objective of the control system can be summarized in [5] as

$$\lim_{t\to\infty} \|p_i(t) - p_0(t) + i \cdot d_{i-1,i}(t)\| = 0 \tag{2.39}$$

$$\lim_{t\to\infty} \|q_i(t) - q_0(t)\| = 0 \tag{2.40}$$

$$\lim_{t\to\infty} \|a_i(t) - a_0(t)\| = 0 \tag{2.41}$$

where $d_{i-1,i}(t)$ is the desired constant spacing between the node $(i-1)$ and the node $i$ for $i = 1, 2, ..., N$. Tracking error can be defined as $\varepsilon_i = \begin{bmatrix} \varepsilon_{p,i} & \varepsilon_{v,i} & \varepsilon_{a,i} \end{bmatrix}^T = x_i - x_{r,i} + L_i(t) = x_i(t) - \Pi_i x_{r,i}(t) + L_i(t)$ for $i \in \mathbb{N}$ where $L_i(t) = \begin{bmatrix} i \cdot d_{i-1,i}(t) & 0 & 0 \end{bmatrix}^T$ so that $A_i L_i(t) = 0$. Nominal control input in (2.28) and (2.29) can be reformulated as

$$u_i^{nom}(t) = -n_i^T \varepsilon_i(t) + \Gamma_i x_{r,i}(t) \tag{2.42}$$

where $n_i = \begin{bmatrix} n_{p,i} & n_{v,i} & n_{a,i} \end{bmatrix}^T$ is the controller gain matrix of the $i^{th}$ vehicle.

According to [5], tracking error dynamics can be expressed as

$$\dot{\varepsilon}_i(t) = (A_i - B_i n_i^T)\varepsilon_i(t) - \Pi_i\big(A_0 x_{r,i}(t) + M_r \sum_{j=1}^{N} a_{ij}(\varepsilon_{r,j}(t) - \varepsilon_{r,i}(t)) - M_r p_{ij}\varepsilon_{r,i}(t)\big) \quad (2.43)$$

by letting $\varepsilon(t) = \begin{bmatrix}\varepsilon_1(t)^T & \varepsilon_2(t)^T & \dots & \varepsilon_N(t)^T\end{bmatrix}$. In conclusion, the state space representation can be obtained as

$$\dot{\varepsilon}(t) = (A - Bn)\varepsilon(t) - \Pi(\mathcal{L}_\mathcal{P} \otimes M_r)\varepsilon_r(t) \quad (2.44)$$

where $n$ is the block diagonal matrix of the controller parameters in (2.28) and (2.29). The matrix denoted by $A$ is the block diagonal matrix of the $A_i$ matrices, $B$ is the block diagonal matrix of the $B_i$ matrices, $\Pi$ is the block diagonal matrix of the $\Pi_i$ matrices for $i = 1, 2, \dots, N$. Tracking error in (2.44) is not only affected by the controller characteristics but also by the observer's erroneous leader state observations. The state space equation for the lumped error $\varepsilon(t) = \begin{bmatrix}\varepsilon(t)^T & \varepsilon_r(t)^T\end{bmatrix}^T$ can be formulated as

$$\dot{\bar{x}} = \bar{A}\bar{x} \quad (2.45)$$

where

$$\bar{A} = \begin{bmatrix} A - Bn & -\Pi(\mathcal{L}_\mathcal{P} \otimes M_r) \\ 0 & I_N \otimes A_0 - \mathcal{L}_\mathcal{P} \otimes M_r \end{bmatrix}. \quad (2.46)$$

The stability criteria for each part of the lumped error state-space in (2.45) are listed below:

1. For the stability of $(I_N \otimes A_0 - \mathcal{L}_\mathcal{P} \otimes M_r)$ in (2.46), Lemma 2.2 should be satisfied.

   **Lemma 2.2** ( [20]). *Let $\{\lambda_i(\mathcal{L}_\mathcal{P})\}_{i=1}^N$ be the eigenvalues of the information flow matrix $\mathcal{L}_\mathcal{P}$, which may or may not be distinct. The vehicle platoon system is asymptotically stable if and only if all the matrices*

   $$A_0 - \lambda_i(\mathcal{L}_\mathcal{P})M_r \quad \textit{for} \quad i = 1, 2, \dots, N \quad (2.47)$$

   *are Hurwitz matrices.*

   The eigenvalues of the matrix $A_0 - \lambda_i(\mathcal{L}_\mathcal{P})M_r$ in Lemma 2.2 are the elements on the main diagonal since it is an upper-triangular matrix. These eigenvalues can be listed as $-\lambda_i(\mathcal{L}_\mathcal{P})m_{r,p}$, $-\lambda_i(\mathcal{L}_\mathcal{P})m_{r,v}$, and $-\lambda_i(\mathcal{L}_\mathcal{P})m_{r,a}$.

These values can only be negative if the observer parameters, $m_{rp}$, $m_{rq}$, and $m_{ra}$, are positive [5].

**2.** Li et al. [5] stated that $A - Bn$ is asymptotically stable if Routh-Hurwitz stability criterion is satisfied for each $A_i - B_i n_i^T$ such that

$$\begin{cases} n_{p,i} > 0, \\ n_{q,i} > \frac{n_{p,i}\tau_i}{n_{a,i}+1}, \quad \text{if} \quad i \in \mathbb{T}_1, \\ n_{a,i} > -1. \end{cases} \quad \begin{cases} n_{p,i} > 0, \\ n_{q,i} > \frac{n_{p,i}\beta_{1,i}}{n_{a,i}+\beta_{2,i}} - 1, \quad \text{if} \quad i \in \mathbb{T}_2 \\ n_{a,i} > -\beta_{2,i}. \end{cases} \quad . \tag{2.48}$$

In summary, the observer and tracking errors for a nonlinear controller are formulated above. The $\bar{A}$ matrix in (2.46) should be analyzed to ensure the stability of the vehicle platoon system. The $I_N \otimes A_0 - \mathcal{L}_\mathcal{P} \otimes M_r$ part in (2.46) is associated with the observer errors like the $-\Pi(\mathcal{L}_\mathcal{P} \otimes M_r)$ part. These matrices including $\mathcal{L}_\mathcal{P}$ demonstrate that the information flow topology involvement in the stability of the vehicle platoon system cannot be ignored. $A - Bn$ element in the $\bar{A}$ matrix in (2.46) does not depend on the information flow topology. If the system matrices and the controller parameters are static, $A - Bn$ will be time-invariant and it will be the same for varying information flow topologies.

## 2.6. Numerical Analysis

This section focuses on conducting simulations and evaluating the outcomes. The parameters used in simulating the vehicle platoon system adhere to the criteria outlined in Section 2.5 and are detailed in Table 2.1 and Table 2.2.

The ISMC and observer gains may vary from one vehicle to another. Nonetheless, the gains are considered to be identical for all of the vehicles in the simulation. In addition, the initial conditions of the vehicle states and the observer states are another aspect of the platoon design that should be taken into account. A vehicle platoon system can start when the followers are in motion or at a standstill. In the simulations, the followers are at $10$ m/s when platooning begins.

Hence, all observer states are initialized at $x_r(t_0) = \begin{bmatrix} N \times d_{i-1,i} & 10 & 0 \end{bmatrix}^T$ while the initial states of the follower vehicles are $x_i(t_0) = \begin{bmatrix} (N-i) \times d_{i-1,i} & 10 & 0 \end{bmatrix}^T$ for $i = 1, \ldots, N = 7$. Note that the sample time $t_s$ is taken as $0.01$ seconds. The information flow topology in Figure 2.4 shows the data exchange between the vehicles in a heterogeneous vehicle platoon system. Not every node receives direct information from the leading vehicle.

Nevertheless, the leader vehicle acts as a root since it can reach all of the nodes one way or another. Moreover, each node has different vehicle dynamics as declared in Table 2.2. $\mathbb{T}_1$ vehicle model is represented as blue circles while $\mathbb{T}_2$ vehicle model is represented as orange circles in Figure 2.4. Inter-vehicle space between each vehicle aimed to be the same constant value as seen in Table 2.1. Table 2.3 lists the external disturbances affecting each vehicle as a function of time.

Vehicles are communicating via V2V communication which can be interrupted by weather conditions such as rain, and snow or by obstacles along the road like buildings. This will lead to communication delays and packet losses in practice. However, communication errors are neglected in the simulations.

Table 2.1. Simulation parameters.

| **Description** | **Symbol** | **Value** |
|---|---|---|
| ISMC gains | $n_{p,i}$ | $0.2$ |
| | $n_{v,i}$ | $0.5$ |
| | $n_{a,i}$ | $0$ |
| Observer gains | $m_{rp,i}$ | $3$ |
| | $m_{rv,i}$ | $2$ |
| | $m_{ra,i}$ | $1$ |
| Desired constant spacing | $d_{i-1,i}$ | 20 m |
| Control gain | $\delta$ | $2$ |
| Boundary layer | $\gamma$ | $0.05$ |

Table 2.2. Vehicle parameters.

| Node ID | Vehicle Model Type | Parameter |
|---|---|---|
| $\alpha_1$ | $\mathbf{T}_1$ | $\tau_1 = 0.20$ |
| $\alpha_2$ | $\mathbf{T}_2$ | $\beta_{1,2} = 6.20,\ \beta_{2,2} = 4.10$ |
| $\alpha_3$ | $\mathbf{T}_2$ | $\beta_{1,3} = 6.50,\ \beta_{2,3} = 2.40$ |
| $\alpha_4$ | $\mathbf{T}_1$ | $\tau_4 = 0.30$ |
| $\alpha_5$ | $\mathbf{T}_2$ | $\beta_{1,5} = 5.50,\ \beta_{2,5} = 3.50$ |
| $\alpha_6$ | $\mathbf{T}_1$ | $\tau_6 = 0.25$ |
| $\alpha_7$ | $\mathbf{T}_1$ | $\tau_7 = 0.30$ |

Table 2.3. External time-varying disturbances.

| Node ID | Symbol | Disturbance |
|---|---|---|
| $\alpha_1$ | $\xi_1(t)$ | $cos(0.2t + \pi/8)$ |
| $\alpha_2$ | $\xi_2(t)$ | $sin(0.5t + \pi/4)$ |
| $\alpha_3$ | $\xi_3(t)$ | $cos(0.3t + \pi/8)$ |
| $\alpha_4$ | $\xi_4(t)$ | $sin(0.2t + \pi/4)$ |
| $\alpha_5$ | $\xi_5(t)$ | $cos(0.1t + \pi/6)$ |
| $\alpha_6$ | $\xi_6(t)$ | $sin(0.1t)$ |
| $\alpha_7$ | $\xi_7(t)$ | $cos(0.2t)$ |

The leading vehicle maintains a constant speed which means there is no acceleration for the leader. Leader's states are initialized at $\begin{bmatrix} N \times d_{i-1,i} & 8 & 0 \end{bmatrix}^T$. Once the setup is finished, the vehicular platoon is tested using the MATLAB environment. Figure 2.4 depicts the graph tested in MATLAB, indicating that the leader vehicle is reaching all nodes within the vehicle platoon system. Therefore, Assumption 2.2 is satisfied.

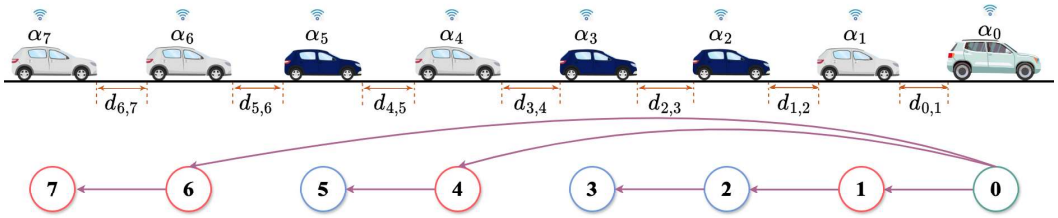


Figure 2.4. Information flow topology.

Figures 2.5-2.7 show observer errors of the follower vehicles. Figures 2.5-2.6 clearly show that the observer errors converge to zero in under $5$ seconds. In both figures, it can be seen from the overlapping lines that observers of some vehicles exhibit the same error behavior for position and velocity states. For example, the line for vehicle $6$ (——) intersects with the lines of vehicles $1$ (——) and $4$ (——). In addition, the line for vehicle $7$ (——) is on top of the lines of vehicles $2$ (——) and $5$ (——). Additionally, Figure 2.7 reveals that the observer error in the acceleration state remains uniform for all of the follower vehicles.

Figures 2.8-2.10 show the observer states of the followers. It can be interpreted that followers can estimate the leading vehicle's states accurately. Figures 2.8 and 2.10 demonstrate that the observations of the leader's position and acceleration by the follower vehicles coincide since the lines in both figures are stacked on top of each other. Furthermore, the observer's velocity states are initialized from $10$ m/s, shown in Figure 2.9, it takes less than $5$ seconds for velocity observation to converge to $8$ m/s which equals to leaders velocity.

Figures 2.11-2.13 display the vehicle states position, velocity, and acceleration, respectively. Figure 2.11 demonstrates that the followers are pursuing the preceding vehicle from a safe distance even with the external time-varying disturbances so there is no collision risk. However, at the beginning of the platooning, followers $3$ and $4$ are moving away from each other for a short amount of time due to a lack of direct communication. Figures 2.12 and 2.13 show that the velocity and acceleration states are converging to the desired states. Vehicles are cruising at a constant velocity approximately after $45$ seconds.

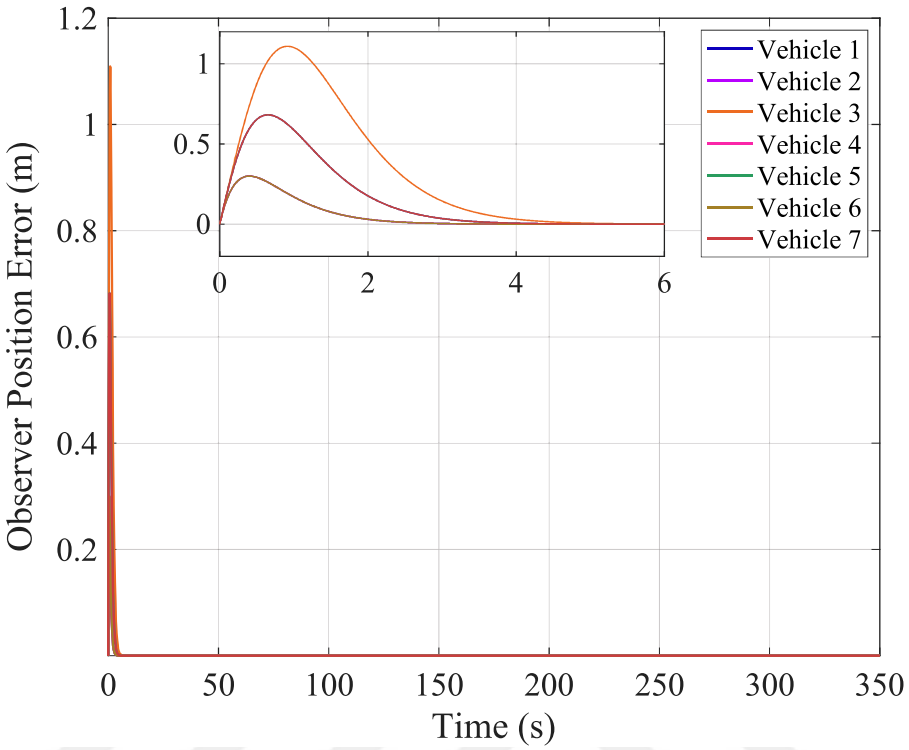


Figure 2.5. Position error of the observer under IFT in Figure 2.4.

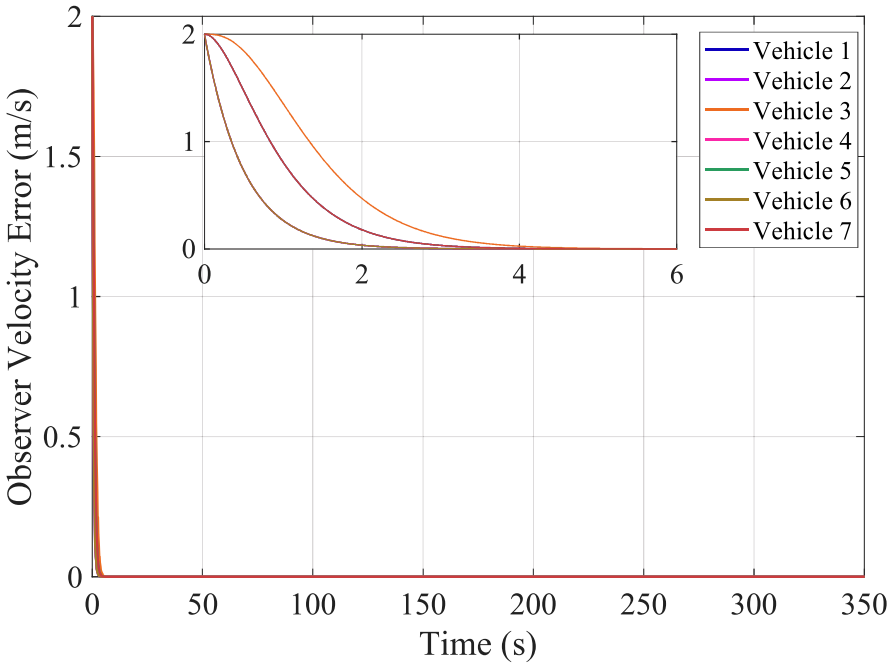


Figure 2.6. Velocity error of the observer under IFT in Figure 2.4.

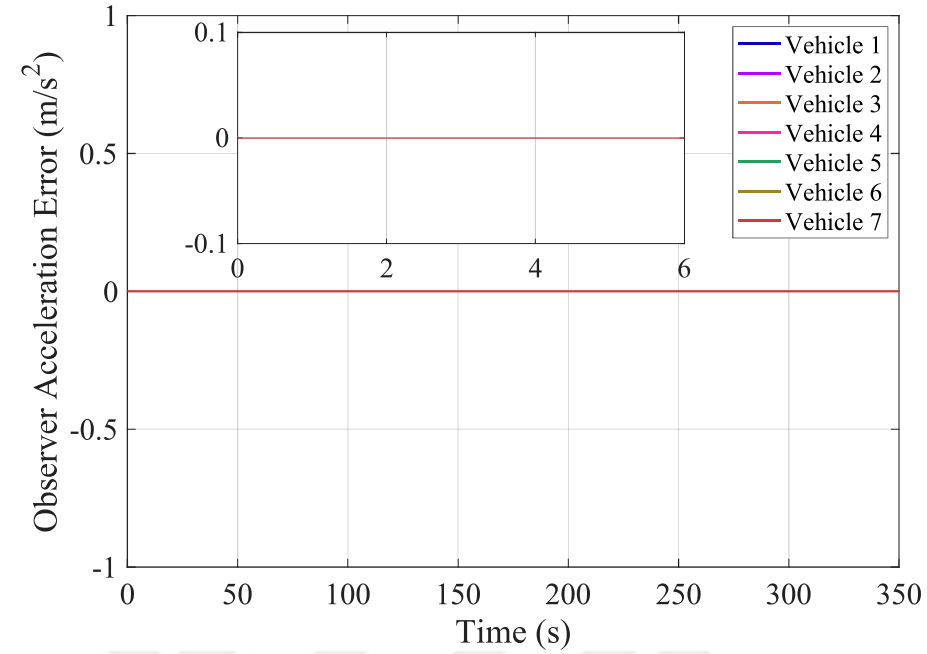


Figure 2.7. Acceleration error of the observer under IFT in Figure 2.4.

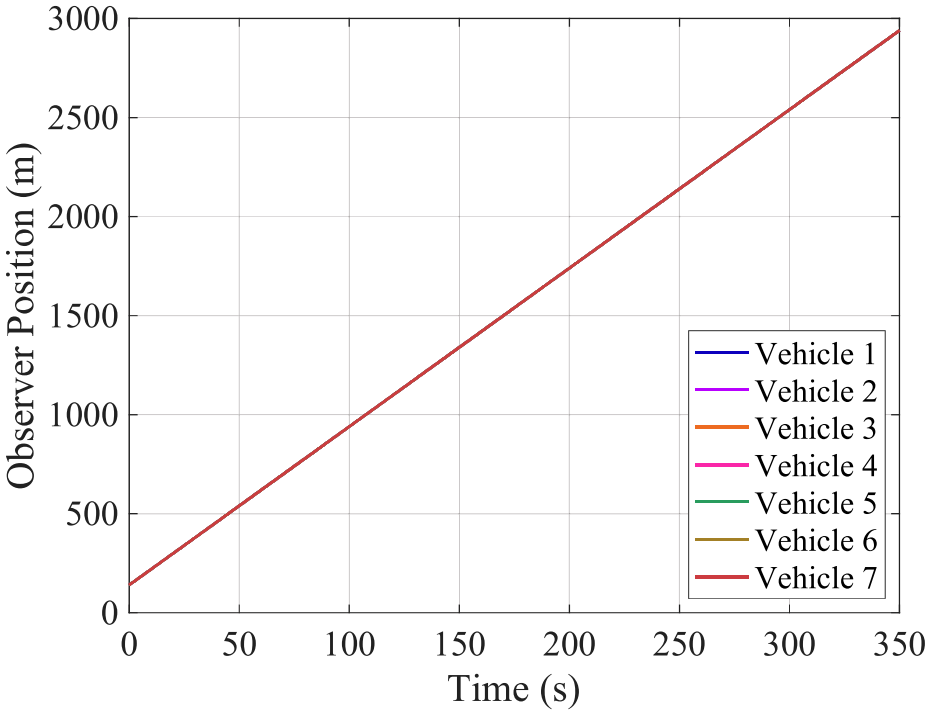


Figure 2.8. Position state of the observer under IFT in Figure 2.4.

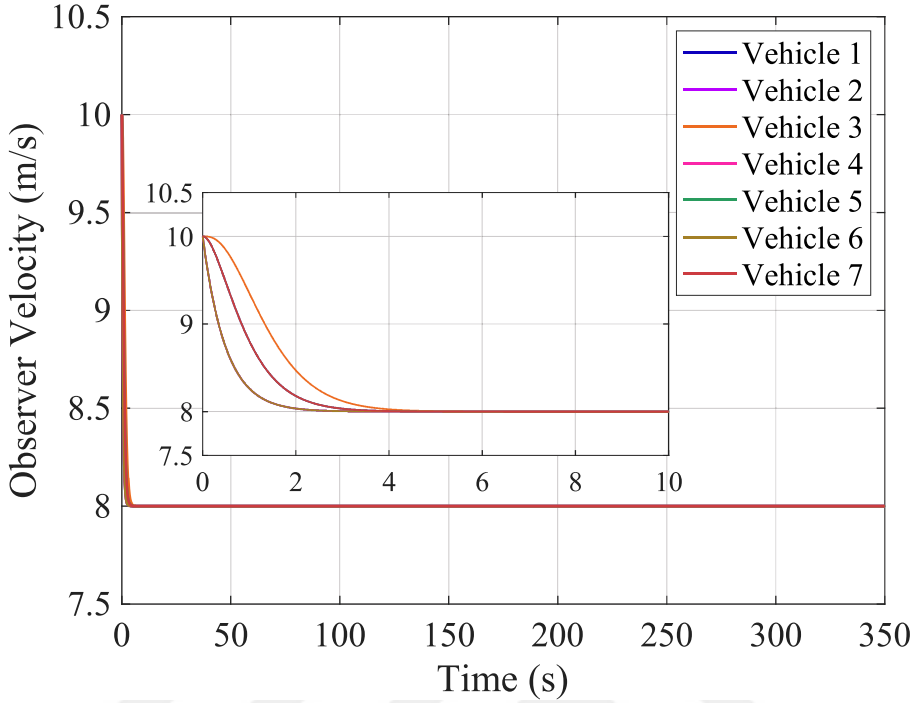


Figure 2.9. Velocity state of the observer under IFT in Figure 2.4.

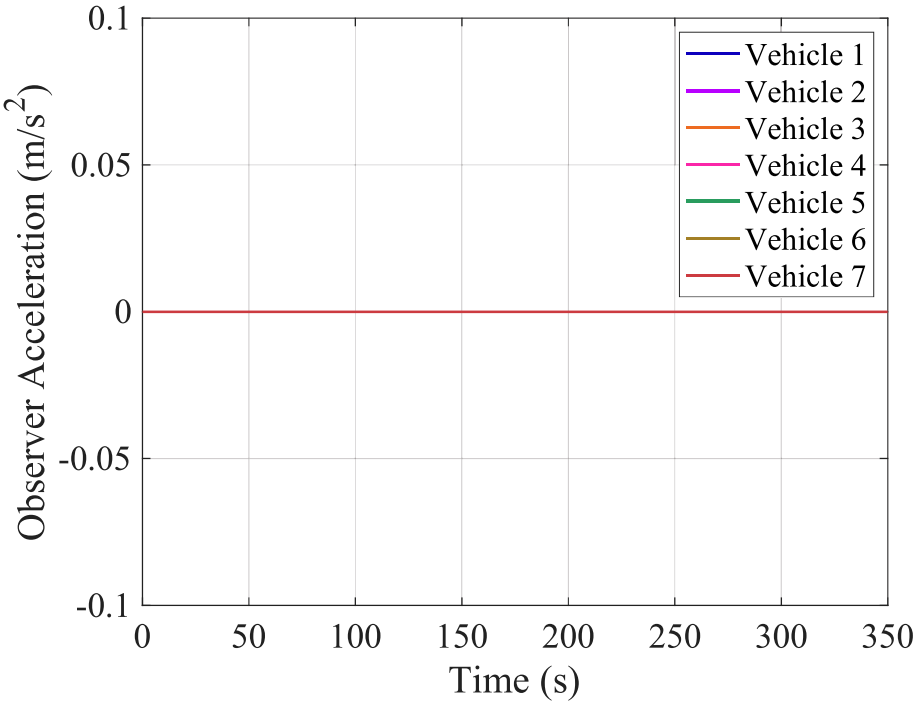


Figure 2.10. Acceleration state of the observer under IFT in Figure 2.4.

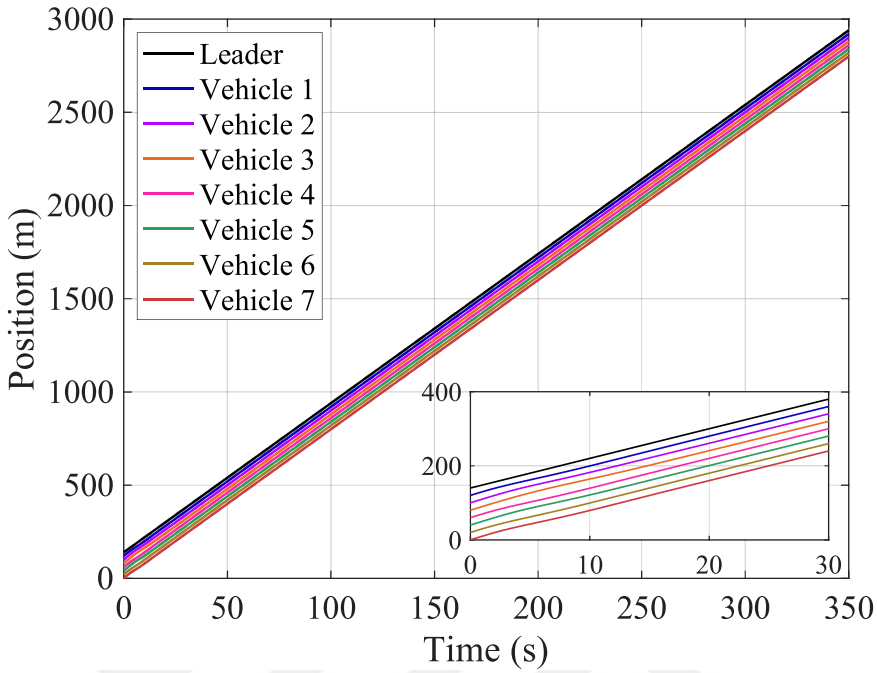


Figure 2.11. Position state of the vehicles under IFT in Figure 2.4.

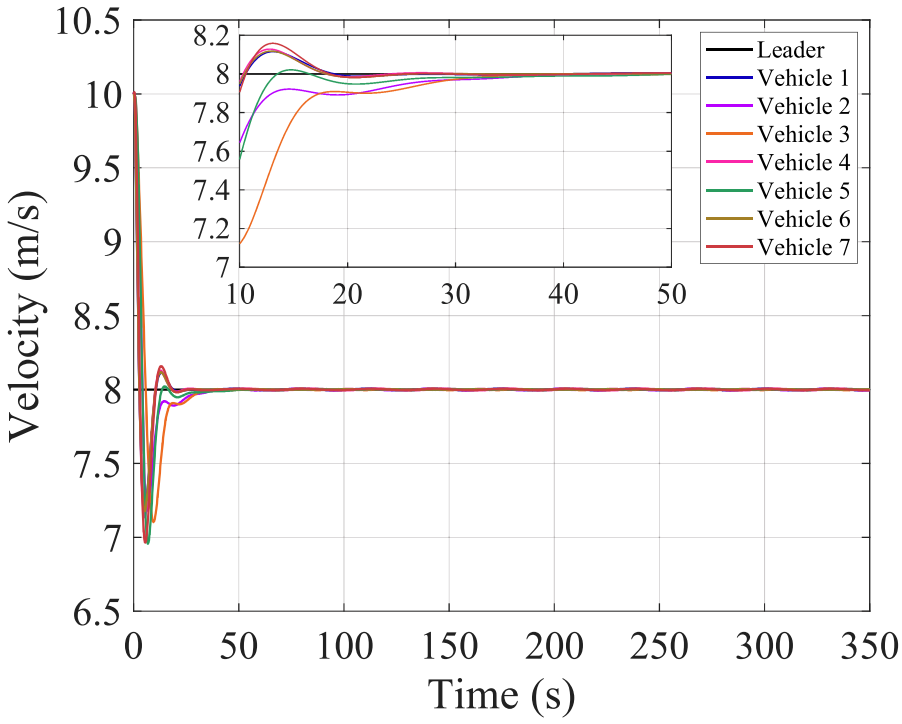


Figure 2.12. Velocity state of the vehicles under IFT in Figure 2.4.

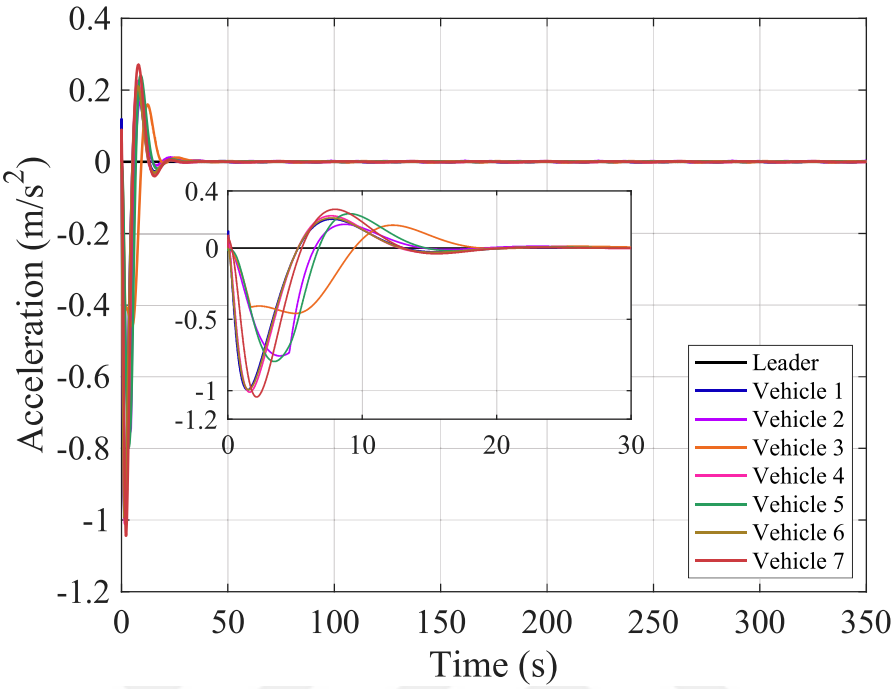


Figure 2.13. Acceleration state of the vehicles under IFT in Figure 2.4.

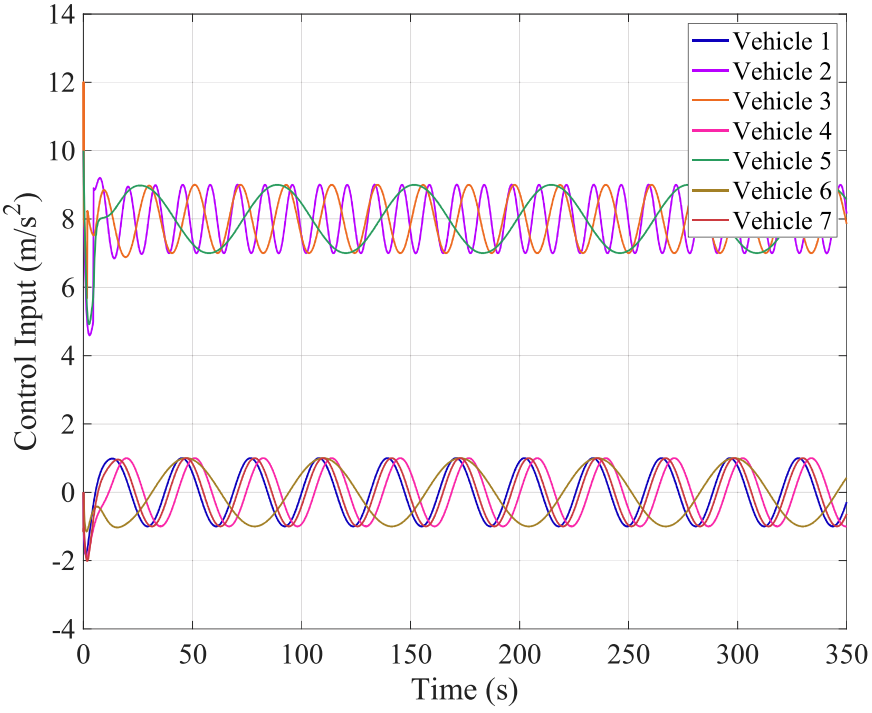


Figure 2.14. Control inputs under IFT in Figure 2.4.

Furthermore, different vehicle types can be explicitly distinguished in Figure 2.14. $\mathbb{T}_2$ model type, $\alpha_2, \alpha_3$, and $\alpha_5$, have the desired velocity as the control input. The remaining vehicles, $\alpha_1, \alpha_4$, $\alpha_6$, and $\alpha_7$, are $\mathbb{T}_1$ model type so their control input is the acceleration.

## 2.7. Summary of the Chapter

This chapter investigates the characteristics of vehicular platoon control systems. Two-layered hierarchical controller proposed by Li et al. in [5] is simulated via MATLAB. Simulation results are examined. Results coincide with the referenced paper, for an IFT that has a spanning tree, the heterogeneous vehicle platoon system tested is asymptotically stable. In this context, different unidirectional and bidirectional information flow topologies that contain a spanning tree will be investigated employing the proposed hierarchical controller in Chapters 3 and 4, respectively. A linear controller also be used for comparison. Additionally, an examination of the stability and convergence of the proposed IFTs will be undertaken.

# 3. ANALYSIS OF UNIDIRECTIONAL TOPOLOGIES

In this chapter, the stability and performance characteristics of a vehicle platoon system under several unidirectional information flow topologies will be analyzed. The analysis considers both homogeneous and heterogeneous platoon types for various unidirectional information flow topologies that are defined. The focus will be on the investigation of the performance of vehicle platoon systems that use the defined information flow topologies. In addition, the influence of the decentralized controller type will also be inspected by the employment of linear and nonlinear controllers in the vehicle platoon system. All arguments will be corroborated with the simulation results.

## 3.1. Unidirectional Information Topologies

Figure 3.1 displays different unidirectional information topologies for the homogeneous vehicle platoon system. These topologies are named based on the number of nodes that receive the leader vehicle information. Unidirectional information topologies, as shown in Figure 3.1, can be described as

- Predecessor Following (PF): In the PF topology, each vehicle follows the preceding vehicle, and the leader information is only available for its neighbor.
- Predecessor Following 2 (PF2): In the PF2 topology, each vehicle follows the preceding vehicle, and the leader information is available for the leader's neighbor and its neighbor's neighbor. Therefore, two vehicles are receiving direct information from the leading vehicle.
- Predecessor Following 3 (PF3): In the PF3 topology, each vehicle follows the preceding vehicle, and the leader information is available for the leader's neighbor and two vehicles that are following the leader's neighbor. Therefore, three vehicles are receiving direct information from the leading vehicle.

- Predecessor Following 4 (PF4): In the PF4 topology, each vehicle follows the preceding vehicle, and the leader information is available for the leader's neighbor and three vehicles that are following the leader's neighbor. Therefore, four vehicles are receiving direct information from the leading vehicle.
- Predecessor Following 5 (PF5): In the PF5 topology, each vehicle follows the preceding vehicle, and the leader information is available for the leader's neighbor and four vehicles that are following the leader's neighbor. Therefore, five vehicles are receiving direct information from the leading vehicle.
- Predecessor Following 6 (PF6): In the PF6 topology, each vehicle follows the preceding vehicle, and the leader information is available for the leader's neighbor and five vehicles that are following the leader's neighbor.
  Therefore, six vehicles are receiving direct information from the leading vehicle.
- Predecessor-Leader Following (PLF): In the PLF topology, each vehicle follows the preceding vehicle, and the leader information is available to all the vehicles in the vehicular platoon.

Figure 3.2 depicts unidirectional information topologies for a heterogeneous vehicle platoon system. Such a platoon system can contain different types of vehicles with varying vehicle dynamics. The leading vehicle, represented by a pink circle (◯), may exhibit different vehicle dynamics compared to the follower vehicles as in Figure 3.2. Vehicles 2, 3, and 5, represented by a blue circle (◯), have identical vehicle dynamics, whereas followers 1, 4, 6, and 7, represented by an orange circle (◯), have similar vehicle dynamics.

The characteristics of the information flow topologies listed above can be represented in matrix forms [21]. These matrices can be listed as

- Adjacency matrix, $\mathcal{A} = [a_{ij}] \in \mathbb{R}^{N\times N}$,
- Laplacian matrix, $\mathcal{L} = [l_{ij}] \in \mathbb{R}^{N\times N}$,
- Pinning matrix, $\mathcal{P} = diag\{p_1, p_2, ..., p_N\}$.

Detailed information related to the matrices mentioned above is available in Chapter 2.

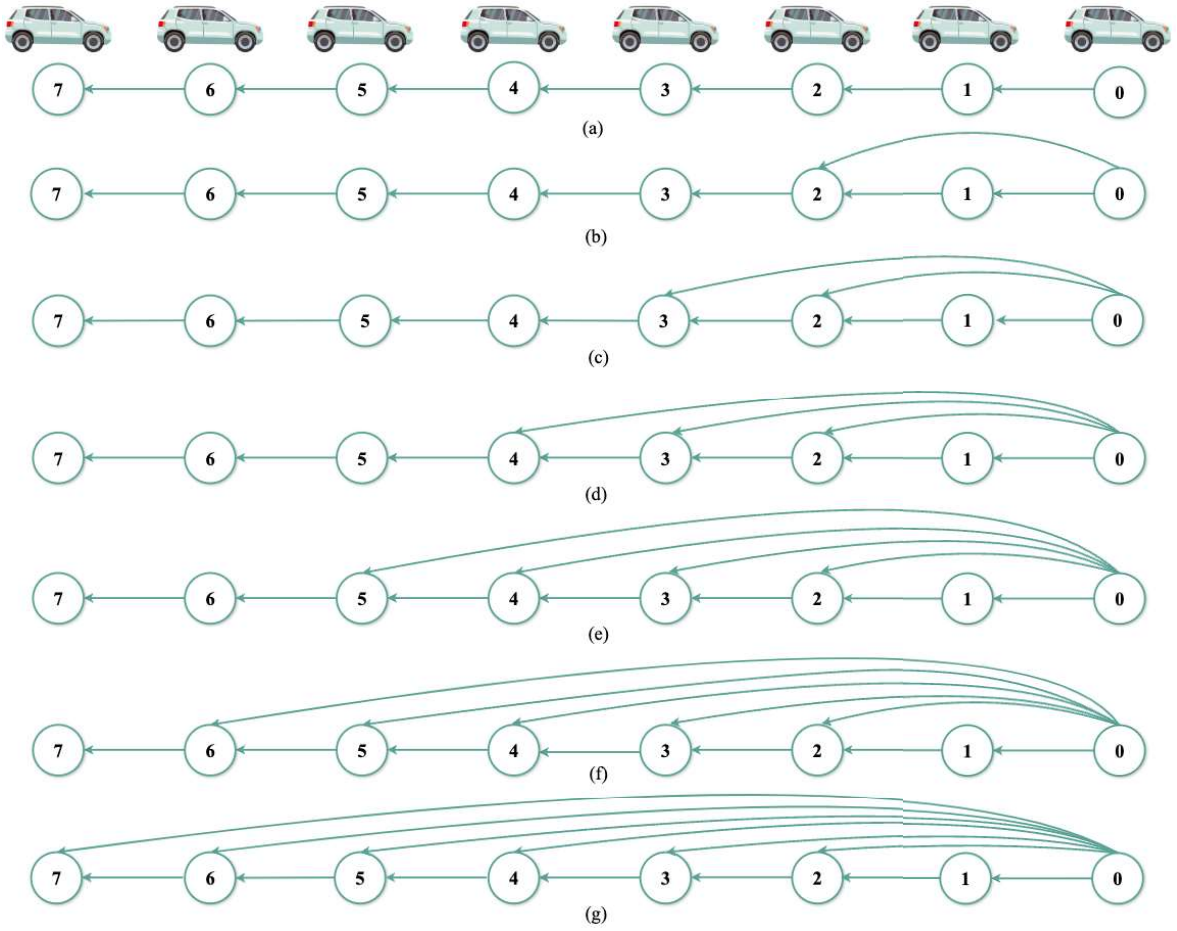


Figure 3.1. Unidirectional IFTs for homogeneous vehicular platoons (a) PF, (b) PF2, (c) PF3, (d) PF4, (e) PF5, (f) PF6, (g) PLF.

If the $i^{th}$ vehicle in the vehicle platoon system is receiving the leader vehicle information then $p_{ii} = 1$. A node set denoted as $\mathbb{P}_i$ for $i = 1, 2, ..., N$, can be defined for each node to indicate the attainability of the leader vehicle information [20]. $\mathbb{P}_i$ is found by

$$\mathbb{P}_i = \begin{cases} \{0\}, & \text{if } p_{ii} = 1 \\ \emptyset, & \text{if } p_{ii} = 0. \end{cases} \tag{3.1}$$

In addition to the leader attainability set, a neighbor set denoted as $\mathbb{N}_i$ for $i = 1, 2, ..., N$ can be defined for each node to indicate the attainability of the vehicle information other than the leader vehicle. The neighbor set for the $i^{th}$ vehicle can be expressed with a set $\mathbb{N}_i = \{j | a_{ij} = 1\}$ as Zheng et al. pointed out [20].

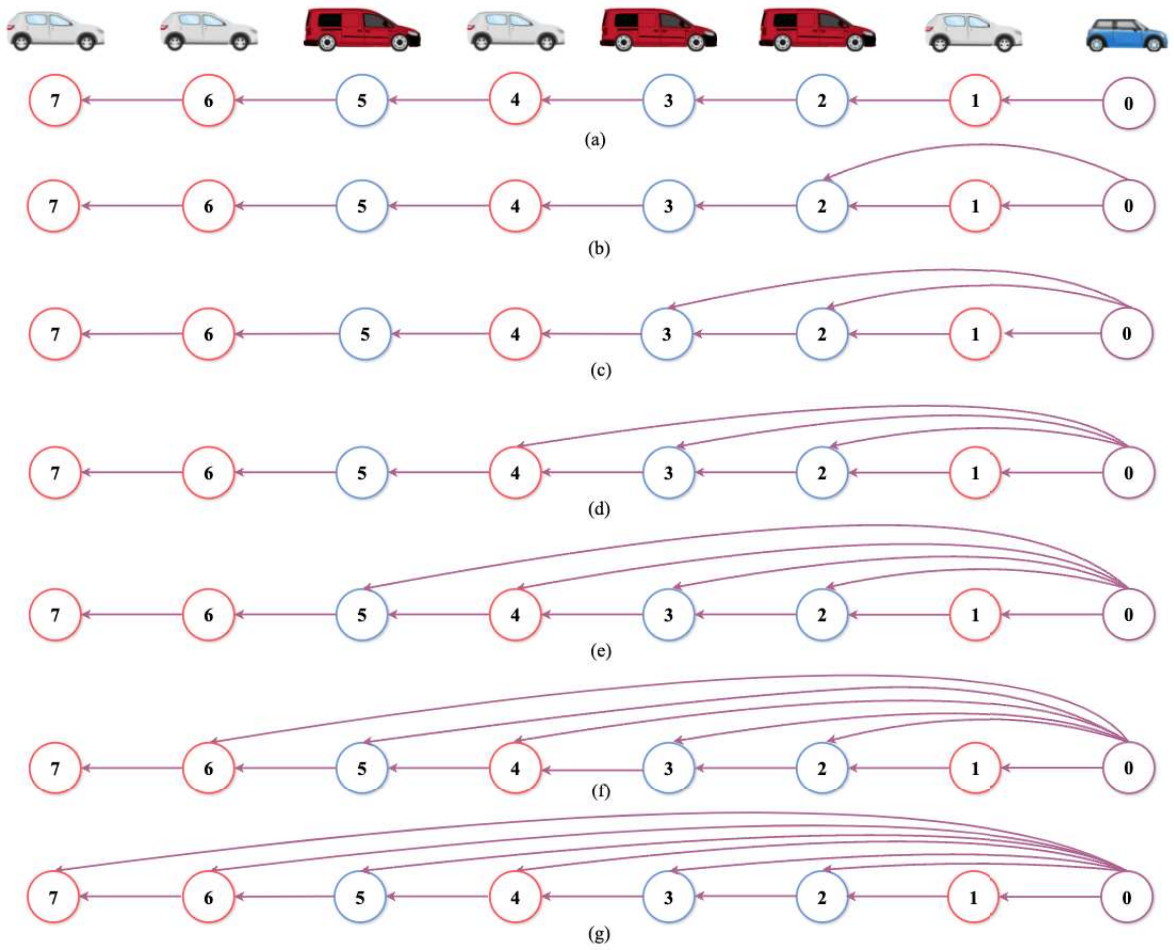


Figure 3.2. Unidirectional IFTs for heterogeneous vehicular platoons (a) PF, (b) PF2, (c) PF3, (d) PF4, (e) PF5, (f) PF6, (g) PLF.

## 3.2. Linear Decentralized Controller Design

Zheng et al. proposed a linearized vehicle dynamics model for the vehicles in vehicle platoon systems [20]. A nonlinear system is linearized using the FBL method as explained in detail in Chapter 2. A control law proportional (P-controller) to the deviation between the actual value and the reference value is applied to the controlled system [20].

The vehicular platoon is designed as a homogeneous system, meaning all the vehicles in the platoon have the same dynamics. Certain assumptions are made in the platoon formation [45].

These assumptions can be described as

(i) Vehicles in the platoon system have identical vehicle dynamics.
(ii) Vehicles in the platoon system have identical controllers.
(iii) The CDG spacing policy is established.
(iv) The leader vehicle is cruising at a constant velocity.

Thus,

$$p_0(t) = v_0(t)t \tag{3.2}$$

where $p_0(t)$ and $v_0(t)$ represent the position and the velocity, respectively, of the leading vehicle. Furthermore, the aim of the vehicle platoon control is to track the velocity of the platoon leader, i.e., $v_i(t) = v_0(t)$ while retaining a secure distance between consecutive vehicles in the vehicle platoon system. To ensure this safe distance, the CDG spacing policy is used so that $p_{i-1}(t) - p_i(t) = d_{i-1,i}(t)$ where $d_{i-1,i}(t)$ is the desired constant spacing between the node $(i-1)$ and the node $i$ for $i = 1, \ldots, N$. Here, the desired inter-vehicle distance between the leading and following vehicles is constant and it is not dependent on the velocity of the vehicles [27].

The decentralized controller law is expressed as

$$u_i(t) = -\sum_{j \in \mathbb{I}_i} [k_1(p_i(t) - p_j(t) - d_{i,j}) + k_2(v_i(t) - v_j(t)) + k_3(a_i(t) - a_j(t))] \tag{3.3}$$

where $k_1$, $k_2$ and $k_3$ are the controller gains of the linear decentralized controller [20].

Equation (3.3) demonstrates that the local controllers are affected by the information flow topology. $\mathbb{I}_i$ parameter in (3.3) is related to the information flow topology. The leader attainability set and the neighbor set for $i = 1, 2, ..., N$ are combined in $\mathbb{I}_i = \mathbb{P}_i \cup \mathbb{N}_i$.

The constant spacing policy obligates a fixed distance between each vehicle in the platoon. The desired trajectory of the vehicle in the $i^{th}$ position is calculated as the difference between the position of the leader vehicle and the sum of the spaces between the leader vehicle and the $i^{th}$ vehicle [20].

Mathematically, this can be represented as

$$p_i^*(t) = p_0(t) - d_{0,i} = p_0(t) - \sum_{j=0}^{i-1} d_{j,j+1}. \tag{3.4}$$

The tracking error of the $i^{th}$ vehicle $\varepsilon_i$ can be written as

$$\varepsilon_i(t) = \begin{bmatrix} \tilde{p}_i(t) \\ \tilde{v}_i(t) \\ \tilde{a}_i(t) \end{bmatrix} = \begin{bmatrix} p_i(t) - p_i^*(t) \\ v_i(t) - \dot{p}_i^*(t) \\ a_i(t) - \ddot{p}_i^*(t) \end{bmatrix} = \begin{bmatrix} p_i(t) - p_i^*(t) \\ v_i(t) - v_0(t) \\ a_i(t) - a_0(t) \end{bmatrix}. \tag{3.5}$$

To put it simply, the lumped tracking error is

$$\varepsilon_i(t) = \sum_{j \in \mathbb{I}_i} (\tilde{x}_i(t) - \tilde{x}_j(t)) \tag{3.6}$$

where $\tilde{x}_i(t) = [\tilde{p}_i(t), \tilde{v}_i(t), \tilde{a}_i(t)]^T$ [20]. Inserting (3.6) into (3.5)

$$u_i(t) = -k^T \varepsilon_i(t) \tag{3.7}$$

where $k = [k_1, k_2, k_3]^T$ [20]. Hereby, the state space model for the closed-loop dynamics of each vehicle can be written down as

$$\begin{aligned} \dot{\tilde{x}}_i(t) &= A\tilde{x}_i(t) - Bk^T \varepsilon_i(t) \\ &= A\tilde{x}_i(t) - Bk^T \left[ \sum_{j=1}^{N} a_{ij}(\tilde{x}_i(t) - \tilde{x}_j(t)) + p_i(\tilde{x}_i(t) - \tilde{x}_0(t)) \right]. \end{aligned} \tag{3.8}$$

Collection of all states in (3.8) can be redesigned as

$$\tilde{x}(t) = \begin{bmatrix} \tilde{x}_1(t) & \tilde{x}_2(t) & \cdots & \tilde{x}_N(t) \end{bmatrix}^T. \tag{3.9}$$

In this way, (3.8) can be reformulated as

$$\dot{\tilde{x}}(t) = \left[ I_N \otimes A - (\mathcal{L}_\mathcal{P}) \otimes Bk^T \right] \tilde{x}(t) \tag{3.10}$$

where the overall closed-loop system matrix is

$$A_c = I_N \otimes A - \mathcal{L}_\mathcal{P} \otimes Bk^T. \tag{3.11}$$

The Kronecker product is denoted by $\otimes$. Assume that $A \in \mathbb{R}^{m\times n}$ and $B \in \mathbb{R}^{p\times q}$, the Kronecker product of $A$ and $B$ can be found as

$$A \otimes B = \begin{bmatrix} a_{11}B & a_{12}B & \dots & a_{1n}B \\ a_{21}B & a_{22}B & \dots & a_{2n}B \\ \vdots & \vdots & \ddots & \vdots \\ a_{m1}B & a_{m2}B & \dots & a_{mn}B \end{bmatrix} \in \mathbb{R}^{pm\times qn}. \tag{3.12}$$

$A_c$ matrix in (3.11) can be divided into three distinct parts. The first part pertains to the node dynamics and is represented by system matrix $A$, as well as the input matrix $B$. The second part pertains to the information flow topology and is represented by the sum of the Laplacian matrix $\mathcal{L}$, and the pinning matrix $\mathcal{P}$ by Definition 2.4. Lastly, the third part pertains to the decentralized controller and is represented by the controller gain matrix $k^T$.

### 3.3. Stability Analysis of Unidirectional Information Flow Topologies

In this section, a stability analysis of the vehicle platoon system for the linear and nonlinear controllers will be made. In Section 3.2, the tracking error of a linear controller is analyzed, and an overall closed-loop system matrix is derived in the case of a linear controller. $A_c$ matrix in (3.11) demonstrates that the stability of the vehicular platoon is closely related to the information flow topology. The first part of the $A_c$ matrix is the Kronecker product of the identity matrix and the system matrix of the nodes. Since the number of vehicles and state matrix of the vehicles is constant, this Kronecker product will also be constant during the platooning of the vehicles. The second part of $A_c$ is the Kronecker product of information flow matrix $\mathcal{L}_\mathcal{P}$ and matrix $Bk^T$ which consists of a time-invariant matrix $B$ and the controller gains.

$A_c$ matrix in (3.11) plays an essential role in the stability analysis of the vehicle platoon system with a linear controller. This matrix has similarities with the $\bar{A}$ matrix in (2.46) that has been studied for the nonlinear controller. Therefore, Lemma 2.2 is also applicable to the linear controller.

Hence, (3.10) for the lumped error state-space is asymptotically stable if and only if the real parts of the eigenvalues of $A - \lambda_i(\mathcal{L}_\mathcal{P})Bk^T$ matrix in Lemma 2.2 for $i = 1, 2, \ldots, N$ are negative. Furthermore, Zheng et al. [20] specified the stability conditions for the controller parameters as $k_1 > 0$, $k_2 > \frac{k_1\tau}{\lambda_i k_3 + 1}$, and $k_3 > -\frac{1}{\lambda_i}$.

Along with Section 2.5, this section shows information flow topology has a great influence on the stability of a vehicle platoon system whether the preferred decentralized controller is linear or nonlinear. Furthermore, examining $\bar{A}$ matrix associated with ISMC in (2.46) and the $A_c$ matrix associated with linear controller in (3.11) reveals that these matrices depend on the information flow topology $\mathcal{L}_\mathcal{P}$ as well as the longitudinal vehicle dynamics and the controller gains.

### 3.4. Performance Analysis of Unidirectional Information Flow Topologies

This section focuses on the performance analysis of the vehicle platoon system under different unidirectional information flow topologies. The aim is to find if there is a correlation between the information flow topology and the speed of the system response. To that end, changes in the location of the eigenvalues from one topology to the next will be put under scope.

The Laplacian matrix of a look-forward type of information topology is a lower triangular matrix since $l_{ij} = 0$ for $i < j$ , as it is stated in [46], i.e.,

$$\mathcal{L} = \begin{bmatrix} l_{11} & & & \\ l_{21} & l_{22} & \mathbf{0} & \\ \vdots & \vdots & \ddots & \\ l_{N1} & l_{N2} & \ldots & l_{NN} \end{bmatrix}. \tag{3.13}$$

The pinning matrix $\mathcal{P}$ is a diagonal matrix for all types of information flow topologies. Thus,

$$\mathcal{P} = \begin{bmatrix} p_{11} & & & \\ & p_{22} & \mathbf{0} & \\ & & \ddots & \\ & \mathbf{0} & & p_{NN} \end{bmatrix}. \tag{3.14}$$

As per Definition 2.4, the information flow matrix $\mathcal{L}_{\mathcal{P}} = \mathcal{L} + \mathcal{P}$ is a lower triangular matrix, where the main diagonal elements are the sum of the Laplacian and the pinning matrices' main diagonal elements:

$$\mathcal{L}_{\mathcal{P}} = \begin{bmatrix} l_{11}+p_{11} & & & \\ l_{21} & l_{22}+p_{22} & & \mathbf{0} \\ \vdots & \vdots & \ddots & \\ l_{N1} & l_{N2} & \dots & l_{NN}+p_{NN} \end{bmatrix}. \tag{3.15}$$

The determinant of a triangular matrix is the product of its main diagonal elements. Therefore, the eigenvalues of a triangular matrix are equal to the elements on the main diagonal [47]. Hence, the eigenvalues of the information flow matrix $\mathcal{L}_{\mathcal{P}}$ are the elements on the main diagonal which can be listed as

$$\sigma(\mathcal{L}_{\mathcal{P}}) = \{l_{11}+p_{11}, l_{22}+p_{22}, \dots, l_{NN}+p_{NN}\}. \tag{3.16}$$

The first main result of this thesis is stated in Theorem 3.1 below.

**Theorem 3.1.** *Let $\{\lambda_i(\mathcal{L}_{\mathcal{P}})\}_{i=1}^N$ denote the eigenvalues of $\mathcal{L}_{\mathcal{P}}$ for a unidirectional IFT under Assumption 2.2. Let $\{\lambda_i(\bar{\mathcal{L}}_{\mathcal{P}})\}_{i=1}^N$ denote the eigenvalues of $\bar{\mathcal{L}}_{\mathcal{P}}$ for an IFT with the addition of a new edge to the existing IFT. Then, all eigenvalues of $\mathcal{L}_{\mathcal{P}}$ and $\bar{\mathcal{L}}_{\mathcal{P}}$ coincide except for a single eigenvalue $i = i^*$ for which*

$$\lambda_{i^*}(\bar{\mathcal{L}}_{\mathcal{P}}) = \lambda_{i^*}(\mathcal{L}_{\mathcal{P}}) + 1. \tag{3.17}$$

*Proof.* The set of eigenvalues of a unidirectional IFT in (3.15) are given by (3.16). Suppose that a new unidirectional edge $(\alpha_i, \alpha_{i^*}) \notin E$, where $i^* \geq i+1$, is added to the existing edge set $E$ so that the new edge set is given by $\bar{E} = E + (\alpha_i, \alpha_{i^*})$. Let the set of eigenvalues of $\bar{\mathcal{L}}_{\mathcal{P}}$ be

$$\sigma(\bar{\mathcal{L}}_{\mathcal{P}}) = \{\bar{l}_{11}+\bar{p}_{11}, \bar{l}_{22}+\bar{p}_{22}, \dots, \bar{l}_{NN}+\bar{p}_{NN}\}. \tag{3.18}$$

Then,

$$\bar{l}_{ii} = l_{ii}, \tag{3.19}$$

$$\bar{p}_{ii} = p_{ii} \tag{3.20}$$

for each $i = 1, \ldots, N$ except for $i = i^*$ where

$$\bar{l}_{ii} = \begin{cases} l_{ii} & \text{if } i = 0, \\ l_{ii} + 1 & \text{if } i = 1, \ldots, N-1 \end{cases}, \quad \bar{p}_{ii} = \begin{cases} p_{ii} + 1 & \text{if } i = 0, \\ p_{ii} & \text{if } i = 1, \ldots, N-1 \end{cases}. \tag{3.21}$$

Therefore, for $i = i^*$

$$\begin{aligned} \bar{l}_{ii} + \bar{p}_{ii} &= \bar{l}_{i^*i^*} + \bar{p}_{i^*i^*} \\ &= l_{ii} + p_{ii} + 1 \\ &= l_{i^*i^*} + p_{i^*i^*} + 1. \end{aligned} \tag{3.22}$$

which implies (3.17). □

**Remark 3.1.** *Theorem 3.1 states that adding a unidirectional link does not decrease the eigenvalues of the new IFM and that at least one of the eigenvalues of the new IFM is strictly greater. By extending this argument, it can be concluded that adding further unidirectional links will increase the eigenvalues. Hence, it can be deduced that the largest eigenvalue of $\bar{\mathcal{L}}_{\mathcal{P}}$ cannot be smaller than that of $\mathcal{L}_{\mathcal{P}}$.*

In conclusion, the lumped error state-space in (3.16) reveals that when comparing two information flow topologies, the graph with a higher number of directed edges will have bigger eigenvalues numerically. Higher eigenvalues can be achieved in two ways: by increasing the number of followers that receive the leader information so that the pinning matrix has more ones on the main diagonal; or by transmitting $i^{th}$ vehicle's information to more of its followers like $(i+1), \ldots, N$, thereby increasing the sum of $a_{ij}$ for $j = 1, 2, \ldots, N$ for the $i^{th}$ vehicle.

All of the directed edges in the PF topology are present in the PF3 topology. Hence, PF topology is the subgraph of the PF3 topology. Table 3.1 shows that PF3 topology is formed by adding 2 more directed edges to the PF topology. These edges are coming from information transfer from the leader to the follower vehicles.

**Example 3.1.** *Find the eigenvalues for PF and PF3 information flow topologies illustrated in Figure 3.1 for a vehicle platoon system that has four followers.*

Table 3.1. Eigenvalues for PF and PF3 information flow topologies with $N = 4$ followers.

| **IFT** | **PF** | **PF3** |
|---|---|---|
| $\mathcal{L}$ | $\begin{bmatrix} 0 & 0 & 0 & 0 \\ -1 & 1 & 0 & 0 \\ 0 & -1 & 1 & 0 \\ 0 & 0 & -1 & 1 \end{bmatrix}$ | $\begin{bmatrix} 0 & 0 & 0 & 0 \\ -1 & 1 & 0 & 0 \\ 0 & -1 & 1 & 0 \\ 0 & 0 & -1 & 1 \end{bmatrix}$ |
| $\mathcal{P}$ | $\begin{bmatrix} 1 & 0 & 0 & 0 \\ 0 & 0 & 0 & 0 \\ 0 & 0 & 0 & 0 \\ 0 & 0 & 0 & 0 \end{bmatrix}$ | $\begin{bmatrix} 1 & 0 & 0 & 0 \\ 0 & 1 & 0 & 0 \\ 0 & 0 & 1 & 0 \\ 0 & 0 & 0 & 0 \end{bmatrix}$ |
| $\mathcal{L}_{\mathcal{P}}$ | $\begin{bmatrix} 1 & 0 & 0 & 0 \\ -1 & 1 & 0 & 0 \\ 0 & -1 & 1 & 0 \\ 0 & 0 & -1 & 1 \end{bmatrix}$ | $\begin{bmatrix} 1 & 0 & 0 & 0 \\ -1 & 2 & 0 & 0 \\ 0 & -1 & 2 & 0 \\ 0 & 0 & -1 & 1 \end{bmatrix}$ |
| $\sigma(\mathcal{L}_{\mathcal{P}})$ | $\{1, 1, 1, 1\}$ | $\{1, 1, 2, 2\}$ |
| $\max(\sigma(\mathcal{L}_{\mathcal{P}}))$ | 1 | 2 |
| $\min(\sigma(\mathcal{L}_{\mathcal{P}}))$ | 1 | 1 |

One of the pinning matrix main diagonal elements equals 1 in the PF topology while three of the pinning matrix main diagonal elements are equal to 1 in the PF3 topology. As a consequence, these additional 2 edges will increment 2 eigenvalues of the information flow matrix by 1.

## 3.5. Numerical Analysis

Information flow topologies in Figure 3.1 are simulated in the MATLAB environment with the linear controller design proposed by Zheng et al. [20]. In the simulations, the number of follower vehicles, $N$, is chosen as 7.

Table 3.2. Simulation parameters for the linear controller.

| **Description** | **Variable** | **Value** |
|---|---|---|
| Controller gain matrix | $\begin{bmatrix} k_1 & k_2 & k_3 \end{bmatrix}^T$ | $\begin{bmatrix} 1 & 2 & 1 \end{bmatrix}^T$ |
| Desired constant spacing | $d_{i-1,i}$ | 20 m |
| Inertial delay of vehicle dynamics | $\tau_i$ | 0.5 |
| Initial conditions of the leader | $\begin{bmatrix} p_0(0) & v_0(0) & a_0(0) \end{bmatrix}^T$ | $\begin{bmatrix} 0 & 20 & 0 \end{bmatrix}^T$ |
| Initial conditions of the followers | $\begin{bmatrix} p_i(0) & v_i(0) & a_i(0) \end{bmatrix}^T$ | $\begin{bmatrix} -i * d_{i-1,i} & 20 & 0 \end{bmatrix}^T$ |
| Sample time | $t_s$ | 0.01 s |

Here, the vehicular platoon is homogeneous meaning all the vehicles in the platoon have the same node dynamics. The system is initialized with zero tracking errors. Simulation parameters are shown in Table 3.2. In the simulations of the linear controller, the speed profile of the leading vehicle is taken as

$$v_0(t) = \begin{cases} 20\ m/s & t \leq 5\ s \\ 10 + 2t\ m/s & 5\ s < t \leq 10\ s \\ 30\ m/s & t > 10\ s \end{cases} \cdot \tag{3.23}$$

The nonlinear ISMC design proposed by Li et al. is used to simulate the information flow topologies in Figure 3.2 in the MATLAB environment [5]. The system is initialized as it is stated in Section 2.6. Simulation parameters are set according to the values provided in Table 2.1. Here the platoon is heterogeneous meaning that the vehicle parameters are not identical. Model types and parameters concerning these types are shown in Table 2.2. Moreover, the external time-varying disturbances are taken as mentioned in Chapter 2. All observer states are initialized at $x_{r,i}(t_0) = \begin{bmatrix} N \times d_{i-1,i} & 10 & 0 \end{bmatrix}^T$ while the initial states of the follower vehicles are $x_i(t_0) = \begin{bmatrix} (N-i) \times d_{i-1,i} & 10 & 0 \end{bmatrix}^T$ for $i = 1, \ldots, N = 7$.

Table 3.3. Eigenvalues of the information flow topologies in Figures 3.1 and 3.2.

| $\lambda_{\#}$ | **PF** | **PF2** | **PF3** | **PF4** | **PF5** | **PF6** | **PLF** |
|---|---|---|---|---|---|---|---|
| **1** | 1 | 1 | 1 | 1 | 1 | 1 | 1 |
| **2** | 1 | 1 | 1 | 1 | 1 | 1 | 2 |
| **3** | 1 | 1 | 1 | 1 | 1 | 2 | 2 |
| **4** | 1 | 1 | 1 | 1 | 2 | 2 | 2 |
| **5** | 1 | 1 | 1 | 2 | 2 | 2 | 2 |
| **6** | 1 | 1 | 2 | 2 | 2 | 2 | 2 |
| **7** | 1 | 2 | 2 | 2 | 2 | 2 | 2 |

The stability analysis of the vehicle platoon system is directly linked to the information flow topology. Equations (2.45) and (3.10) lend weight to the information flow matrix $\mathcal{L}_{\mathcal{P}}$. The type of controller used does not affect the information flow matrix. Hence, the stability analysis applies to either linear or nonlinear decentralized controller types. In relation to this, in Table 3.3 the eigenvalues for each tested topology can be seen. Table 3.3 shows the eigenvalues of different types of information flow matrix $\mathcal{L}_{\mathcal{P}}$ and it is independent of the decentralized controller type. Note that the velocity of the leader vehicle is constant at $8$ m/s.

PF topology in Figure 3.1 has $7$ directed edges while PF2 topology illustrated in the same figure has $8$ directed edges. Therefore, the amount of exchanged information in the PF2 topology is more than in the PF topology. It can be stated that eigenvalues for the information flow matrices for PF and PF2 topologies satisfy (3.17) in Theorem 3.1. All eigenvalues of $\mathcal{L}_{\mathcal{P}}$ for PF topology are ones ($\{\lambda_{PF_i}(\mathcal{L}_{\mathcal{P}})\}_{i=1}^{7} = 1$). For PF2 topology, there are $(N-1)$ one eigenvalues and one of the eigenvalues is $2$ ($\{\lambda_{PF2_i}(\mathcal{L}_{\mathcal{P}})\}_{i=1}^{6} = 1$, and $\lambda_{PF2_7}(\mathcal{L}_{\mathcal{P}}) = 2$). On that account, eigenvalues will have a mathematical relation as

$$\lambda_{PF2_7}(\mathcal{L}_{\mathcal{P}}) = \lambda_{PF_7}(\mathcal{L}_{\mathcal{P}}) + 1. \tag{3.24}$$

Note that the eigenvalues of the information flow matrix $\mathcal{L}_{\mathcal{P}}$ for all topologies listed in Table 3.3 are positive real numbers so $\sigma(\lambda_{\mathcal{L}_{\mathcal{P}}}) > 0$ condition in Lemma 2.1 is confirmed.

1: Start the time at $t_0 = 0$, the sampling time is $t_s$ and stop the time at $t_{end}$. So, vector of the simulation is found by $t = t_0 : t_s : t_{end}$
2: **for** $i = 1 : N$ **do**
3: Compute the difference between the actual vehicle state and the desired vehicle state as $\sigma_i(t) = |x_i(t) - x_0(t)|$.
4: Then, check if the difference is lower than a predefined tolerance threshold
5: **if** $\sigma_i(t) < tolerance$ **then**
6: $\delta_i(t) = 1$
7: **else**
8: $\delta_i(t) = 0$
9: **end if**
10: Find the locations of the rising edges, $r_i$, in the $\delta_i$ vector by $r_i = find(\delta_i(t) = 1)$
11: Find the index of the latest rising edge by $(index_i = r_i(end))$
12: Find the corresponding time for the $index_i$ in time vector, by $t_{settling_i} = t(index_i)$
13: **end for**=0

Figure 3.3. Settling time calculation algorithm.

Additionally, information about the overall performance of the vehicular platoon will be provided in this section. Unlike the stability analysis, the linear and nonlinear decentralized controller cases should be examined separately since they have different control laws.

To inspect the rate of convergence, the algorithm in Figure 3.3 is used to calculate the settling time in seconds for different vehicle platoon systems. The same algorithm is used for the linear and nonlinear controllers. In the vehicle platoon system with the linear controller, the leading vehicle changes its velocity in the $5$ seconds and the $10$ seconds after starting the simulation. Thus, settling time is expected to be more than $10$ seconds.

The velocity state of the followers is taken into account in calculations of the algorithm in Figure 3.3. Tables 3.4 and 3.5 show the results of the algorithm in seconds for linear and nonlinear controllers, respectively. The results in Tables 3.4 and 3.5 show that having access to the leader's information is crucial for faster system response.

Table 3.4. Settling time in seconds for the linear controller with $1\ \%$ speed tolerance under different information flow topologies in Figure 3.1.

| Vehicle No | PF | PF2 | PF3 | PF4 | PF5 | PF6 | PLF |
|---|---|---|---|---|---|---|---|
| **1** | 13.24 | 13.24 | 13.24 | 13.24 | 13.24 | 13.24 | 13.24 |
| **2** | 14.17 | 13.24 | 13.24 | 13.24 | 13.24 | 13.24 | 13.24 |
| **3** | 17.94 | 14.17 | 13.24 | 13.24 | 13.24 | 13.24 | 13.24 |
| **4** | 19.12 | 17.94 | 14.17 | 13.24 | 13.24 | 13.24 | 13.24 |
| **5** | 19.88 | 19.12 | 17.94 | 14.17 | 13.24 | 13.24 | 13.24 |
| **6** | 23.95 | 19.88 | 19.12 | 17.94 | 14.17 | 13.24 | 13.24 |
| **7** | 25.01 | 23.95 | 19.88 | 19.12 | 17.94 | 14.17 | 13.24 |

Table 3.5. Settling time in seconds for the nonlinear controller with $1\ \%$ speed tolerance under different information flow topologies in Figure 3.2.

| Vehicle No | PF | PF2 | PF3 | PF4 | PF5 | PF6 | PLF |
|---|---|---|---|---|---|---|---|
| **1** | 17.20 | 17.20 | 17.20 | 17.20 | 17.20 | 17.20 | 17.20 |
| **2** | 31.07 | 29.69 | 29.69 | 29.69 | 29.69 | 29.69 | 29.69 |
| **3** | 35.37 | 34.80 | 33.93 | 33.93 | 33.93 | 33.93 | 33.93 |
| **4** | 23.52 | 22.84 | 22.05 | 20.90 | 20.90 | 20.90 | 20.90 |
| **5** | 38.92 | 37.32 | 35.15 | 30.51 | 27.28 | 27.28 | 27.28 |
| **6** | 24.65 | 24.02 | 23.32 | 22.51 | 21.27 | 17.08 | 17.08 |
| **7** | 25.19 | 24.64 | 24.06 | 23.45 | 22.77 | 21.99 | 20.85 |

The settling time of a node reduces as soon as it receives the leader's information. The settling time also shortens if the neighbor of the node (includes the neighbors $j = 1, \ldots, i-1$ for the $i^{ith}$ node) receives the leader's information. Once a node receives the leader's information, the settling time for the node's velocity state will remain the same regardless of the other nodes' leader accessibility. For example, in the linear controller case, the settling time in the first row of Table 3.4 has remained constant at $13.24$ seconds.

Additionally, the settling time stays at $17.20$ seconds in the first row of Table 3.5. Therefore, it can be said that the settling behavior observed in the linear controller also applies to the nonlinear controller. The reason for this is that the first follower vehicle has access to the leader vehicle's information in every topology option in Figures 3.1 and 3.2. Additionally, in the linear controller, it has been seen that all vehicles reach the leader vehicle's speed within the same duration of $13.24$ seconds in the PLF topology.

Lastly, the space error between consecutive vehicles for unidirectional IFTs will be examined. Figure 3.4 belongs to the information topology with the smallest number of directed edges since the leader information is only accessible to the first follower.

Figure 3.5 plots the space error between consecutive vehicles for the PLF topology where all nodes have access to the leader information. In this topology, only the first follower has a spacing error other than zero. Consequently, the magnitude of space error in the PF topology ranges between $-3\ m$ and $4\ m$ approximately, see Figure 3.4 while in the PLF topology, it ranges between $-0.11\ m$ and $2.13\ m$ approximately, see Figure 3.5. In a vehicle platoon system with homogeneous vehicles that have identical vehicle dynamics, zero space error can be explained by the direct interaction with the leader and the zero initial errors.

Figures 3.6 and 3.7 pertain to the space error between adjacent vehicles in a vehicle platoon system with nonlinear decentralized controllers and heterogeneous vehicle dynamics. In the simulations, external time-varying disturbances, specific to each vehicle, are applied. Disturbances have a negative impact on the vehicle platoon system since they increase the risk of collision. For instance, Figure 3.7 demonstrates that the followers $2$ and $3$ (——) and the followers $4$ and $5$ (——) are cruising close to each other in the beginning. Nevertheless, with the hierarchical controller design proposed by Li et al. [5], the spacing error between consecutive vehicles converges to zero in approximately $55$ seconds.

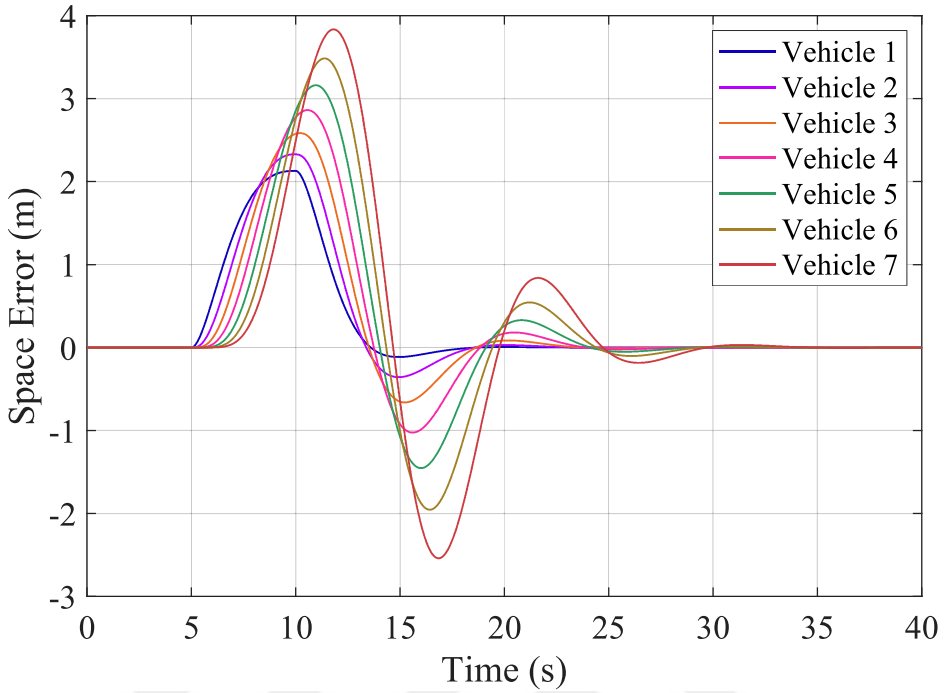


Figure 3.4. Space error with linear controller for unidirectional PF IFT in Figure 3.1.

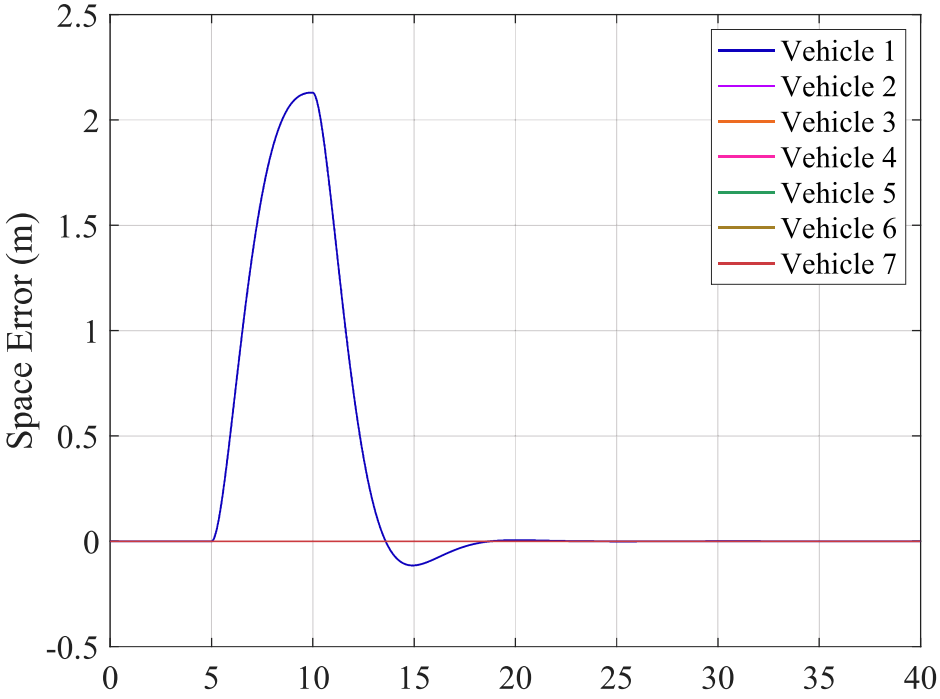


Figure 3.5. Space error with linear controller for unidirectional PLF IFT in Figure 3.1.

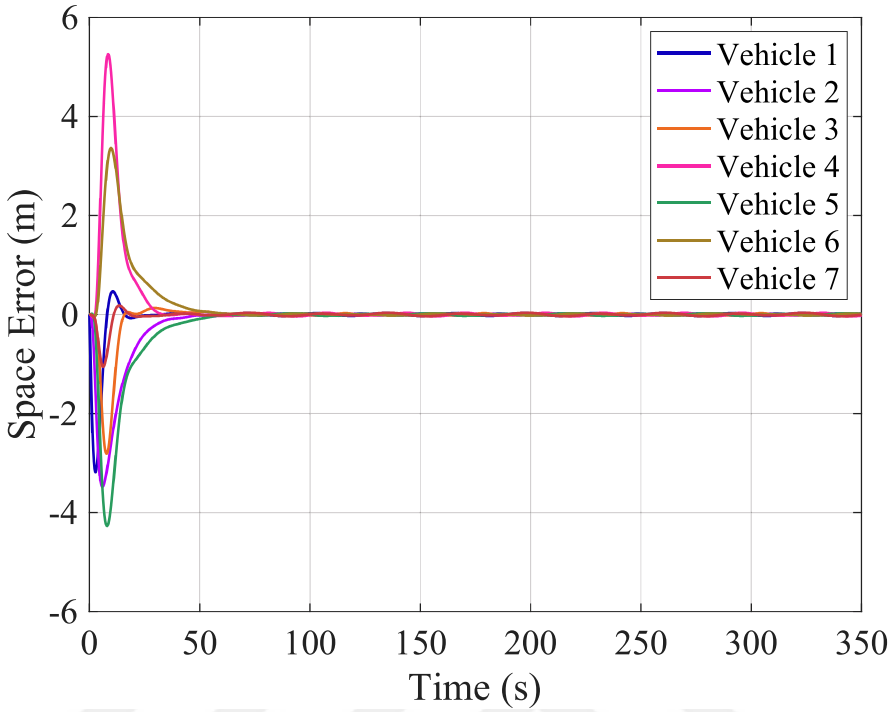


Figure 3.6. Space error with nonlinear controller for unidirectional PF IFT in Figure 3.2.

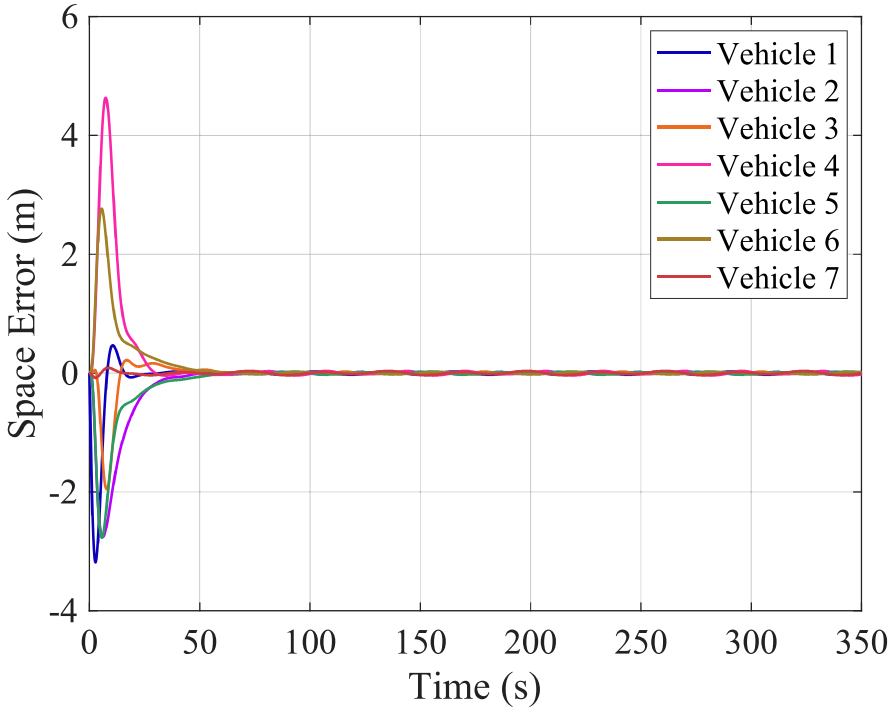


Figure 3.7. Space error with nonlinear controller for unidirectional PLF IFT in Figure 3.2.

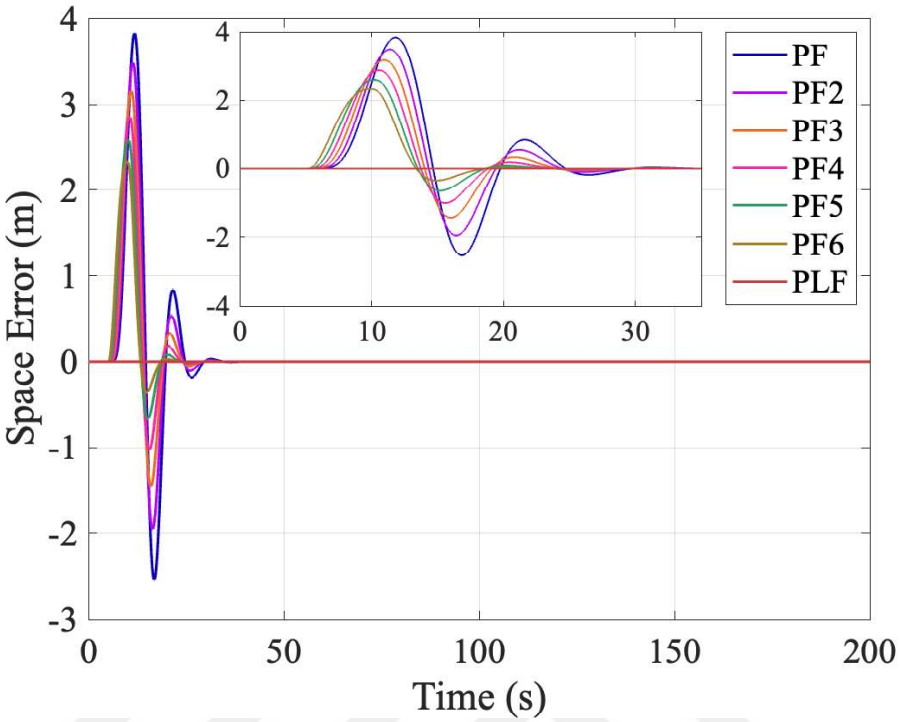


Figure 3.8. Space error for vehicle 7 with linear controller for unidirectional IFTs in Figure 3.1.

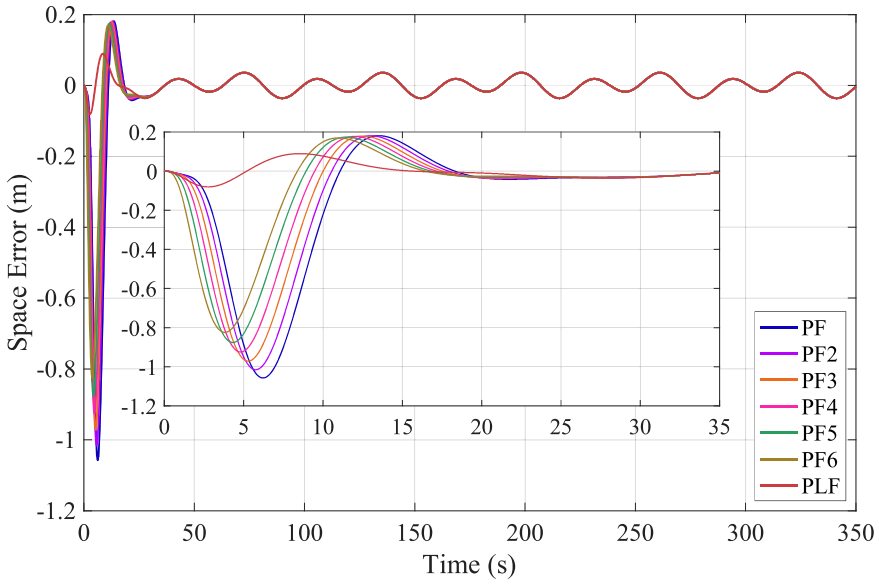


Figure 3.9. Space error for vehicle 7 with nonlinear controller for unidirectional IFTs in Figure 3.2.

Figure 3.8 shows the space error of the $7^{th}$ follower from PF topology to PLF topology for linear controller case. As number of the directed edges increases the space error converges to zero faster. It is evident that adding a direct link to the leading vehicle has significantly reduced the magnitude of the space error.

Moreover, Figure 3.9 shows space error of the $7^{th}$ follower under topologies in Figure 3.2 for the ISMC case. The results from Figure 3.9 support the conclusions derived from Figure 3.8. Once, vehicle 7 receives the leader state information, the magnitude of its tracking error notably decreases.

## 3.6. Summary of the Chapter

This chapter introduces various unidirectional information topologies to explore the behavior of the vehicle platoon system under different information structures. Both homogeneous linearly controlled and heterogeneous nonlinearly controlled vehicle platoon systems are examined. The simulation outcomes align with Lemma 2.1 in Chapter 2 and Theorem 3.1 indicating that the system exhibits quicker response time with an expanded information network. As the next step of the study, bidirectional information flow topologies will be investigated in Chapter 4.

# 4. ANALYSIS OF BIDIRECTIONAL TOPOLOGIES

In this chapter, similar concepts to Chapter 3 will be discussed but this time the analysis will be conducted for bidirectional information flow topologies. Node dynamics, linear and nonlinear decentralized controller laws, and formation geometry, which depend on the constant spacing policy, are already explained exhaustively in the previous chapter. As a matter of course, this chapter will focus on the differences that arise due to the bidirectional topology in terms of matrix properties and how these differences impact the stability and performance of the vehicle platoon system.

## 4.1. Bidirectional Information Topologies

Figure 4.1 displays different bidirectional information topologies for a vehicle platoon system. As is the case with unidirectional information topologies, bidirectional information topologies are also named according to the number of nodes that receive the leader vehicle information. Bidirectional information topologies, as shown in Figure 4.1, can be described as below:

- Bidirectional (BD): In the BD topology, each vehicle communicates with its adjacent vehicle by simultaneously transmitting and receiving information.
- Bidirectional 2 (BD2): In the BD2 topology, each vehicle communicates with its adjacent vehicle by transmitting and receiving information, and the leader information is available for the leader's neighbor and its neighbor's neighbor. Therefore, two vehicles are receiving direct information from the leading vehicle.
- Bidirectional 3 (BD3): In the BD3 topology, each vehicle communicates with its adjacent vehicle by transmitting and receiving information, and the leader information is available for the leader's neighbor and two vehicles that are following the leader's neighbor. Therefore, three vehicles are receiving direct information from the leading vehicle.

- Bidirectional 4 (BD4): In the BD4 topology, each vehicle communicates with its adjacent vehicle by transmitting and receiving information and the leader information is available for the leader's neighbor and three vehicles that are following the leader's neighbor. Therefore, four vehicles are receiving direct information from the leading vehicle.
- Bidirectional 5 (BD5): In the BD5 topology, each vehicle communicates with its adjacent vehicle by transmitting and receiving information, and the leader information is available for the leader's neighbor and four vehicles that are following the leader's neighbor. Therefore, five vehicles are receiving direct information from the leading vehicle.
- Bidirectional 6 (BD6): In the BD6 topology, each vehicle communicates with its adjacent vehicle by transmitting and receiving information, and the leader information is available for the leader's neighbor and five vehicles that are following the leader's neighbor. Therefore, six vehicles are receiving direct information from the leading vehicle.
- Bidirectional-Leader (BDL): In the BDL topology, each vehicle communicates with its adjacent vehicle by transmitting and receiving information, and the leader information is available to all the vehicles in the vehicular platoon.

Figure 4.2 illustrates bidirectional information topologies for a heterogeneous vehicle platoon system. The leading vehicle, represented by an orange circle, operates according to its distinct vehicle dynamics as in Figure 4.2. Followers $2$, $3$, and $5$, represented by a green circle, have indistinguishable vehicle dynamics, whereas followers $1$, $4$, $6$, and $7$, represented by a purple circle, have the same vehicle dynamics.

## 4.2. Stability Analysis of Bidirectional Information Flow Topologies

Stability analysis of the vehicular platoon is directly connected to the information flow topology. As discussed in Section 3.3, Lemma 2.1 which states $Re(\lambda_i(\mathcal{L}_{\mathcal{P}})) > 0$ must be satisfied for a stable vehicle platoon system.

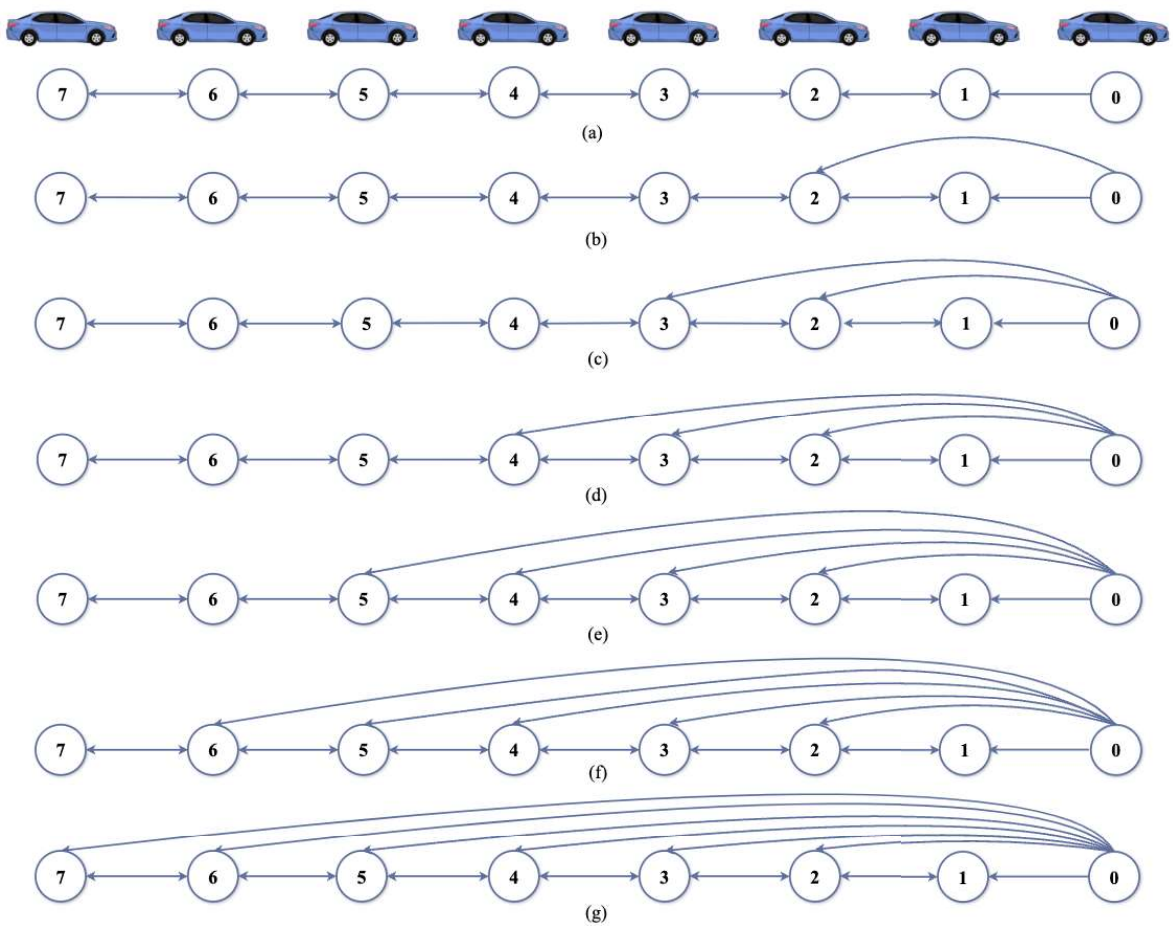


Figure 4.1. Bidirectional IFTs for homogeneous vehicular platoons (a) BD, (b) BD2, (c) BD3, (d) BD4, (e) BD5, (f) BD6, (g) BDL.

This requirement is mandatory for both unidirectional and bidirectional information flow topologies. Furthermore, it does not depend on the control law implementation as the structure of $\bar{A}$ in (2.46) and $A_c$ in (3.11) are alike.

### 4.3. Performance Analysis of Bidirectional Information Flow Topologies

The Laplacian matrix $\mathcal{L}$ of a look-forward and look-backward type information topology is a symmetric matrix since $l_{ij} = l_{ji}$ for $i, j \in \mathbb{Z}^+$.

$\mathcal{L}$ can be expressed as

$$\mathcal{L} = \begin{bmatrix} l_{11} & l_{12} & \dots & l_{1N} \\ l_{12} & l_{22} & \dots & l_{2N} \\ \vdots & \vdots & \ddots & \vdots \\ l_{1N} & l_{2N} & \dots & l_{NN} \end{bmatrix}. \tag{4.1}$$

The pinning matrix $\mathcal{P}$ is a diagonal matrix whose form is as in (3.14). As per Definition 2.4, the information flow matrix is a symmetric matrix, where the main diagonal elements are the sum of the Laplacian and the pinning matrices' main diagonal elements.

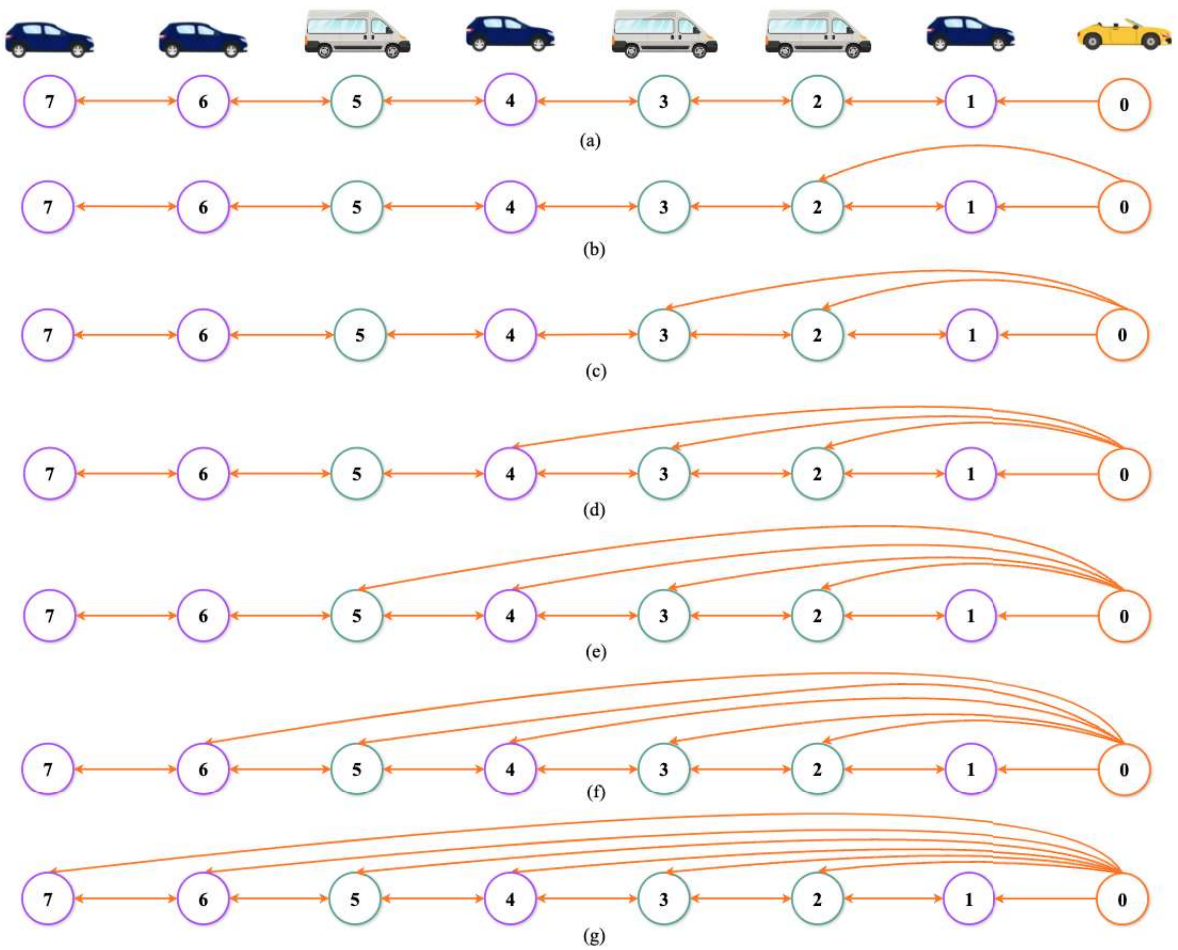


Figure 4.2. Bidirectional IFTs for heterogeneous vehicular platoons (a) BD, (b) BD2, (c) BD3, (d) BD4, (e) BD5, (f) BD6, (g) BDL.

$\mathcal{L}_{\mathcal{P}}$ can be represented as

$$\mathcal{L}_{\mathcal{P}} = \begin{bmatrix} l_{11}+p_1 & l_{12} & \dots & l_{1N} \\ l_{12} & l_{22}+p_2 & \dots & l_{2N} \\ \vdots & \vdots & \ddots & \vdots \\ l_{1N} & l_{2N} & \dots & l_{NN}+p_N \end{bmatrix}. \tag{4.2}$$

A real symmetric matrix is a Hermitian matrix that is defined as a matrix that is equal to its conjugate transpose. If $A$ and $B$ matrices are Hermitian, $(aA + bB)$ is also Hermitian for any real $a$ and $b$ scalars [48]. Therefore, the Laplacian matrix in (4.1) and the pinning matrix in (3.14) are Hermitian matrices. Thus, the information flow matrix $\mathcal{L}_{\mathcal{P}}$ is Hermitian so it has real eigenvalues [48]. To discuss eigenvalues of $\mathcal{L}_{\mathcal{P}}$ further, firstly Lemma 4.1 will be inspected.

**Lemma 4.1** (Weyl's Inequality [48])**.** *Suppose that $A, B \in \mathbb{R}^{n\times n}$ are Hermitian matrices. Let the eigenvalues of $A$ be $\{\lambda_i(A)\}_{i=1}^n$, the eigenvalues of $B$ be $\{\lambda_i(B)\}_{i=1}^n$, and the eigenvalues of $A+B$ be $\{\lambda_i(A+B)\}_{i=1}^n$ in algebraically nondecreasing order. Then,*

$$\lambda_i(A+B) \leq \lambda_{i+j}(A) + \lambda_{n-j}(B) \tag{4.3}$$

*where $i = 1, \dots, n$ and $j = 0, 1, \dots, n-i$, with equality for some pair $i, j$ if and only if there is a nonzero vector $x$ so that $Ax = \lambda_{i+j}(A)x$, $Bx = \lambda_{n-j}(B)x$, and $(A+B)x = \lambda_i(A+B)x$. In addition,*

$$\lambda_{i-j+1}(A) + \lambda_j(B) \leq \lambda_i(A+B) \tag{4.4}$$

*where $i = 1, \dots, n$ and $j = 1, \dots, i$, with equality for some pair $i, j$ if and only if there is a nonzero vector $x$ so that $Ax = \lambda_{i-j+1}(A)x$, $Bx = \lambda_j(B)x$, and $(A+B)x = \lambda_i(A+B)x$. If $A$ and $B$ have no common eigenvector, then every inequality in (4.3) and (4.4) is a strict inequality.*

Weyl's inequalities in Lemma 4.1 explain how the eigenvalues change if a Hermitian matrix $A$ is added up with a Hermitian matrix $B$. This concept will be helpful in the interpretation of the system behavior to the modifications in the information topology for bidirectional topologies.

The second main result of this thesis is stated in Lemma 4.2 below.

**Lemma 4.2.** *Let* $\{\lambda_i(L_P)\}_{i=1}^N$ *denote the eigenvalues of* $\mathcal{L}_\mathcal{P}$ *in algebraically nondecreasing order for a bidirectional IFT under Assumption 2.2. Let* $\{\lambda_i(\bar{L}_P)\}_{i=1}^N$ *denote the eigenvalues of* $\bar{\mathcal{L}}_\mathcal{P}$ *in algebraically nondecreasing order for an IFT with the addition of a new edge to the existing IFT. Then,*

$$\lambda_1(\mathcal{L}_\mathcal{P}) \leq \lambda_1(\bar{\mathcal{L}}_\mathcal{P}) \leq \lambda_2(\mathcal{L}_\mathcal{P}) \leq \lambda_2(\bar{\mathcal{L}}_\mathcal{P}) \leq \cdots \leq \lambda_N(\mathcal{L}_\mathcal{P}) \leq \lambda_N(\bar{\mathcal{L}}_\mathcal{P}). \tag{4.5}$$

*Proof.* Let $\mathcal{L}_\mathcal{P}$ and $\bar{\mathcal{L}}_\mathcal{P}$ be the information flow matrices for the directed graphs $\mathcal{G} = (V, E)$ and $\bar{\mathcal{G}} = (\bar{V}, \bar{E})$, respectively where $\bar{\mathcal{G}}$ is obtained by adding a new edge $e$ to $\mathcal{G}$, i.e., $\bar{E} = E + e$ where $e \in \bar{E}$ and $e \notin E$. Let $\{\lambda_i(\delta\mathcal{L}_\mathcal{P})\}_{i=1}^N$ denote the eigenvalues of $\delta\mathcal{L}_\mathcal{P}$ in algebraically nondecreasing order where

$$\delta\mathcal{L}_\mathcal{P} = \bar{\mathcal{L}}_\mathcal{P} - \mathcal{L}_\mathcal{P}. \tag{4.6}$$

There are two cases to consider: Case $(i)$ $e$ is coming from the leading vehicle and case $(ii)$ $e$ is not coming from the leading vehicle. Each case is analyzed separately below.

Case $(i)$ ($e = (\alpha_i, \alpha_j)$, $i = 0$ ). The addition of $e = (\alpha_0, \alpha_i)$ will change the information flow matrix by $\delta\mathcal{L}_\mathcal{P}$ whose elements are zero except from the $\delta\mathcal{L}_\mathcal{P}(i,i)$ which is 1. Hence, $\delta\mathcal{L}_\mathcal{P}$ is a diagonal matrix. The characteristic polynomial of $\delta\mathcal{L}_\mathcal{P}$ is given by

$$\det(\lambda I - \delta\mathcal{L}_\mathcal{P}) = \lambda^{N-1}(\lambda - 1), \tag{4.7}$$

which leads to $(N-1)$ eigenvalues at 0 and one eigenvalue at 1.

Case $(ii)$ ($e = (\alpha_i, \alpha_j)$, $i \neq 0$ ). The addition of $e = (\alpha_i, \alpha_j)$ will change the information flow matrix by $\delta\mathcal{L}_\mathcal{P}$ whose nonzero elements are $\delta\mathcal{L}_\mathcal{P}(i,j) = \delta\mathcal{L}_\mathcal{P}(j,i) = -1$ and $\delta\mathcal{L}_\mathcal{P}(i,i) = \delta\mathcal{L}_\mathcal{P}(j,j) = 1$ for $i = 1, \ldots, N-1$ and $j > i+1$. Hence, $\delta\mathcal{L}_\mathcal{P}$ is a symmetric real matrix. The characteristic polynomial of $\delta\mathcal{L}_\mathcal{P}$ is given by

$$\det(\lambda I - \delta\mathcal{L}_\mathcal{P}) = \lambda^{N-1}(\lambda - 2), \tag{4.8}$$

which leads to $(N-1)$ eigenvalues at 0 and one eigenvalue at 2.

Applying Lemma 4.1 with $A = \mathcal{L}_\mathcal{P}$, $B = \delta\mathcal{L}_\mathcal{P}$ and $A + B = \bar{\mathcal{L}}_\mathcal{P}$, (4.3) becomes

$$\lambda_1(\bar{\mathcal{L}}_\mathcal{P}) \leq \lambda_2(\mathcal{L}_\mathcal{P}) + \lambda_{N-1}(\delta\mathcal{L}_P) \quad \text{for } i = 1\,, j = 1. \tag{4.9}$$

Since $\lambda_{N-1}(\delta\mathcal{L}_P)$ is found as $0$ in both (4.8) and (4.7), (4.9) can be expressed as

$$\lambda_1(\bar{\mathcal{L}}_{\mathcal{P}}) \leq \lambda_2(\mathcal{L}_{\mathcal{P}}). \tag{4.10}$$

Furthermore, for $i = 1$ and $j = 1$, (4.4) leads to

$$\lambda_1(\mathcal{L}_{\mathcal{P}}) + \lambda_1(\delta\mathcal{L}_P) \leq \lambda_1(\bar{\mathcal{L}}_{\mathcal{P}}). \tag{4.11}$$

Since $\lambda_1(\delta\mathcal{L}_P) = 0$ in both (4.8) and (4.7), (4.11) can be expressed as

$$\lambda_1(\mathcal{L}_{\mathcal{P}}) \leq \lambda_1(\bar{\mathcal{L}}_{\mathcal{P}}). \tag{4.12}$$

Combining (4.10) and (4.12) gives

$$\lambda_1(\mathcal{L}_{\mathcal{P}}) \leq \lambda_1(\bar{\mathcal{L}}_{\mathcal{P}}) \leq \lambda_2(\mathcal{L}_{\mathcal{P}}). \tag{4.13}$$

The above procedure can be repeated using (4.3) for $i = 2, \ldots, N-1$ and $j = 1$. Equation (4.4) should be calculated for $i = 2, \ldots, N$ and $j = 1$ in order to find the result in (4.5). □

In the next result, it is demonstrated that the first eigenvalue of $\mathcal{L}_{\mathcal{P}}$ is strictly less than that of $\bar{\mathcal{L}}_{\mathcal{P}}$.

**Corollary 4.1.**

$$\lambda_1(\mathcal{L}_{\mathcal{P}}) < \lambda_1(\bar{\mathcal{L}}_{\mathcal{P}}). \tag{4.14}$$

*Proof.* From Lemma 4.2 it follows that $\lambda_1(\mathcal{L}_{\mathcal{P}}) \leq \lambda_1(\bar{\mathcal{L}}_{\mathcal{P}})$. Furthermore, the inequality is strict if $A = \mathcal{L}_P$ and $B = \delta\mathcal{L}_P$ have no common eigenvector as it is stated in Lemma 4.1.

Note that $\lambda_1(\delta\mathcal{L}_P) = 0$ in both (4.8) and (4.7) so that $(\delta\mathcal{L}_P)\nu = \lambda_1(\delta\mathcal{L}_P)\nu = 0$ for $i = j = 1$ from Lemma 4.1. Suppose that edge $e = (\alpha_i, \alpha_j)$ is added.

The $N-2$ normalized eigenvectors of $\delta\mathcal{L}_P$ are $N-2$ of the vectors from the following set, with 1s neither in the $i^{th}$ nor in the $j^{th}$ location,

$$\left\{ \begin{bmatrix} 1 \\ 0 \\ 0 \\ \vdots \\ 0 \end{bmatrix}, \begin{bmatrix} 0 \\ 1 \\ 0 \\ \vdots \\ 0 \end{bmatrix}, \ldots, \begin{bmatrix} 0 \\ 0 \\ 0 \\ \vdots \\ 1 \end{bmatrix} \right\}. \tag{4.15}$$

An $(N-1)^{th}$ eigenvector $\nu_{N-1} \in \mathbb{R}^N$ consists all zeros except for the 1s in the $i^{th}$ and $j^{th}$ locations whereas $N^{th}$ eigenvector $\nu_N \in \mathbb{R}^N$ can be constructed as all zeros except for 1 in the $i^{th}$ location and $-1$ in the $j^{th}$ location.

It is known from (4.7) and (4.8) that $N-1$ eigenvalues of $\lambda_1(B)$ are equal to zero. Thus, $N-1$ eigenvectors corresponding to this eigenvalue will be considered. Next, it will be shown that $\nu_1, \nu_2, \ldots, \nu_{N-1}$ are not eigenvectors of $\mathcal{L}_P$ by contradiction. Let $\mathcal{L}_\mathcal{P}$, $\delta\mathcal{L}_\mathcal{P}$ and $\bar{\mathcal{L}}_\mathcal{P}$ be denoted by $A$, $B$ and $(A+B)$, respectively for the sake of simplicity. Suppose $\nu_i$ is an eigenvector of $A$, such that $A\nu_i = \lambda_i(A)\nu_i$ for each $i = 1, \ldots, N$. From Weyl's inequalities, for $i = j = 1$, it is possible that

$$Ax = \lambda_1(A)x \tag{4.16}$$

$$Bx = \lambda_1(B)x \tag{4.17}$$

$$(A+B)x = \lambda_1(A+B)x. \tag{4.18}$$

Note that $\lambda_1(B) = 0$, i.e., $Bx = 0$ so that $x$ shall be one of the eigenvectors associated with 0 eigenvalue. In addition, from Lemma 2.1, it is known that $\lambda_1(A) > 0$. Considering (4.15), the product $\lambda_1(A)x$ picks the $i^{th}$ column of the matrix $A$ for $x = \nu_i$ for $i = 1, 2, \ldots, N-2$. As a result, for $x = \nu_i$ where $i = 1, 2, \ldots, N-2$, $Ax$ is not a multiple of $x$. This is because each vehicle in the platoon system exchanges information with another vehicle based on the spanning tree assumption, i.e., the BD topology in Figure 4.1. Consequently, there will be a nonzero entry in at least one off-diagonal element of the IFM, which is denoted as $A$.

For the remaining and the $(N-1)^{st}$ eigenvector which corresponds to $0$ eigenvalue, $Ax$ for $x = \nu_i$ for $i = N-1$ can be expressed as

$$\begin{aligned} Ax &= \begin{bmatrix} a_{11} & a_{12} & \dots & a_{1N} \\ a_{21} & a_{22} & \dots & a_{2N} \\ \vdots & \vdots & \ddots & \vdots \\ a_{N1} & a_{N1} & \dots & a_{NN} \end{bmatrix} \begin{bmatrix} x_1 \\ x_2 \\ \vdots \\ x_N \end{bmatrix} \\ &= \begin{bmatrix} \sum_{k=1}^{N} a_{1k}x_k \\ \sum_{k=1}^{N} a_{2k}x_k \\ \vdots \\ \sum_{k=1}^{N} a_{Nk}x_k \end{bmatrix} \end{aligned} \tag{4.19}$$

where $A = [a_{ij}] \in \mathbb{R}^{N \times N}$ and $x = [x_i] \in R^N$ which have 1s in the $i^{th}$ and $j^{th}$ locations. Therefore, $l^{th}$ row of the $Ax$ will be $(a_{li} + a_{lj})$ for $j = 1, \dots, N$. In the case of $l \neq i$ and $l \neq j$, $Ax$ can be a multiple of $x$ if both

$$a_{li} + a_{lj} = 0, \tag{4.20}$$

and,

$$a_{ii} + a_{ij} = a_{ji} + a_{jj} \tag{4.21}$$

are satisfied. Since $A$ is a symmetric matrix for a bidirectional IFT, $a_{ij} = a_{ji}$. Hence, (4.21) becomes

$$a_{ii} = a_{jj}. \tag{4.22}$$

Suppose (4.22) is satisfied, then (4.20) should also be fulfilled for $Ax$ to be a multiple of $x$. In this case, both $a_{li}$ and $a_{lj}$ should be $0$ or $a_{li} = -a_{lj}$ for all values of $l$ except from $i$ and $j$. $a_{li}$ cannot be equal to $-a_{lj}$ since both elements are off-diagonal elements due to $l \neq i$ and $l \neq j$ conditions. Therefore, $a_{li} \leq 0$ and $a_{lj} \leq 0$. In addition, in the case of both $a_{li}$ and $a_{lj}$ are being $0$, there are no directional edges from $l$ to $i$ and $j$ for $l = 1, \dots, N$, $l \neq i$ and $l \neq j$. This cannot be satisfied since it is a contradiction to the spanning tree assumption. $\square$

**Remark 4.1.** *Based upon Corollary 4.1, minimum eigenvalue of the $\mathcal{L}_{\mathcal{P}}$ is smaller than the minimum eigenvalue of $\bar{\mathcal{L}}_{\mathcal{P}}$ so that the vehicle platoon system response with $\bar{\mathcal{L}}_{\mathcal{P}}$ converges faster than that of the vehicle platoon system response with $\mathcal{L}_{\mathcal{P}}$.*

**Lemma 4.3.** *Let $\{\lambda_i(\mathcal{L}_{\mathcal{P}})\}_{i=1}^{N}$ denote the eigenvalues of $\mathcal{L}_{\mathcal{P}}$ in algebraically nondecreasing order for a bidirectional IFT under Assumption 2.2. Let $\{\lambda_i(\tilde{\mathcal{L}}_{\mathcal{P}})\}_{i=1}^{N}$ denote the eigenvalues of $\tilde{\mathcal{L}}_{\mathcal{P}}$ in algebraically nondecreasing order for an IFT with the addition of one or more edges to the existing IFT. Then,*

$$\lambda_1(\mathcal{L}_{\mathcal{P}}) < \lambda_1(\tilde{\mathcal{L}}_{\mathcal{P}}) \tag{4.23}$$

$$\lambda_i(\mathcal{L}_{\mathcal{P}}) \leq \lambda_i(\tilde{\mathcal{L}}_{\mathcal{P}}) \quad for\ i = 2, \ldots, N. \tag{4.24}$$

*Proof.* Equation (4.23) follows from (4.14) in Corollary 4.14. The upcoming part of the proof deals with (4.24). Adding multiple edges is equivalent to iterating the process in Lemma 4.2 which results in (4.23). Let $\mathcal{L}_{\mathcal{P}}$, $\bar{\mathcal{L}}_{\mathcal{P}}$ and $\tilde{\mathcal{L}}_{\mathcal{P}}$ be the information flow matrices for the directed graphs $\mathcal{G} = (V, E)$, $\bar{\mathcal{G}} = (\bar{V}, \bar{E})$ and $\tilde{\mathcal{G}} = (\tilde{V}, \tilde{E})$, respectively where $\bar{\mathcal{G}}$ is obtained by adding a new edge $e$ to $\mathcal{G}$, i.e., $\bar{E} = E + e$ where $e \in \bar{E}$, $e \in \tilde{E}$, $e \notin E$ and $\tilde{\mathcal{G}}$ is obtained by adding a new edge $f$ to $\bar{\mathcal{G}}$, i.e., $\tilde{E} = \bar{E} + f$ where $f \in \tilde{E}$, $f \notin E$, $f \notin \bar{E}$. Then, for $i = j = 1$, (4.13) can be expressed as

$$\lambda_1(\mathcal{L}_{\mathcal{P}}) \leq \lambda_1(\bar{\mathcal{L}}_{\mathcal{P}}) \leq \lambda_2(\mathcal{L}_{\mathcal{P}}) \leq \lambda_2(\bar{\mathcal{L}}_{\mathcal{P}}) \tag{4.25}$$

$$\lambda_1(\bar{\mathcal{L}}_{\mathcal{P}}) \leq \lambda_1(\tilde{\mathcal{L}}_{\mathcal{P}}) \leq \lambda_2(\bar{\mathcal{L}}_{\mathcal{P}}) \leq \lambda_2(\tilde{\mathcal{L}}_{\mathcal{P}}). \tag{4.26}$$

So that

$$\lambda_1(\mathcal{L}_{\mathcal{P}}) \leq \lambda_1(\bar{\mathcal{L}}_{\mathcal{P}}) \leq \lambda_1(\tilde{\mathcal{L}}_{\mathcal{P}}) \leq \lambda_2(\mathcal{L}_{\mathcal{P}}) \leq \lambda_2(\bar{\mathcal{L}}_{\mathcal{P}}) \leq \lambda_2(\tilde{\mathcal{L}}_{\mathcal{P}}). \tag{4.27}$$

The above procedure can be repeated using (4.3) for $i = 2, \ldots, N-1$ and $j = 1$; and using (4.4) for $i = 2, \ldots, N$ and $j = 1$ in order to arrive at the result in (4.24). □

**Example 4.1.** *Find the eigenvalues for BD and BD3 information flow topologies illustrated in Figure 4.1 for a vehicle platoon system that has four followers.*

Table 4.1 displays that the minimum eigenvalue of the information flow matrix $\mathcal{L}_{\mathcal{P}}$ is lower for the BD topology than it is for the BD3 topology. The difference between these topologies is the additional 2 directed edges from the leader to the two distinct followers.

Table 4.1. Eigenvalues for look-forward and look-backward information flow topologies with $N = 4$ followers.

| **IFT** | **BD** | **BD3** |
|---|---|---|
| $\mathcal{L}$ | $\begin{bmatrix} 1 & -1 & 0 & 0 \\ -1 & 2 & -1 & 0 \\ 0 & -1 & 2 & -1 \\ 0 & 0 & -1 & 1 \end{bmatrix}$ | $\begin{bmatrix} 1 & -1 & 0 & 0 \\ -1 & 2 & -1 & 0 \\ 0 & -1 & 2 & -1 \\ 0 & 0 & -1 & 1 \end{bmatrix}$ |
| $\mathcal{P}$ | $\begin{bmatrix} 1 & 0 & 0 & 0 \\ 0 & 0 & 0 & 0 \\ 0 & 0 & 0 & 0 \\ 0 & 0 & 0 & 0 \end{bmatrix}$ | $\begin{bmatrix} 1 & 0 & 0 & 0 \\ 0 & 1 & 0 & 0 \\ 0 & 0 & 1 & 0 \\ 0 & 0 & 0 & 0 \end{bmatrix}$ |
| $\mathcal{L}_{\mathcal{P}}$ | $\begin{bmatrix} 2 & -1 & 0 & 0 \\ -1 & 2 & -1 & 0 \\ 0 & -1 & 2 & -1 \\ 0 & 0 & -1 & 1 \end{bmatrix}$ | $\begin{bmatrix} 2 & -1 & 0 & 0 \\ -1 & 3 & -1 & 0 \\ 0 & -1 & 3 & -1 \\ 0 & 0 & -1 & 1 \end{bmatrix}$ |
| $\sigma(\mathcal{L}_{\mathcal{P}})$ | $\{0.12, 1.00, 2.35, 3.53\}$ | $\{0.49, 1.32, 2.83, 4.36\}$ |
| $\min(\sigma(\mathcal{L}_{\mathcal{P}}))$ | 0.12 | 0.49 |
| $\max(\sigma(\mathcal{L}_{\mathcal{P}}))$ | 3.53 | 4.36 |

This increase in the number of directed edges will increment two of the main diagonal elements in the information flow matrix $\mathcal{L}_{\mathcal{P}}$. Additional edges will increase the information flow matrix by $\delta\mathcal{P}$ that can be written as

$$\delta\mathcal{P} = \begin{bmatrix} 0 & 0 & 0 & 0 \\ 0 & 1 & 0 & 0 \\ 0 & 0 & 1 & 0 \\ 0 & 0 & 0 & 0 \end{bmatrix}. \tag{4.28}$$

There is a relationship between the $\sigma(\mathcal{L}_{\mathcal{P}})$ for the BD topology, colored in pink, and the BD3 topology, colored in gray, can be expressed as

$$0.12 < 0.49 < 1.00 < 1.32 < 2.35 < 2.83 < 3.53 < 4.36.$$

To put a finer point on it, the information flow matrix $\mathcal{L}_{\mathcal{P}}$ eigenvalues for the BD topology interlaces with the BD3 topology's eigenvalues. The BD3 topology will have a faster system response since it has a higher minimum eigenvalue.

Equations (2.45) and (3.10) attest that the vehicle platoon system performance cannot be dissociated from the information flow topology. Information flow topologies with smaller eigenvalues of $\mathcal{L}_{\mathcal{P}}$ will adversely affect the tracking error [22].

## 4.4. Numerical Analysis

This section provides the simulation results obtained from running experiments in the MATLAB/Simulink environment. For the linearly controlled vehicle platoon system, dynamics in (3.10) is implemented. In the case of the vehicular platoon with the nonlinear decentralized controller, (2.45) is used to model the system. In order to observe the impact of changes in the information flow topology, the simulation parameters are kept constant, as detailed in Chapter 2 and Chapter 3.

The eigenvalues of the bidirectional information flow topology matrix are examined to assess their impact on stability. This matrix illustrates the information exchange between followers and the direct pinning to the leading vehicle.

Table 4.2 displays the eigenvalues of $\mathcal{L}_{\mathcal{P}}$ with changing bidirectional information flow topologies. It is clear that Lemma 4.2 is satisfied since the edge addition to any topology generates a new topology whose eigenvalues have a relation as in (4.13).

To give an example, in bidirectional information flow topologies shown in Figure 4.1 and Figure 4.2, for BD2 and BD4 topologies, the eigenvalue relation of the information flow matrix becomes

$$\lambda_{BD2_1} < \lambda_{BD4_1} < \lambda_{BD2_2} < \lambda_{BD4_2} < \cdots < \lambda_{BD2_7} < \lambda_{BD4_7}.$$

Table 4.2. Eigenvalues for different information flow topologies in Figures 4.1 and 4.2 .

| $\lambda_{\#}$ | **BD** | **BD2** | **BD3** | **BD4** | **BD5** | **BD6** | **BDL** |
|---|---|---|---|---|---|---|---|
| **1** | 0.0437 | 0.0644 | 0.0929 | 0.1428 | 0.2451 | 0.4999 | 1.0000 |
| **2** | 0.3820 | 0.5389 | 0.7424 | 1.0000 | 1.0788 | 1.0789 | 1.1901 |
| **3** | 1.0000 | 1.2132 | 1.2607 | 1.2996 | 1.5720 | 1.6101 | 1.7530 |
| **4** | 1.7909 | 1.8036 | 2.0000 | 2.1662 | 2.2368 | 2.4393 | 2.5550 |
| **5** | 2.6180 | 2.6898 | 2.8906 | 3.0000 | 3.0966 | 3.3696 | 3.4450 |
| **6** | 3.3383 | 3.5483 | 3.5496 | 3.7537 | 4.0319 | 4.2100 | 4.2470 |
| **7** | 3.8271 | 4.1419 | 4.4598 | 4.6377 | 4.7388 | 4.7922 | 4.8019 |

Any two bidirectional information topologies chosen from the defined set will meet the requirements of Lemma 4.1 with the addition of a single edge. Additionally, if multiple edges are added, two randomly selected bidirectional information topologies will satisfy Lemma 4.3. The eigenvalues of the information flow matrix $\mathcal{L}_{\mathcal{P}}$ for all topologies listed in Table 4.2 are positive real numbers so $Re(\lambda_i(\mathcal{L}_{\mathcal{P}})) > 0$ condition for $i = 1, 2, \ldots, N$ in Lemma 2.1 is fulfilled under the spanning tree assumption (Assumption 2.2).

To understand the system behavior, the eigenvalues of the information flow matrix can be pondered. It is foreseen that an increasing trend in the eigenvalues will result in faster system response according to Remark 4.1 that is based on Lemma 4.2. The performance analysis in this section includes linear and nonlinear control types on an individual basis.

Table 4.3 displays the settling time calculated for velocity state using the algorithm in Figure 3.3 for bidirectional topologies in the case of a linear controller. The results align with Table 3.4 as increased information exchange reduces the settling time. The results suggest that it is essential to have access to the leader's information to facilitate a faster response from the system.

Table 4.3. Settling time in seconds for the linear controller with $1\ \%$ speed tolerance under different information flow topologies in Figure 4.1 .

| Vehicle No | BD | BD2 | BD3 | BD4 | BD5 | BD6 | BDL |
|---|---|---|---|---|---|---|---|
| **1** | 70.17 | 33.49 | 13.80 | 13.53 | 13.38 | 13.28 | 13.24 |
| **2** | 86.55 | 46.61 | 20.15 | 14.10 | 13.53 | 13.31 | 13.24 |
| **3** | 101.12 | 60.65 | 31.22 | 17.62 | 14.10 | 13.41 | 13.24 |
| **4** | 102.35 | 72.58 | 50.54 | 26.53 | 15.51 | 13.63 | 13.24 |
| **5** | 115.58 | 73.59 | 52.27 | 35.29 | 21.71 | 14.06 | 13.24 |
| **6** | 116.32 | 83.78 | 60.19 | 36.04 | 23.32 | 14.59 | 13.24 |
| **7** | 116.61 | 84.39 | 61.21 | 42.68 | 28.35 | 18.51 | 13.24 |

Table 4.4. Settling time in seconds for the nonlinear controller with $1\ \%$ speed tolerance under different information flow topologies in Figure 4.2 .

| Vehicle No | BD | BD2 | BD3 | BD4 | BD5 | BD6 | BDL |
|---|---|---|---|---|---|---|---|
| **1** | 47.23 | 25.63 | 21.46 | 17.15 | 17.23 | 17.21 | 17.20 |
| **2** | 68.83 | 46.31 | 35.30 | 30.77 | 29.89 | 29.72 | 29.69 |
| **3** | 69.59 | 53.49 | 40.22 | 35.03 | 34.06 | 33.94 | 33.93 |
| **4** | 62.13 | 41.72 | 28.58 | 16.38 | 17.23 | 20.97 | 20.90 |
| **5** | 78.27 | 60.60 | 50.31 | 42.17 | 32.92 | 27.96 | 27.28 |
| **6** | 65.18 | 45.40 | 31.93 | 16.21 | 19.13 | 17.54 | 17.08 |
| **7** | 64.95 | 46.23 | 32.10 | 24.93 | 23.50 | 22.49 | 20.85 |

Moreover, increasing the number of nodes receiving information from the leader vehicle positively affects not just the subjected nodes but also improves the overall vehicle platoon system by decreasing the settling time. Table 4.4 gives similar information to Table 4.3 except for the nonlinear controller type. This table points out the time in seconds for the velocity set point to be reached with $1\ \%$ tolerance. Going from left to right in Table 4.4, it can be generalized that the information shared increases while the settling time shortens for model type $\mathbb{T}_2$ vehicles.

In this study, it is also found that whether the information exchange type is unidirectional or bidirectional, if leader information is accessible to all of the followers, the settling time is the same. In this regard, it can be seen that the PLF column in Table 3.4 and the BDL column in Table 4.3 are identical. Additionally, the settling time for the corresponding followers in the PLF column of Table 3.5 and the BDL column of Table 4.4 are equal to each other.

Moreover, Figure 4.3 shows the effect of increasing the amount of information shared with vehicle 7 on its space error. Space error converges to zero faster as the number of directed edges in the IFT increases. Figure 4.4 shows the parallel outputs for the vehicle platoon system with a nonlinear controller.

Figure 4.5 and Figure 4.6 show the space error for the vehicle platoon system with a linear controller. Here, if a node itself or the node's neighbor receives the leader's state information, the distance between the node and the preceding vehicle notably approaches the desired inter-vehicle space value. Naturally, it takes longer for vehicles to maintain the desired distance between each other if the BD topology is utilized as shown in Figure 4.5.

The settling time significantly reduces as the vehicular platoon is encouraged to share more information. Note that if all of the nodes receive the leader information, the space error plot for the PLF topology, Figure 3.5, and the BDL topology, Figure 4.6, become congruous. It should also be highlighted that regardless of the controller type, the settling time values for the PLF and BDL topologies are the same in Tables 3.4 and 4.3 and Tables 3.5 and 4.4, respectively. This indicates that if all followers are receiving the leader's information, changing the link between the consecutive followers from a one-way, unidirectional information flow to a two-way, bidirectional flow will not reduce the settling time.

Lastly, space error for the ISM controlled vehicle platoon system is shown in Figures 4.7 and 4.8. In all of the IFTs tested, the space error converges to zero eventually. But, it takes visibly longer for the BD topology in Figure 4.7 than the BDL topology in Figure 4.8 since the information sharing is more strict for the BD topology.

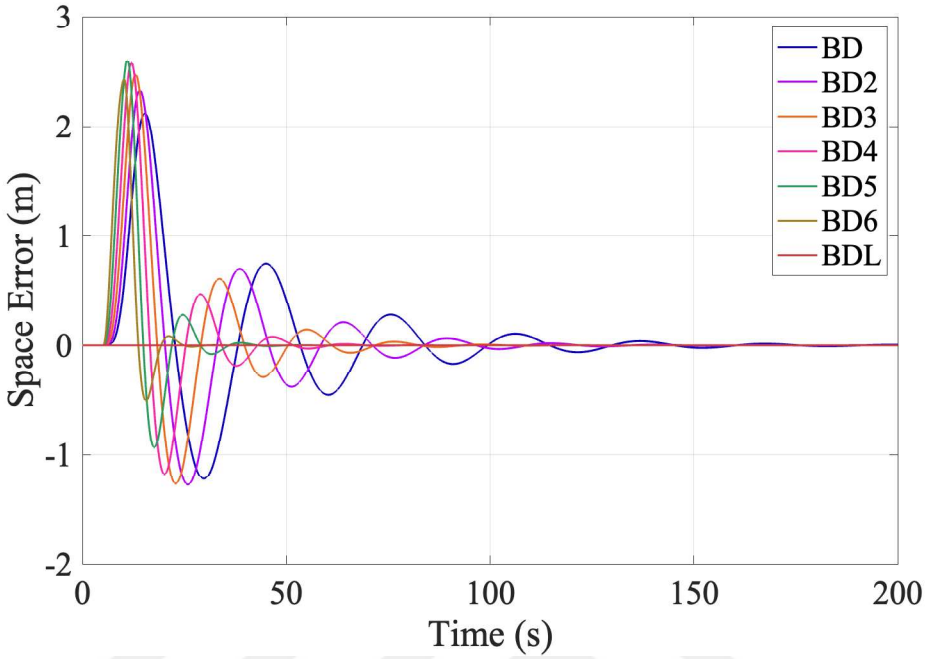


Figure 4.3. Space error for vehicle 7 with linear controller under bidirectional IFTs in Figure 4.1.

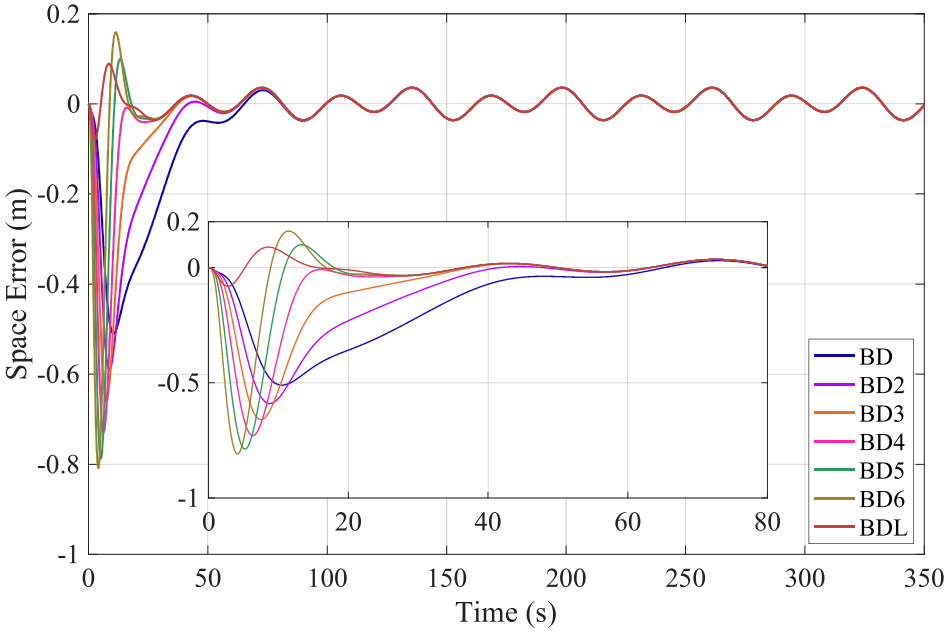


Figure 4.4. Space error for vehicle 7 with nonlinear controller under bidirectional IFTs in Figure 4.2.

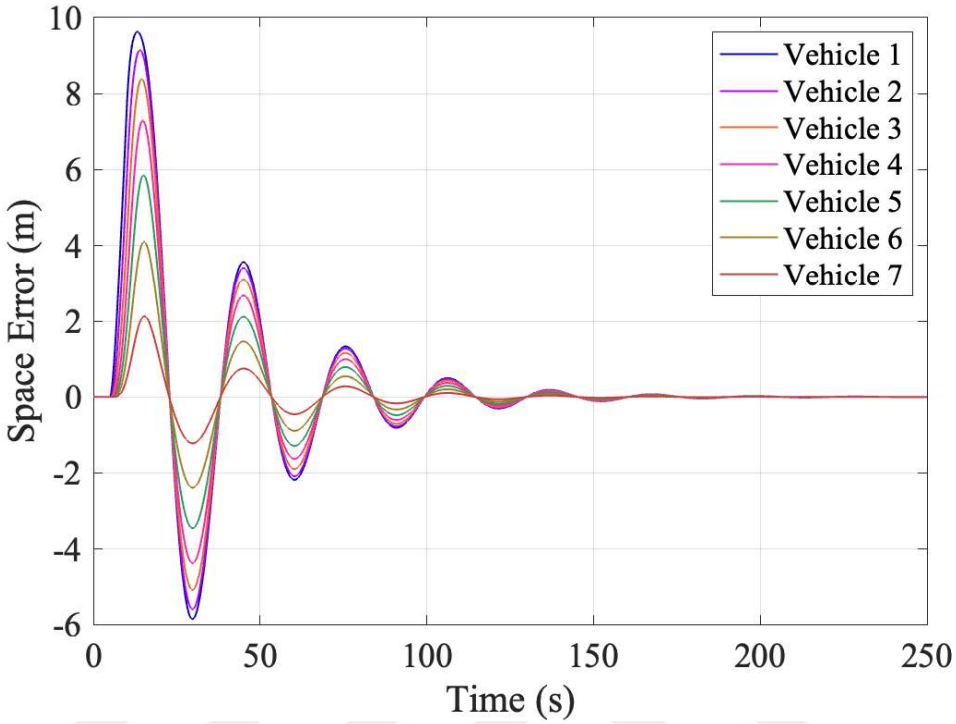


Figure 4.5. Space error with linear controller for bidirectional BD IFT in Figure 4.1.

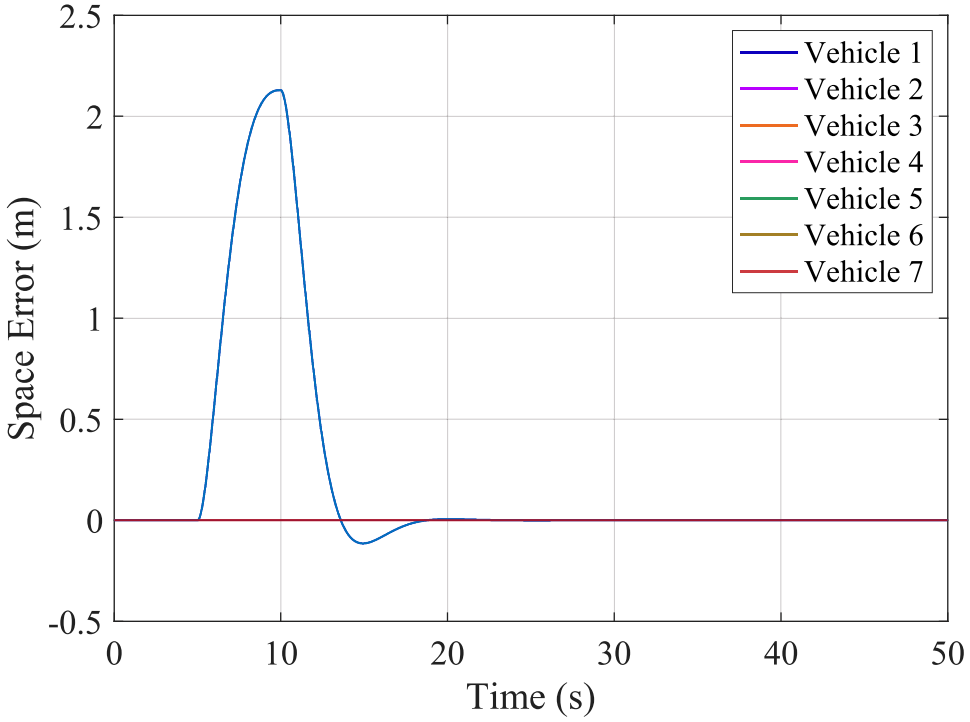


Figure 4.6. Space error with linear controller for bidirectional BDL IFT in Figure 4.1.

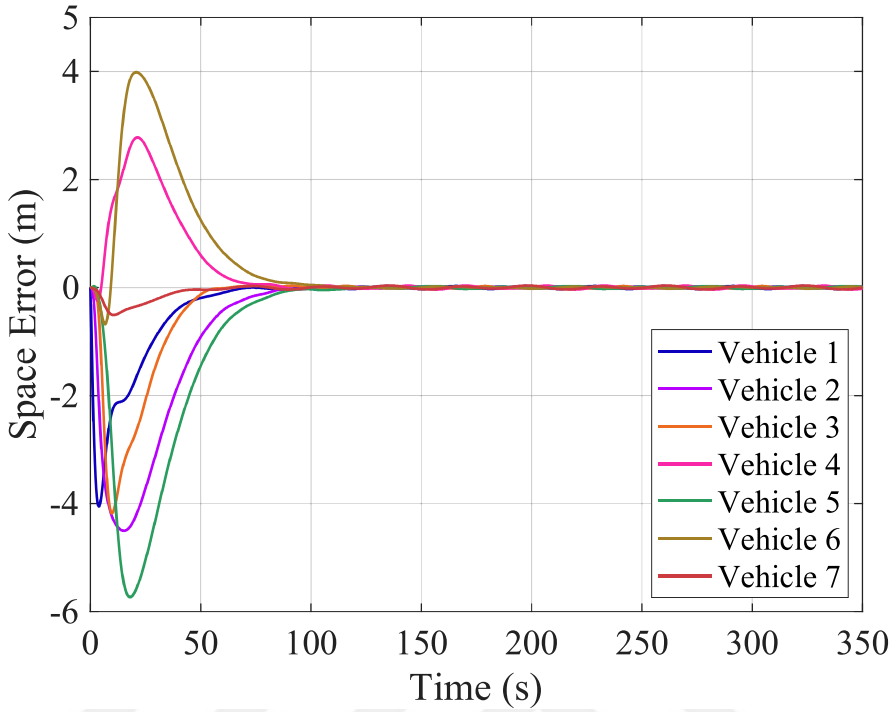


Figure 4.7. Space error with nonlinear controller for bidirectional BD IFT in Figure 4.2.

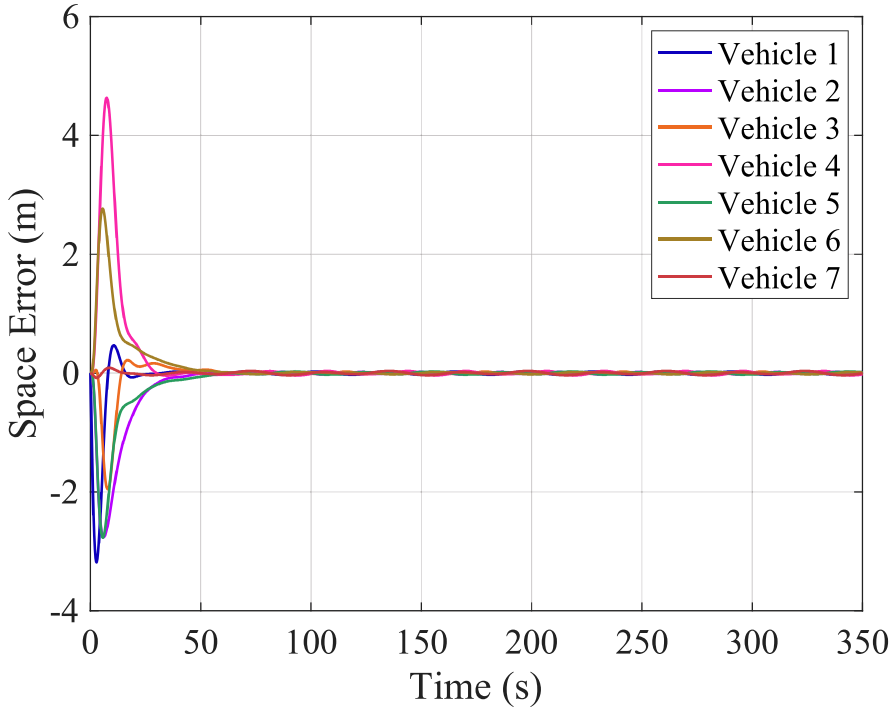


Figure 4.8. Spacing error with nonlinear controller for bidirectional BDL IFT in Figure 4.2.

## 4.5. Summary of the Chapter

To sum up, this chapter explains the control system performance under several bidirectional IFTs. On the stability side, system requirements are the same as the unidirectional information topology. However, the shift in eigenvalue positions in response to changes in information flow topology varies because the matrix structure differs from that of the unidirectional case. Up to this chapter, all topologies inspected were satisfying the spanning tree assumption. In Chapter 5, the necessity for an information flow topology to contain a spanning tree will be eliminated and the behavior of the vehicle platoon system under such information flow topologies will be examined.

# 5. ANALYSIS OF TOPOLOGIES WITHOUT A SPANNING TREE

This chapter focuses on various aspects of information topologies without a spanning tree. The stability analysis of a vehicle platoon system that does not have a spanning tree will be conducted. Furthermore, the consequences of choosing such topologies in a vehicle platoon system are investigated. If the information flow topology does not have a spanning tree, sub-platoon groups are formed in the vehicle platoon system. The underlying reason behind sub-platoon grouping is examined and explained with accompanying simulation results.

## 5.1. Graph Partition

In Chapter 2, the properties of a graph are explained in detail. It is stated that the graph has a spanning tree if there exists a vertex from which directed routes exist to all other vertices. Next, in Chapter 3 and Chapter 4, vehicle platoon systems are formed with information flow topologies that contain a spanning tree. In these information flow topologies, the leading vehicle acts as a root node. Therefore, leader information access is granted to every node in the vehicle platoon system via direct or indirect connection. It has been inspected that the spanning tree assumption implies that the vehicle platoon system achieves a consensus. However, examining the vehicle platoon system in situations without a spanning tree is another research topic that should be emphasized. Within this framework, graph partition algorithms will be inspected in this thesis.

Over the last thirty years, there has been significant research focus on graph partitioning. Partition of electric circuits was the main concern in the initial studies of graph partition [49]. Mu et al. classify graph partitioning into two categories: Vertex and edge partitioning [50]. Vertex partition is based on a balanced node division where each node belongs to a single subgroup. A good vertex partition should avoid cut edges as much as possible in order to reduce communication costs [49]. The cut edge occurs when two linked nodes are divided into two separate subgraphs. On the other hand, the edge partition is based on a balanced edge division where each edge belongs to a single subgroup.

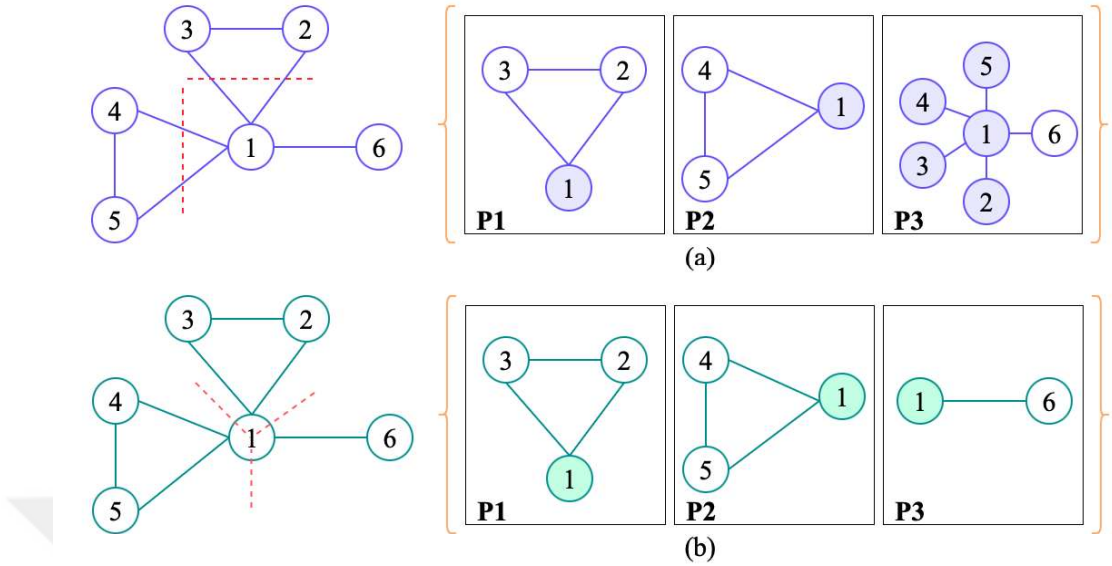


Figure 5.1. Graph partition categories (a) Vertex partitioning, (b) Edge partitioning.

Vertex and edge partitioning methods are compared in Figure 5.1 where repetitive vertices are highlighted. Moreover, Ayall et al. add hybrid partition as a third category to the graph partition classification. As its name indicates, it is a method which blends vertex and edge partitioning.

## 5.2. Graph Partition Algorithms

A graph partitioning technique must meet certain criteria, including minimizing edge cuts and maximizing load balance, as outlined in [51]. In the same study, it is also highlighted that graphs have a dynamic nature since the addition or subtraction of vertices or edges may occur as time passes.

A graph to part into subgroups is represented as $\mathcal{G} =(\mathcal{V}, E)$ where the set of nodes are $\mathcal{V} = \{\alpha_0, \alpha_1, \alpha_2, \ldots, \alpha_n\}$ and the set of edges are $E \subseteq \mathcal{V} \times \mathcal{V}$. It is assumed that $\mathcal{G}$ does not contain a spanning tree. Under this assumption, consecutive followers may have difficulty in protecting a safe distance due to a lack of communication with the leader or the neighbors. If there is no spanning tree in the IFT, the vehicle platoon is expected to split into sub-platoons due to a lack of interaction. The next step of the study is to analyze the nature of the divisions and how sub-platoons are formed.

Erkan et al. introduced an innovative graph partitioning technique aimed at dividing a graph into distinct subgroups, namely primary and secondary layer subgroups [45]. This section will provide an overview of the proposed algorithm. Following that, an evaluation will be conducted to determine the suitability of employing the approach outlined in [45] for dividing sub-platoons within a vehicle platoon lacking a spanning tree.

**Definition 5.1** (Primary Layer Subgraph (PLS) [52]). *Let $\mathcal{G}$ =($\mathcal{V}, E$) be the graph representation for a vehicle platoon system. There exists a unique number of PLS $l_p$, which satisfies $l_p \geq 1$, and subgraphs $\mathcal{G}_{p,i}$ =($\mathcal{V}_{p,i}, E_{p,i}$) for $i = 1, 2, \ldots, l_p$ where vertex subset $\mathcal{V}_{p,i}$ is the largest possible set which contains a spanning tree. Additionally, vertices $\mathcal{V}_{p,i}$ can only transmit information to the vertices in the other subgraphs and the reverse communication relationship is not possible.*

**Definition 5.2** (Secondary Layer Subgraph (SLS) [52]). *Let $\hat{\mathcal{V}}$ be the vertices that are not part of any PLS. Then, $\hat{\mathcal{V}} = V / \bigcup_{i=1}^{l_p} \mathcal{V}_{p,i}$ for $i = 1, 2, \ldots, l_s$ where $l_s$ is the number of secondary subgraphs and the union of vertex subsets $\mathcal{V}_{s,i}$ are equal to $\hat{\mathcal{V}}$. Every subgraph $\mathcal{G}_{s,i}$ contains a spanning tree where the root vertex receives information from a minimum of two vertices in distinct subgraphs and the remaining vertices only communicate within the secondary group they belong.*

The algorithm to detect PLS and SLS is detailed in [52]. Total number of primary subgraphs are denoted by $\bar{n}_p = \sum_{i=1}^{l_p} n_{p,i}$ and $\bar{n}_s = \sum_{j=1}^{l_s} n_{s,j}$ is denoting the the total number of secondary subgroups. The number of nodes in subgraphs is denoted by $n_{p,i}$ for the $i^{th}$ PLS, and $n_{s,j}$ for the $j^{th}$ SLS. Furthermore, in [53], PLS and SLS detection algorithms are utilized.

In [53], it is emphasized that due to the arrangement of subgraph dynamics, the equilibrium points of primary and secondary layers are the convex combination of primary and secondary layer elements, respectively. Next, the stability requirements for these subgroups need to be investigated. Consequently, the following section is dedicated to the stability analysis of IFTs that do not include a spanning tree.

## 5.3. Stability Analysis of Information Flow Topologies Without a Spanning Tree

The stability analysis of a convoy of vehicles is related to how information is communicated among the vehicles. In a vehicle platoon system without a spanning tree in its information flow topology, there isn't a network path that ensures every node can be reached from any other node. The absence of a spanning tree introduces potential problems such as data loops or inconsistent information to the vehicle platoon system. Hence, the vehicle platoon system could be driven towards an unstable state.

In this chapter, conditions for asymptotic stability on a vehicle platoon system with no spanning tree will be established. To analyze the system stability, first the closed-loop system matrices in (2.46) and (3.11) should be inspected. Note that the stability of $I_N \otimes A - \mathcal{L}_{\mathcal{P}} \otimes Bk^T$ is equivalent to that of $A - \lambda_i(\mathcal{L}_{\mathcal{P}})Bk^T$ for $i \in \mathbb{N}$, via eigenvalue decomposition [5]. This is also valid for a vehicle platoon system with matrix $\bar{A}$ in (2.46).

In the case of a communication network with a spanning tree, the eigenvalues of $\mathcal{L}_{\mathcal{P}}$ are real numbers both for unidirectional and bidirectional IFTs. However, this does not apply to an IFT without a spanning tree meaning such a system may have real and complex eigenvalues. In this case, the following result will be used to characterize the stability conditions of the vehicle platoon system.

**Lemma 5.1** ([54]). *A third-order characteristic polynomial of the form*

$$f(\lambda) = \lambda^3 + a_1\lambda^2 + a_2\lambda + a_3 \tag{5.1}$$

*with complex coefficients has roots in the OLHP if and only if*

*(1)* $Re(a_1) > 0\,,$

*(2)* $Re(a_1) \cdot Re(a_1\bar{a}_2 - a_3) - (Im(a_2))^2 > 0\,,$

*(3)* $[Re(a_1) \cdot Re(a_2\bar{a}_3) - (Re(a_3))^2][Re(a_1) \cdot Re(a_1\bar{a}_2 - a_3) - (Im(a_2))^2]$
$- [Re(a_1) \cdot Im(\bar{a}_1 a_3) + Re(a_3) \cdot Im(a_2)]^2 > 0\,.$

Recall that, in the analyzed case, the characteristic polynomial of $(A - \lambda_i(\mathcal{L}_\mathcal{P})Bk^T)$ can be written as

$$|sI - (A - \lambda_i(\mathcal{L}_\mathcal{P})Bk^T)| = s^3 + \frac{\lambda_i(\mathcal{L}_\mathcal{P})k_3 + 1}{\tau}s^2 + \frac{\lambda_i(\mathcal{L}_\mathcal{P})k_2}{\tau}s + \frac{\lambda_i(\mathcal{L}_\mathcal{P})k_1}{\tau} \tag{5.2}$$

where the internal lag of the vehicle is $\tau > 0$ and $k_1$, $k_2$, $k_3$ are the controller gains of the linear decentralized controller [20]. By letting

$$a_1 = \frac{\lambda_i(\mathcal{L}_\mathcal{P})k_3 + 1}{\tau} \tag{5.3}$$

$$a_2 = \frac{\lambda_i(\mathcal{L}_\mathcal{P})k_2}{\tau} \tag{5.4}$$

$$a_3 = \frac{\lambda_i(\mathcal{L}_\mathcal{P})k_1}{\tau} \tag{5.5}$$

the stability conditions can be stated as follows

$$\frac{Re(\lambda_i(\mathcal{L}_\mathcal{P}))k_3 + 1}{\tau} > 0 \tag{5.6}$$

$$\frac{Re(\lambda_i(\mathcal{L}_\mathcal{P}))k_3 + 1}{\tau} \cdot Re\Big(\frac{\lambda_i(\mathcal{L}_\mathcal{P})k_3 + 1}{\tau} \cdot \frac{\bar{\lambda}_i(\mathcal{L}_\mathcal{P})k_2}{\tau} - \frac{\lambda_i(\mathcal{L}_\mathcal{P})k_1}{\tau}\Big) - Im\Big(\frac{\lambda_i(\mathcal{L}_\mathcal{P})k_2}{\tau}\Big)^2 > 0 \tag{5.7}$$

$$\Big[\frac{Re(\lambda_i(\mathcal{L}_\mathcal{P}))k_3 + 1}{\tau} \cdot Re\Big(\frac{\lambda_i(\mathcal{L}_\mathcal{P})k_2}{\tau} \cdot \frac{\bar{\lambda}_i(\mathcal{L}_\mathcal{P})k_1}{\tau}\Big) - \Big(\frac{Re(\lambda_i(\mathcal{L}_\mathcal{P}))k_1}{\tau}\Big)^2\Big] \cdot \Big[\frac{Re(\lambda_i(\mathcal{L}_\mathcal{P}))k_3 + 1}{\tau} \cdot Re\Big(\frac{\lambda_i(\mathcal{L}_\mathcal{P})k_3 + 1}{\tau} \cdot \frac{\bar{\lambda}_i(\mathcal{L}_\mathcal{P})k_2}{\tau} - \frac{\lambda_i(\mathcal{L}_\mathcal{P})k_1}{\tau}\Big) - \Big(\frac{Im((\lambda_i(\mathcal{L}_\mathcal{P}))k_2}{\tau}\Big)^2\Big] - \Big[\frac{Re(\lambda_i(\mathcal{L}_\mathcal{P}))k_3 + 1}{\tau} \cdot Im\Big(\frac{\bar{\lambda}_i(\mathcal{L}_\mathcal{P})k_3 + 1}{\tau} \cdot \frac{\lambda_i(\mathcal{L}_\mathcal{P})k_1}{\tau}\Big) + \frac{Re(\lambda_i(\mathcal{L}_\mathcal{P}))k_1}{\tau} \cdot \frac{Im(\lambda_i(\mathcal{L}_\mathcal{P}))k_2}{\tau}\Big]^2 > 0 \tag{5.8}$$

for all nonzero eigenvalues of $\mathcal{L}_\mathcal{P}$ $(\lambda_i(\mathcal{L}_\mathcal{P}) \neq 0)$.

Equations (5.6)-(5.8) summarize the necessary conditions for a stable system with an information flow topology in the absence of a spanning tree condition. Moreover, condition (5.6) can be simplified as

$$k_3 > -\frac{1}{Re(\lambda_i(\mathcal{L}_\mathcal{P}))}. \tag{5.9}$$

## 5.4. Numerical Analysis

In this section, an IFT without a spanning tree is determined, as shown in Figure 5.2. Then, the numerical analysis of the vehicle platoon system using the specified IFT is conducted. To analyze the stability of the system, firstly the information flow matrix $\mathcal{L}_P$ for the IFT in Figure 5.2 is found as

$$\mathcal{L}_P = \begin{bmatrix} 4 & -1 & 0 & 0 & -1 & 0 & -1 \\ 0 & 0 & 0 & 0 & 0 & 0 & 0 \\ 0 & -1 & 1 & 0 & 0 & 0 & 0 \\ -1 & 0 & -1 & 3 & -1 & 0 & 0 \\ 0 & 0 & 0 & 0 & 1 & -1 & 0 \\ 0 & 0 & 0 & -1 & 0 & 1 & 0 \\ -1 & 0 & 0 & 0 & 0 & 0 & 1 \end{bmatrix}. \tag{5.10}$$

The set of eigenvalues of the $\mathcal{L}_P$ matrix in (5.10) can be listed as follows:

$$\sigma(\mathcal{L}_P) = \{0.00, 0.28, 0.77, 1.00, 2.30 - 0.33i, 2.30 + 0.33i, 4.36\}. \tag{5.11}$$

In order to select the linear controller gains, $k_1$, $k_2$, and $k_3$, (5.7), (5.8) and, (5.9) will be used for each nonzero eigenvalue of the $\mathcal{L}_\mathcal{P}$ $(\lambda_i(\mathcal{L}_\mathcal{P}) \neq 0)$. Considering all eigenvalues of $\mathcal{L}_\mathcal{P}$ for $i = 1, \ldots, N$, (5.9) can be rearranged as

$$k_3 > -\frac{1}{\max\limits_{i\in\{1,\ldots,N\}} Re(\lambda_i(\mathcal{L}_\mathcal{P}))}. \tag{5.12}$$

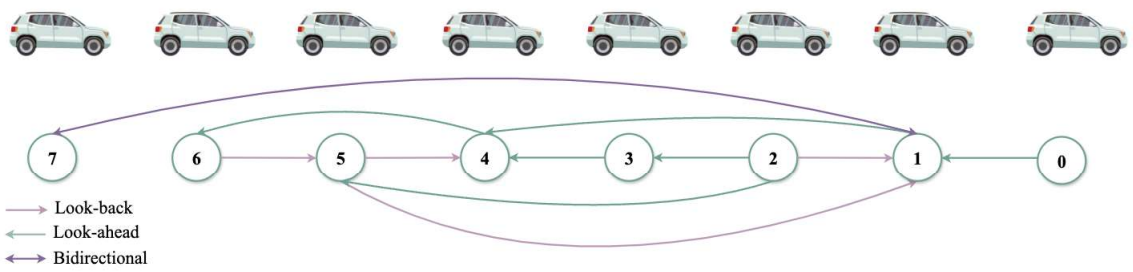


Figure 5.2. Homogeneous platoon without a spanning tree.

Table 5.1. Coefficients for eigenvalues in (5.11) where $\tau = 0.5$.

| $i$ | $Re(\lambda_i)$ | $Im(\lambda_i)$ | $a_1$ | $a_2$ | $a_3$ |
|---|---|---|---|---|---|
| 1 | 0.00 | 0.00 | NA | NA | NA |
| 2 | 0.28 | 0.00 | $0.56k_3 + 2$ | $0.56k_2$ | $0.56k_1$ |
| 3 | 0.77 | 0.00 | $1.54k_3 + 2$ | $1.54k_2$ | $1.54k_1$ |
| 4 | 1.00 | 0.00 | $2k_3 + 2$ | $2k_2$ | $2k_1$ |
| 5 | 2.30 | $-0.33$ | $4.6k_3 + 2 - 0.66k_3i$ | $4.6k_2 - 0.66k_2i$ | $4.6k_1 - 0.66k_1i$ |
| 6 | 2.30 | 0.33 | $4.6k_3 + 2 + 0.66k_3i$ | $4.6k_2 + 0.66k_2i$ | $4.6k_1 + 0.66k_1i$ |
| 7 | 4.36 | 0.00 | $8.72k_3 + 2$ | $8.72k_2$ | $8.72k_1$ |

As shown in Table 5.1, the largest real part of the eigenvalues in (5.11) is $4.36$. Thus, (5.12) becomes

$$k_3 > -\frac{1}{4.36} = -0.23. \tag{5.13}$$

Furthermore, to select controller gains $k_2$ and $k_3$, it is needed to be verified that the conditions in (5.7) and (5.8) are satisfied for each nonzero eigenvalues of $\mathcal{L}_\mathcal{P}$. For example, for $\lambda_5(\mathcal{L}_\mathcal{P}) = 2.30 - 0.33i$ , (5.7) can be expressed as

$$(4.6k_3 + 2) \cdot Re\Big((4.6k_3 + 2 - 0.66k_3i) \cdot (4.6k_2 + 0.66k_2i) - (4.6k_1 - 0.66k_1i)\Big) \\ -\Big(Im(4.6k_2 - 0.66k_2i)\Big)^2 > 0. \tag{5.14}$$

By rearranging (5.15)

$$(4.6k_3 + 2)(-4.6k_1 + 9.2k_2 + 21.60k_2k_3) - 0.44k_2^2 > 0 \tag{5.15}$$

can be obtained. From (5.13) it is known that $k_3 > -0.23$ so that $4.6k_3 + 2 > 0$. Therefore, (5.15) can be simplified as

$$(-4.6k_1 + 9.2k_2 + 21.6k_2k_3) > \frac{0.44k_2^2}{4.6k_3 + 2}. \tag{5.16}$$

Moreover, condition in (5.8) should also be checked for $\lambda_5(\mathcal{L}_\mathcal{P}) = 2.30 - 0.33i$ as follows

$$\begin{aligned} &\Big[(4.6k_3+2)(21.60k_1k_2) - (21.16k_1^2)\Big] \\ \cdot&\Big[(4.6k_3+2)(-4.6k_1+9.2k_2+21.6k_2k_3) - 0.44k_2^2\Big] \\ -&\Big[((4.6k_3+2)(-1.32)k_1 - 3.04k_1k_2)^2\Big] \;>\; 0. \end{aligned} \tag{5.17}$$

Suppose that $k_3$ is chosen as $0.4$ so that condition in (5.13) is met. Furthermore, $k_1$ and $k_2$ are selected as $0.6$ and $0.8$, respectively. Substituting these values in (5.15) it can be confirmed that

$$(-4.6 \times 0.4 + 9.2 \times 0.6 + 21.6 \times 0.6 \times 0.8) = 14.05 > \frac{0.44 \times (0.6)^2}{4.6 \times 0.8 + 2} = 0.03. \tag{5.18}$$

For the same parameter values (5.19) becomes

$$\begin{aligned} &((4.6 \times 0.8 + 2)(21.60 \times 0.4 \times 0.6) - 21.6 \times 0.4^2) \\ \cdot&((4.6 \times 0.8 + 2)(-4.6 \times 0.4 + 9.2 \times 0.6 + 21.6 \times 0.6 \times 0.8) - 0.44 \times 0.6^2) \\ -&(-6.07 \times 0.4 \times 0.8 - 2.64 \times 0.4 - 3.04 \times 0.4 \times 0.6)^2 = 2060.59 > 0. \end{aligned} \tag{5.19}$$

Consequently, the conditions in (5.7), (5.8) and, (5.9) are satisfied with the chosen controller gains when the coefficients related to $\lambda_5(\mathcal{L}_\mathcal{P})$ are used. It is important to calculate $a_1$, $a_2$, and $a_3$ for each non-zero eigenvalue and confirm the conditions specified in Lemma 5.1 to determine appropriate controller gains for a stable vehicle platoon system without a spanning tree.

Table 5.2 shows the coefficient values associated with each nonzero eigenvalue using the selected controller gains. Additionally, controller parameters are validated in Table 5.3 to ensure the stability of the vehicle platoon system using the coefficients in Table 5.2. As it can be seen from Table 5.3, all conditions in Lemma 5.1 are fulfilled for $k_1 = 0.4$ , $k_2 = 0.6$ and, $k_3 = 0.8$ can be used in the analysis of the IFT in Figure 5.2.

Table 5.2. Coefficients in Table (5.1) for $k_1 = 0.4$ , $k_2 = 0.6$ and, $k_3 = 0.8$.

| $i$ | $Re(\lambda_i)$ | $Im(\lambda_i)$ | $a_1$ | $a_2$ | $a_3$ |
|---|---|---|---|---|---|
| 2 | 0.28 | 0.00 | 2.45 | 0.34 | 0.22 |
| 3 | 0.77 | 0.00 | 3.23 | 0.92 | 0.62 |
| 4 | 1.00 | 0.00 | 3.60 | 1.20 | 0.80 |
| 5 | 2.30 | $-0.33$ | $5.68 - 0.53i$ | $2.76 - 0.40i$ | $1.84 - 0.26i$ |
| 6 | 2.30 | 0.33 | $5.68 + 0.53i$ | $2.76 + 0.40i$ | $1.84 + 0.26i$ |
| 7 | 4.36 | 0.00 | 8.98 | 5.23 | 3.49 |

Table 5.3. Validation of conditions in (5.7), (5.8) and, (5.9) for coefficients in Table 5.2.

| $i$ | (5.6) | (5.7) | (5.8) |
|---|---|---|---|
| 2 | $2.45 > 0$ | $1.46 > 0$ | $0.20 > 0$ |
| 3 | $3.23 > 0$ | $7.66 > 0$ | $11.19 > 0$ |
| 4 | $3.60 > 0$ | $12.67 > 0$ | $35.68 > 0$ |
| 5 | $5.68 > 0$ | $79.62 > 0$ | $2060.59 > 0$ |
| 6 | $5.68 > 0$ | $79.62 > 0$ | $2060.59 > 0$ |
| 7 | $8.98 > 0$ | $390.23 > 0$ | $59173.49 > 0$ |

It should be noted that the vehicle platoon system is initialized with zero tracking errors similar to the linear controller case described in Chapter 3. The speed profile of the leader vehicle is taken as in (3.23) and the sample time is taken as $0.01$ seconds. Now that the simulation parameters have been chosen, the next step is to execute the simulation on MATLAB.

Figure 5.3 illustrates the inclination toward inter-vehicle clustering. It is possible to identify the sub-platoon groups formed from Figure 5.3. For instance, vehicles $1$ (- - -) and 7 (- - -) can be declared as one of the subgroups formed under IFT in Figure 5.2 by inspecting Figure 5.3(a).

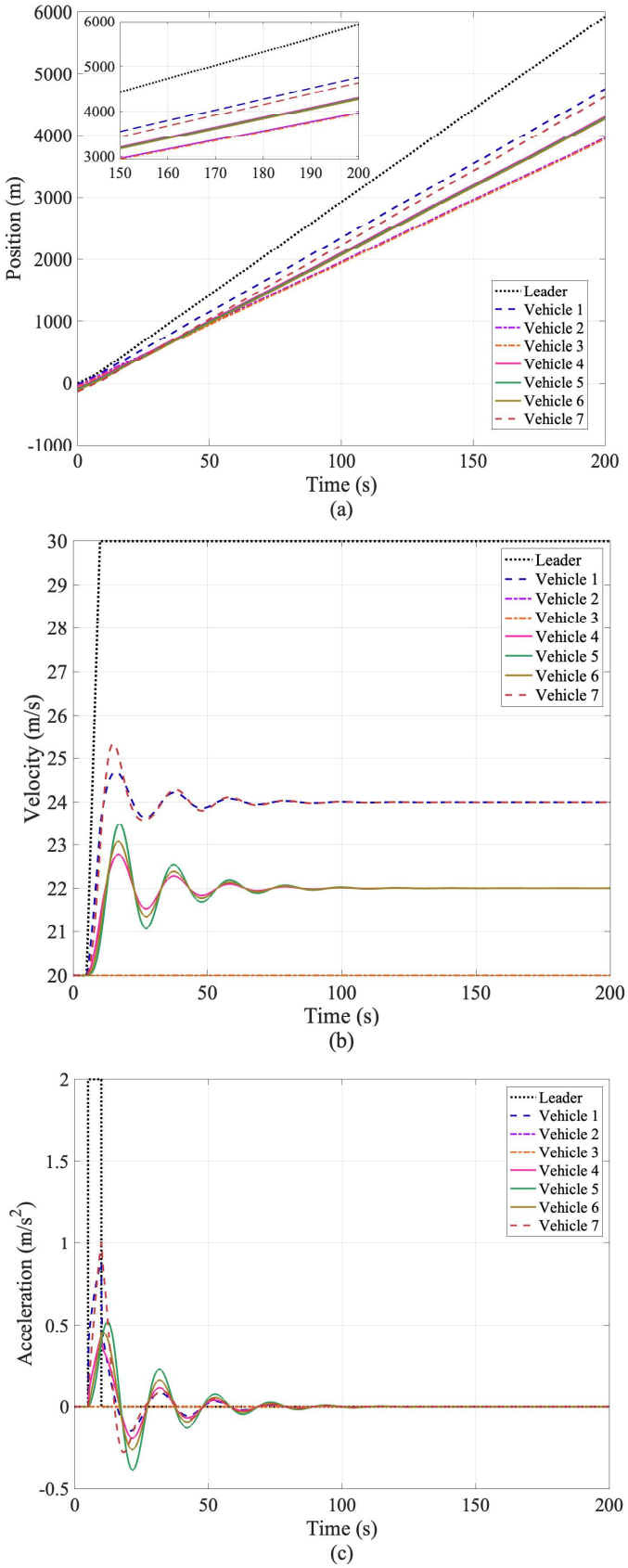


Figure 5.3. Vehicle states of IFT in Figure 5.2 (a) Position, (b) Velocity, (c) Acceleration.

Vehicles 2 (-·-·-) and 3 (-·--) are another sub-platoon group as it can be seen from Figure 5.3(b). These two vehicles are cruising at a constant speed of 20 $m/s$, which means they are not receiving the leading vehicle information directly or indirectly. Since they are the slowest vehicles, they are following the other vehicles from behind as visualized in Figure 5.3(a). Finally, vehicles 4 (——), 5 (——), and 6 (——) can be considered as the nodes belong to a different sub-platoon group formed under IFT in Figure 5.2. The velocity of these vehicles converges to 22 $m/s$ as shown in Figure 5.3(b). Furthermore, in Figure 5.3(c) it can be seen that the acceleration of all vehicles converges to 0 after 100 seconds.

To explain the division of the vehicle platoon system into sub-platoon groups in the case of an IFT with no spanning tree employed, the PLS and SLS algorithms introduced by Develer et al. in [53] can be used. The PLS algorithm found $\bar{n}_p = 2$ and the SLS algorithm found $\bar{n}_s = 2$ layers on the primary and secondary subgraphs, respectively as shown in Figure 5.4 for IFT in Figure 5.2. The leading vehicle is in PLS1 while the PLS2 subgraph consists of followers 2 and 3. In this subgraph, there is a spanning tree, and follower 2 acts as a root node since it sends information to follower 3 meaning the control input of follower 3 will be updated according to the information coming from follower 2. Moreover, SLS1 contains vehicles 1 and 7. The remaining vehicles are part of SLS2 as shown in Figure 5.4.

The primary layer subgraphs are self-sufficient since they do not rely on information coming from the neighboring subgraphs. As stated above, PLS2 is not connected to PLS1 so the vehicles in PLS2 fail to track the velocity of the leading vehicle. Therefore, they maintain their initial velocity and acceleration values. In this SLS1, vehicle 3 is a follower and vehicle 2 acts like the leading vehicle. Lastly, vehicles 4, 5, and 6 are split into a SLS2 subgraph. SLS2 receives information from both PLS2 and SLS1 subgraphs. Therefore, as Develer et al. state in [53], SLS1's equilibrium point for velocity is 22 m/s which is the average of the equilibrium point of PLS2, 20 m/s, and SLS1 24 m/s. Eventually, PLS and SLS algorithms have divided the vehicle platoon system into 4 sub-platoons in total.

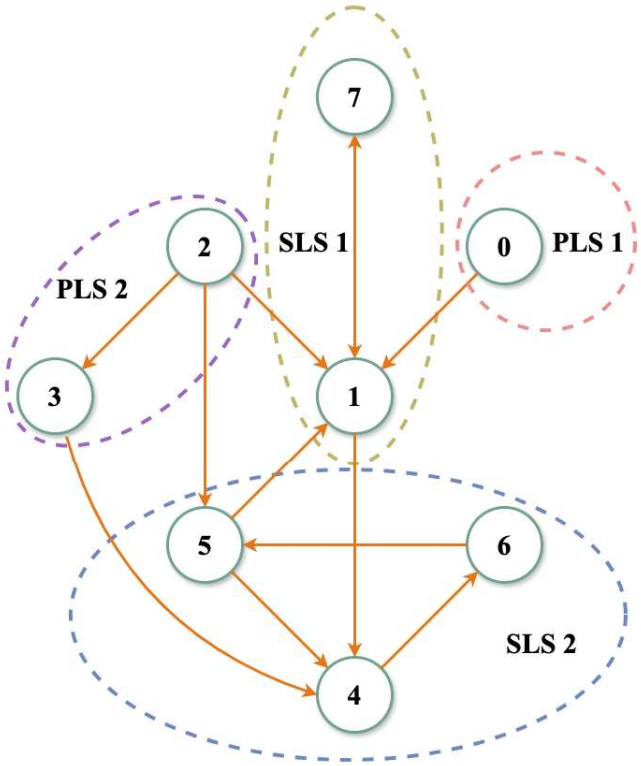


Figure 5.4. Two primary and two secondary layer subgraphs for IFT in Figure 5.2.

In a vehicle platoon system under an IFT without a spanning tree, vehicles may not always be able to maintain a safe distance from the preceding vehicle. To examine if the vehicles keep a safe inter-vehicle distance, space errors between the consecutive vehicles are checked. SAE standardized the message set directory for Vehicle to Everything (V2X) communication in [55]. In this standard, the communication range is specified as less than 1000 meters. Therefore, this threshold can be applied with a safety margin for detecting communication loss.

**Assumption 5.1.** *If the space error exceeds 500 meters, the communication between the vehicles is considered to be lost.*

Considering the safe distance between the vehicles, based on the Assumption 5.1, the upper threshold for the communication loss detection is $500-d_{i-1,i}$ where $d_{i-1,i}$ is the desired distance between the $i-1^{th}$ and the $i^{th}$ vehicles, and $-500-d_{i-1,i}$ is the lower threshold for the space error.

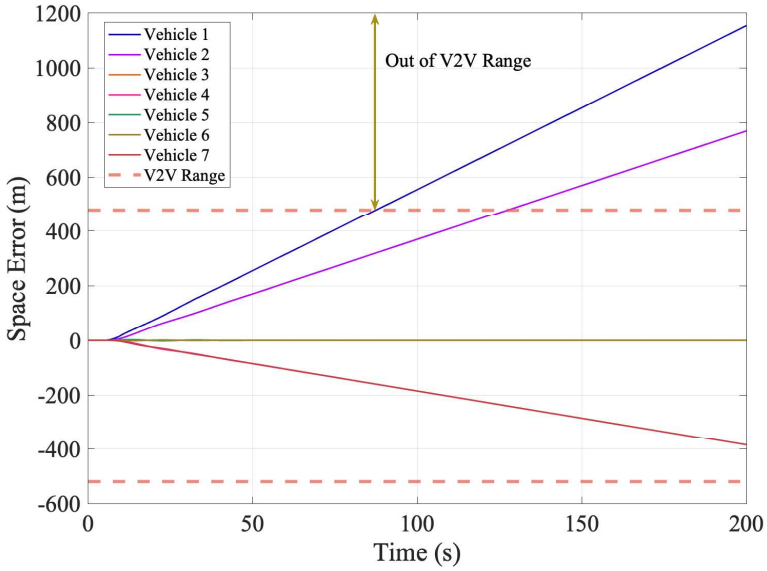


Figure 5.5. Space error for IFT in Figure 5.2 between consecutive vehicles with linear controller.

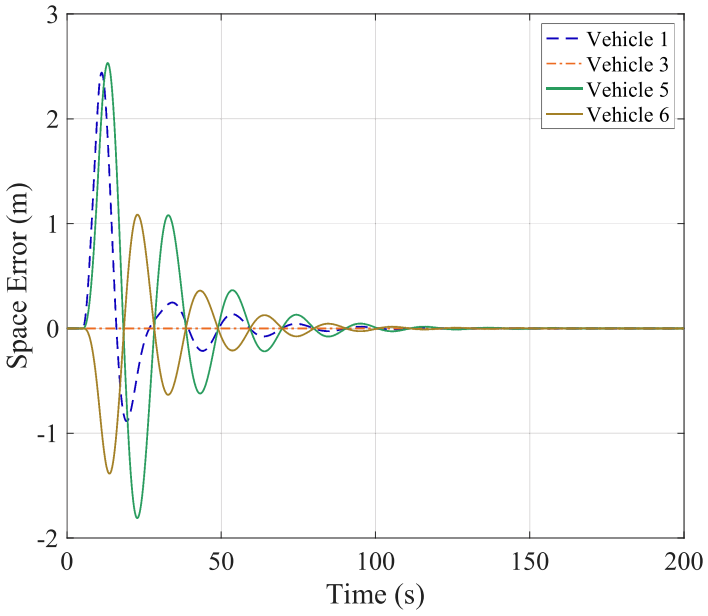


Figure 5.6. Space error for IFT in Figure 5.2 between vehicles in PLS2, SLS1, and SLS2 with linear controller.

In the tested IFT, shown in Figure 5.2, a communication loss error is detected under Assumption 5.1. The simulation results in Figure 5.5 demonstrate that some of the followers have left the convoy and therefore failed to meet the vehicle platoon system's requirements.

At this point, it would be reasonable to check sub-platoons formed in compliance with the graph partition algorithms in [52] to understand the clustering behavior of the vehicles which is one of the fundamental contributions of this thesis.

Note that it is assumed that vehicles in the sub-platoons formed can change their lane to prevent collisions. The follower 7 will track the follower 1 so that the desired space between these two vehicles is $6 \times d_{i-1,i}$. Figure 5.6 demonstrates that the sub-platoon groups formed in Figure 5.4 are successful in maintaining a safe distance between consecutive nodes.

It is possible to propose several IFTs that lack a spanning tree to test various scenarios. To expand the use cases in the thesis, IFT in Figure 5.7 has also been taken into consideration. The information flow matrix $\mathcal{L}_P$ for the IFT in Figure 5.7 is found as

$$\mathcal{L}_P = \begin{bmatrix} 1 & 0 & 0 & 0 & 0 & 0 & 0 \\ 0 & 1 & -1 & 0 & 0 & 0 & 0 \\ 0 & 0 & 1 & 0 & 0 & 0 & 0 \\ 0 & 0 & 0 & 1 & 0 & 0 & -1 \\ 0 & 0 & -1 & 0 & 1 & 0 & 0 \\ 0 & 0 & -1 & 0 & 0 & 2 & -1 \\ 0 & 0 & 0 & 0 & 0 & 0 & 0 \end{bmatrix}. \tag{5.20}$$

The set of eigenvalues of the $\mathcal{L}_P$ matrix in (5.20) are

$$\sigma(\mathcal{L}_P) = \{0, 1, 1, 1, 1, 1, 2\}. \tag{5.21}$$

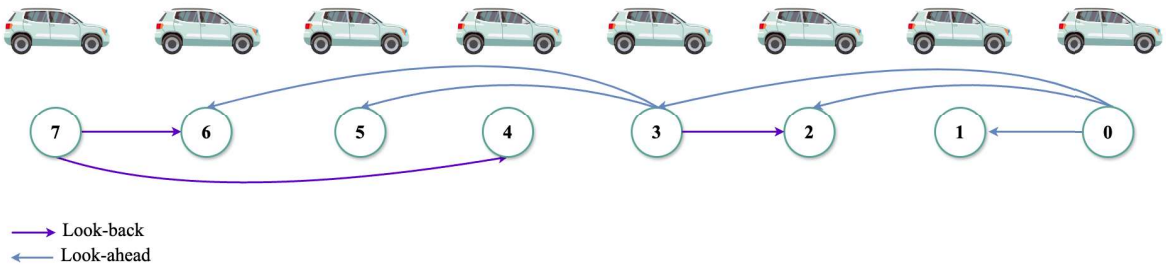


Figure 5.7. Homogeneous platoon without a spanning tree.

There is a zero eigenvalue associated with the follower 7 since this node does not receive information from any other node, and it only sends information to followers $4$ and $6$. Nonetheless, all of the eigenvalues of the corresponding $\mathcal{L}_P$ are real numbers so that the Routh-Hurwitz stability criterion is in third order as stated in [20]. Hence, controller gain parameters can be determined using (5.7), (5.8), and (5.9). From (5.9) it can be found that

$$k_3 > -0.5 \tag{5.22}$$

so let $k_3$ be $1$ as in Chapter 3 and Chapter 4. Using $k_3 = 1$, (5.7) can be rearranged as

$$k_2 > 0.5k_1. \tag{5.23}$$

In addition to (5.23),

$$k_1 > 0 \tag{5.24}$$

should also be satisfied to have a stable vehicle platoon system. Thus, it is possible to choose controller gain parameters $k_1 = 1$ and $k_2 = 2$ as in Chapter 3 and Chapter 4.

The PLS algorithm found $\bar{n}_p = 2$ and the SLS algorithm found $\bar{n}_s = 1$ layers on the primary and secondary subgraphs, respectively as shown in Figure 5.9 for IFT in Figure 5.7. Nodes in PLS$1$ are the leader vehicle and followers $1, 2, 3$, and $5$. This primary subgraph contains a spanning tree and the leader acts as a root node. PLS$2$ subgraph consists of followers $7$ and $4$. In this subgraph, there is a spanning tree, and follower $7$ acts as a root node since it sends information to follower $4$ meaning the control input of follower $4$ will be updated according to the information coming from follower $7$.

Follower 6 forms a secondary layer subgraph by itself. It receives information from PLS$1$ and PLS$2$ since it is linked to followers 3 and 7 as shown in Figure 5.9. Eventually, PLS and SLS algorithms have divided the vehicle platoon system into $3$ sub-platoons in total when the IFT in Figure 5.7 is employed. The next step is to check the equilibrium points for each subgroup. Vehicles within PLS$1$ demonstrate that they are capable of following the desired leader velocity and as a result, these vehicles are attaining the highest velocity, positioning them ahead of other vehicles in the different subgraphs.

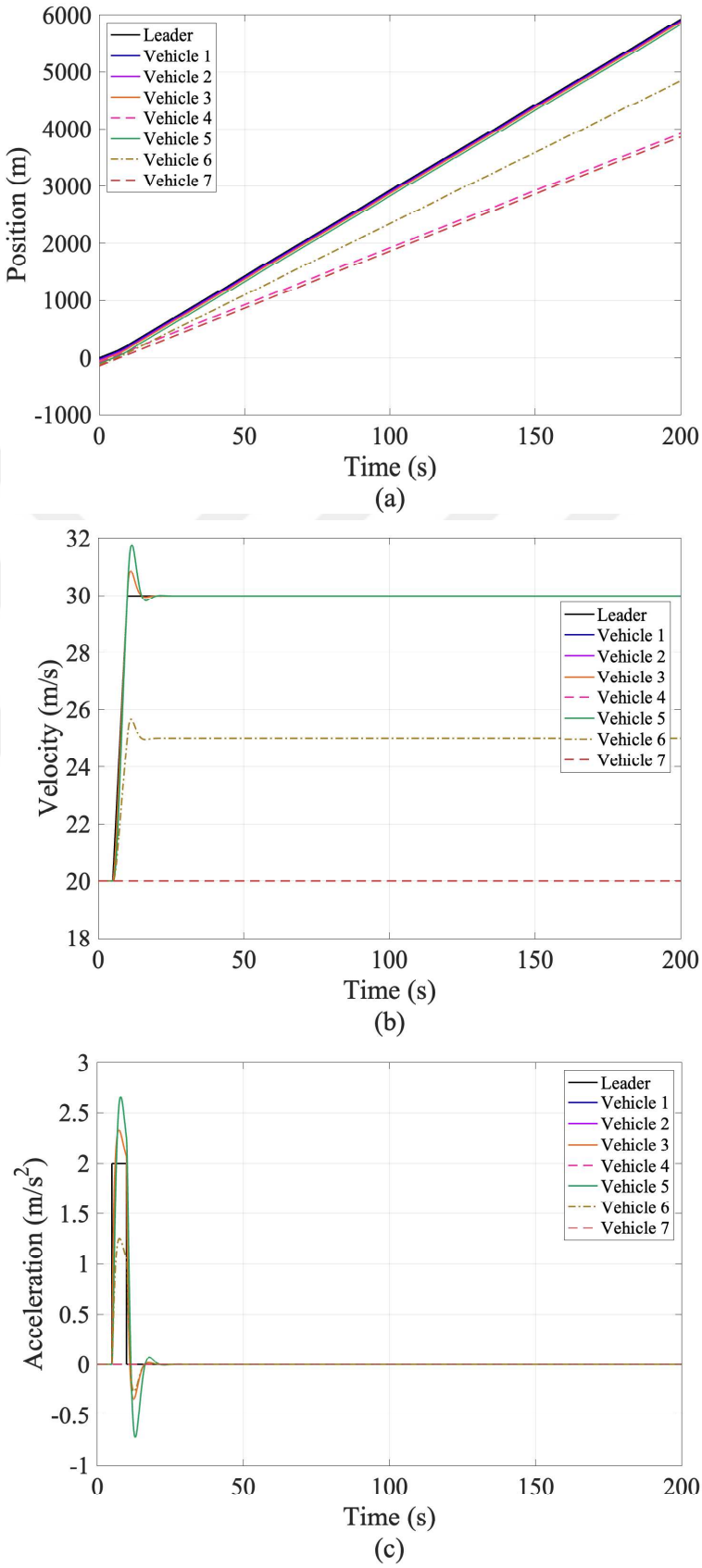


Figure 5.8. Vehicle states of IFT in Figure 5.7 (a) Position, (b) Velocity, (c) Acceleration.

Vehicles 4 and 7 in the PLS2 have no information coming from other subgraphs therefore they maintain their initial velocity and acceleration values. In this sub-platoon, vehicle 4 is the follower, and vehicle 7 is the leading vehicle. Lastly, vehicle 6 is split into the SLS1 subgraph on its own. It receives information from both PLS1 and PLS2 subgraphs so that SLS1's equilibrium point for velocity is 25 m/s which is the average of the equilibrium point of PLS1, 30 m/s, and PLS2 20 m/s as Develer et al. state in [53].

Figure 5.10 shows that the space error between followers 3 and 4 (——), followers 4 and 5 (——) are exceeding the allowable V2V range so the communication between the vehicles will not be possible via V2V. In addition, it is obvious that the space error between followers 5 and 6 (——) and followers 6 and 7 (——) will exceed the allowable limit after 100 seconds.

Figure 5.11 shows the space error within each sub-platoon for the linear controller. Since vehicle 6 individually forms SLS1, it is not included. The first four nodes of the vehicle platoon system (leader (——), follower 1 (——), 2 (——), and 3 (——) in Figure 5.8) will follow the preceding vehicle so the desired space between the vehicles is equal to $d_{i-1,i}$, which is the desired space between the follower $i-1$ and $i$.

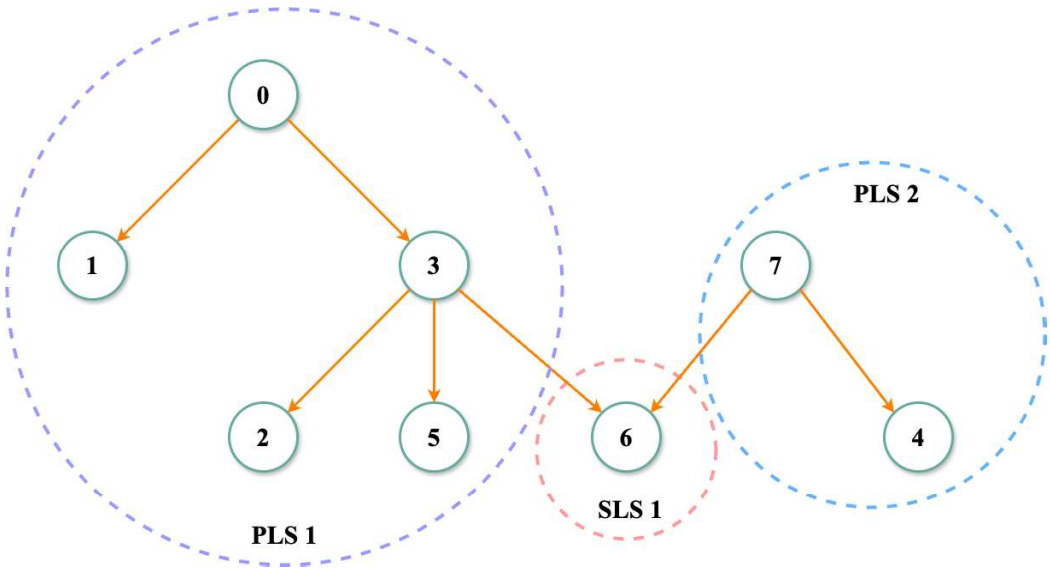


Figure 5.9. Two primary and one secondary layer subgraphs.

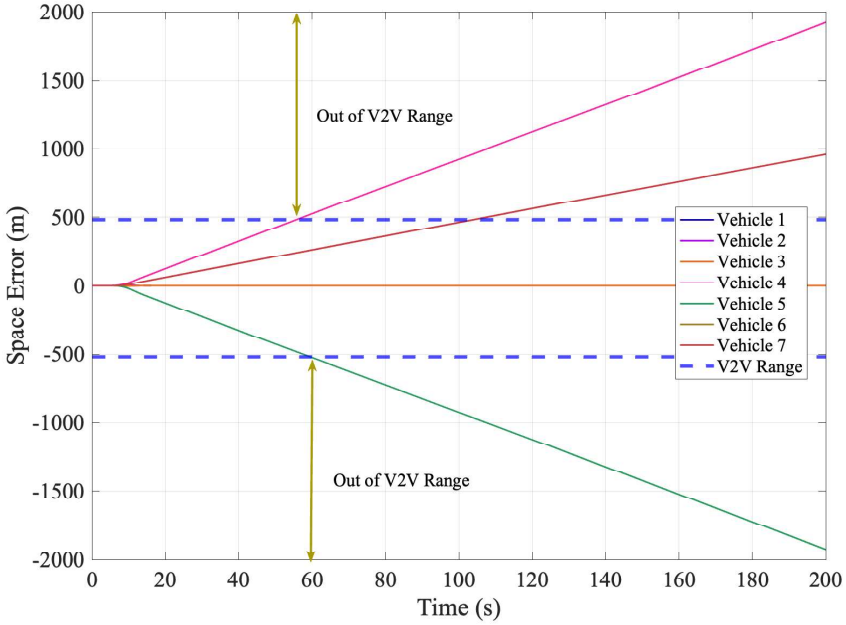


Figure 5.10. Space error for IFT in Figure 5.7 between consecutive vehicles with linear controller.

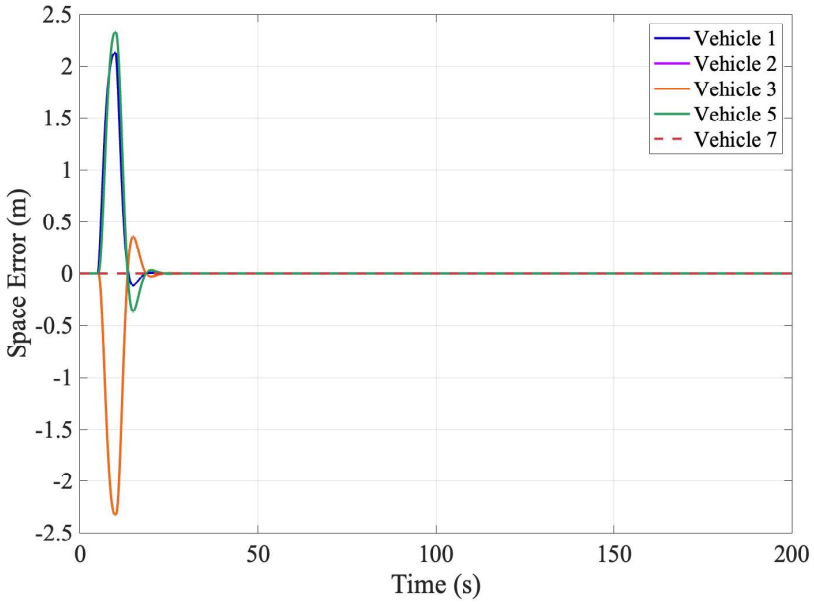


Figure 5.11. Space error within the primary layer subgraphs with the linear controller.

In conclusion, Figures 5.2 and 5.8 demonstrate that when controller parameters satisfy the conditions specified in (5.7), (5.8), and (5.9) both primary and secondary layer subgraphs can establish stable sub-platoon systems.

## 5.5. Summary of the Chapter

This chapter discusses the use of an information flow topology without a spanning tree in a vehicle platoon system. It has been observed that if the information flow topology does not contain a spanning tree, there is no guarantee of direct or indirect leader information reaching the followers. As a result, sub-platoons are formed. These sub-platoon formations align with the graph partition algorithm proposed by Erkan et al. [52]. After detecting subgraphs with PLS and SLS algorithms, the inter-vehicle distance and equilibrium points of each sub-platoon are analyzed. The stability criteria for these subgraphs are derived from Lemma 5.1 based on (5.1). The stability conditions are computed for a vehicle platoon system with a linear controller. The next chapter will review the thesis study and provide a brief analysis of the conclusions.

# 6. CONCLUSION

This study investigates the effects of various information topologies on the control of platoon systems. In this context, different information topologies are tested using a linear and nonlinear controller. The impact of information augmentation through increasing the number of edges in both unidirectional and bidirectional IFTs is analyzed under the assumption of a spanning tree, as described in Assumption 2.2.

A hierarchical controller, introduced by Li et al. in [5], is used as the nonlinear controller. The proposed hierarchical controller is a combination of an observer and an ISMC, and it is capable of compensating external time-varying disturbances. Simulation results align with those of [5], as the topologies examined in Chapter 3 and Chapter 4 are string stable. Based on these results, the followers can track the leader while preserving the designated distance, and the desired acceleration, velocity, and position are achieved.

A linear controller proposed by Zheng et al. [20], which is a P-controller that takes the state error as a basis of the control input, is used in the linear controller implementations in this paper. The essential design point in this type of controller is the specification of the controller gains. Routh-Hurwitz stability criterion comes to aid in that regard. As in the nonlinear controller implementation, simulation results for the topologies assessed in Chapter 3 and Chapter 4 exhibit parallel outcomes with the cited paper.

The performance of the vehicle platoon system strongly correlates with eigenvalue analysis. In this study, it has been understood that the eigenvalue interpretation of the information flow topology matrix aids in comprehending the behavior of the vehicle platoon system. Moreover, the analysis of eigenvalues has been conducted individually for unidirectional and bidirectional topologies due to variations in matrix structures. In addition, settling time, which is found by using the algorithm in Figure 3.3, is taken as an indicator in measuring the performance of the vehicle platoon system. It has been seen that increasing the minimum eigenvalue of the system shortens the settling time significantly.

In this thesis, it is explained that the unidirectional topologies form a lower triangular IFT matrix structure. Consequently, increasing the diagonal elements of the IFT matrix creates an effect similar to increasing the eigenvalues of the IFT. If an edge is added to an IFT, the eigenvalues of the original and the new IFTs have a relationship like in (3.17) as indicated in Theorem 3.1 which is one of the fundamental contributions of this study. As noted in Remark 3.1, edge addition will lead to a shorter time to reach the desired vehicle states.

This study further deduced that IFT matrices of bidirectional topologies are symmetric Hermitian matrices. As a consequence, adding an edge to a system will be equal to adding a Hermitian matrix to the original IFT since interactions with the leader vehicle affect the main diagonal elements and the follower-related interactions are symmetric. According to Lemma 4.2, eigenvalues of the new IFT formed by the addition of a single edge will interlace with the eigenvalues of the existing IFT. Besides, an eigenvalue of the new IFT, $\lambda_i(\bar{\mathcal{L}}_{\mathcal{P}})$, formed by the addition of multiple edges will never be smaller than a corresponding eigenvalue of the existing IFT, $\lambda_i(\mathcal{L}_{\mathcal{P}})$, for any $i = 1, 2, \ldots, N$. This analysis related to bidirectional topologies is another fundamental contribution of this thesis. Ultimately, in Remark 4.1 it is stated that interventions that increase at least one of the eigenvalues of IFT will result in a faster vehicle platoon system.

In addition, this thesis offers a fresh perspective on vehicle platoon systems by exploring topologies that diverge from the commonly analyzed spanning tree topologies found in traditional literature. In the examined IFTs, there are no spanning trees so the leader does not act as the root node of the vehicle platoon system. In both scenarios, the linear controller fails to maintain a safe distance between consecutive vehicles. In such cases, the integrity of the vehicle platoon system has been compromised. Nonetheless, the vehicle platoon system no longer acts as a single unit, and sub-platoons consistent with the algorithms inspected in Chapter 5 are formed. Additionally, in Section 5.3 it has been shown that the stability of each subgroup is ensured if conditions in Lemma 5.1 are met. This section of the thesis provides a perspective on the criteria for ensuring stability in topologies without a spanning tree.

## 6.1. Future Work

This study has been carried out relying on various assumptions, including the neglect of lateral vehicle dynamics and no packet loss in V2V communication. However, it is possible to assess a vehicle platoon system under diverse conditions. For this purpose, some improvement opportunities that can contribute to the vehicle platoon control problem are listed below:

- Incorporating lateral control techniques would improve this study. Combined control entails managing both longitudinal and lateral vehicle dynamics. In this method, the control input includes acceleration for longitudinal control and steering angle for lateral control.
- Potential communication interruptions should be taken into account to test more realistic scenarios. Hence, addressing communication delays and packet losses becomes crucial for sustaining the stability of the platoon system. In addition, MATLAB's V2V toolbox, which involves an algorithm for the transmission and receipt process for the BSMs, can be utilized in communication error test scenarios.
- This study is based on a fixed communication topology and a constant spacing policy. While a vehicle platoon design may work well for a specific information exchange structure, it could fail for a different IFT. Therefore, a vehicle platoon system that can adapt to different information topologies, and thus avoid instability and poor performance of the system in network topology switch cases, can be designed as a future study.
- This study examines two distinct IFTs within simulations involving topologies that do not have a spanning tree. It is important to highlight that there is a chance to undertake more in-depth research into the stability analysis of the IFTs in the absence of a spanning tree. In addition, the analysis focuses solely on a linear decentralized controller for topologies lacking a spanning tree. However, a nonlinear decentralized controller could also be examined.

# REFERENCES


1. EL-Zaher, M., B. Dafflon, F. Gechter and J.-M. Contet, “Vehicle Platoon Control with Multi-Configuration Ability”, *Procedia Computer Science*, Vol. 9, pp. 1503–1512, 2012.

2. Amoozadeh, M., H. Deng, C.-N. Chuah, H. M. Zhang and D. Ghosal, “Platoon Management with Cooperative Adaptive Cruise Control Enabled by VANET”, *Vehicular Communications*, Vol. 2, No. 2, pp. 110–123, 2015.

3. Wu, Y., S. E. Li, Y. Zheng and J. K. Hedrick, “Distributed Sliding Mode Control for Multi-Vehicle Systems with Positive Definite Topologies”, *IEEE 55th Conference on Decision and Control (CDC)*, pp. 5213–5219, Las Vegas, USA, 2016.

4. Wu, Y., S. E. Li, J. Cortés and K. Poolla, “Distributed Sliding Mode Control for Nonlinear Heterogeneous Platoon Systems with Positive Definite Topologies”, *IEEE Transactions on Control Systems Technology*, Vol. 28, No. 4, pp. 1272–1283, 2020.

5. Li, Y., Z. Qin, H. Zhu, S. Peeta and X. Gao, “Platoon Control of Connected Vehicles with Heterogeneous Model Structures Considering External Disturbances”, *Green Energy and Intelligent Transportation*, Vol. 1, No. 3, p. 100038, 2022.

6. Sheikholeslam, S. and C. A. Desoer, *Longitudinal Control of a Platoon of Vehicles; Ill: Nonlinear Model*, Tech. rep., University of California, 1990.

7. Kazemi, A., I. Sharifi and H. Talebi, “Longitudinal and Lateral Control of Vehicle Platoons using Laguerre-Based and Robust MPC with Merge and Exit maneuvers”, *Control Engineering Practice*, Vol. 142, p. 105737, 2024.

8. He, C., Y. Li, J. Xu and W. Hao, “Third-Order Model Based Nonlinear Longitudinal Control for Heterogeneous Connected Vehicle Platoon”, *IEEE International Conference on Real-time Computing and Robotics (RCAR)*, pp. 106–111, Irkutsk, Russia, 2019.

9. Zhao, H. and W. Li, “L2 String Stability Analysis for Vehicle Platooning System with Switching Topologies”, *36th Youth Academic Annual Conference of Chinese Association of Automation (YAC)*, pp. 61–65, Nanchang, China, 2021.

10. Li, S. E., Y. Zheng, K. Li, Y. Wu, J. K. Hedrick, F. Gao and H. Zhang, “Dynamical Modeling and Distributed Control of Connected and Automated Vehicles: Challenges and Opportunities”, *IEEE Intelligent Transportation Systems Magazine*, Vol. 9, No. 3, pp. 46–58, 2017.

11. Huang, A., L. Guo, P. Chen, M. Sun and H. Chen, “Distributed Model Predictive Control Considering Fuel Economy for Heterogeneous Vehicle Platoons”, *35th Chinese Control and Decision Conference (CCDC)*, pp. 709–714, Yichang, Hubei Province, China, 2023.

12. Cheng, F., H. Zheng, C. Gong and C. Kaku, “Longitudinal Cruise Control of Truck Platoon Based on Distributed Sliding Mode Control Strategy”, *6th CAA International Conference on Vehicular Control and Intelligence (CVCI)*, pp. 1–5, Nanjing, China, 2022.

13. Chen, H., Y. Li, S. Yu and S. Shi, “Integral Sliding-Mode Platoon Control for Connected Vehicles with Disturbance Observer”, *6th CAA International Conference on Vehicular Control and Intelligence (CVCI)*, pp. 1–6, Nanjing, China, 2022.

14. Li, F., L. Wang and C. Liao, “CAN (Controller Area Network) Bus Communication System Based on Matlab/Simulink”, *4th International Conference on Wireless Communications, Networking and Mobile Computing*, pp. 1–4, Dalian, China, 2008.

15. Jiang, D. and L. Delgrossi, “IEEE 802.11p: Towards an International Standard for Wireless Access in Vehicular Environments”, *IEEE Vehicular Technology Conference*, pp. 2036 – 2040, Calgary, Canada, 2008.

16. Saleh, A., V. Chirila, M. Ruel and P. Villemure, “Empirical Performance of Dedicated Short-Range Communication in Various Road and Environmental Conditions”, *IEEE*

*Intelligent Vehicles Symposium (IV)*, pp. 336–341, Nagoya, Japan, 2021.

17. Carpenter, S. E. and M. L. Sichitiu, "Analysis of Packet Loss in a Large-Scale DSRC Field Operational Test", *International Conference on Performance Evaluation and Modeling in Wired and Wireless Networks (PEMWN)*, pp. 1–6, Paris,France, 2016.

18. Society of Automotive Engineers (SAE), "Vehicle Level Validation Test Procedures for V2V Safety Communications", *J2945/1A_202007*, SAE International Technical Standard, 2020.

19. Zhang, Y., Z. Xu, Z. Wang, X. Yao and Z. Xu, "Impacts of Communication Delay on Vehicle Platoon String Stability and Its Compensation Strategy: A Review", *Journal of Traffic and Transportation Engineering*, Vol. 10, No. 4, pp. 508–529, 2023.

20. Zheng, Y., S. Eben Li, J. Wang, D. Cao and K. Li, "Stability and Scalability of Homogeneous Vehicular Platoon: Study on the Influence of Information Flow Topologies", *IEEE Transactions on Intelligent Transportation Systems*, Vol. 17, No. 1, pp. 14–26, 2016.

21. Zheng, Y., S. E. Li, K. Li and L.-Y. Wang, "Stability Margin Improvement of Vehicular Platoon Considering Undirected Topology and Asymmetric Control", *IEEE Transactions on Control Systems Technology*, Vol. 24, No. 4, pp. 1253–1265, 2016.

22. Gao, F., X. Hu, S. E. Li, K. Li and Q. Sun, "Distributed Adaptive Sliding Mode Control of Vehicular Platoon With Uncertain Interaction Topology", *IEEE Transactions on Industrial Electronics*, Vol. 65, No. 8, pp. 6352–6361, 2018.

23. Kwon, J.-W. and D. Chwa, "Adaptive Bidirectional Platoon Control Using a Coupled Sliding Mode Control Method", *IEEE Transactions on Intelligent Transportation Systems*, Vol. 15, No. 5, pp. 2040–2048, 2014.

24. Jun, M., L. Zuo, M. Yan and J. Zhang, "Distributed Vehicle Platoon Tracking Control for Optimal Energy Consumption with Switching Topologies", *35th Chinese Control and*

*Decision Conference (CCDC)*, pp. 161–167, Yichang, Hubei Province, China, 2023.

25. Zhang, L., J. Sun and T. Cai, "Distributed Topology Switching Strategy Designing for Heterogeneous Vehicle Platoons", *2018 IEEE 14th International Conference on Control and Automation (ICCA)*, pp. 734–738, Alaska, USA, 2018.

26. Wang, P., H. Deng, J. Zhang, L. Wang, M. Zhang and Y. Li, "Model Predictive Control for Connected Vehicle Platoon Under Switching Communication Topology", *IEEE Transactions on Intelligent Transportation Systems*, Vol. 23, No. 7, pp. 7817–7830, 2022.

27. Swaroop, D. and J. K. Hedrick, "Constant Spacing Strategies for Platooning in Automated Highway Systems", *Journal of Dynamic Systems, Measurement, and Control*, Vol. 121, No. 3, pp. 462–470, 1999.

28. Godsil, C. and G. F. Royle, *Algebraic Graph Theory*, Graduate Texts in Mathematics, Springer, New York, 2001.

29. Li, S. E., Y. Zheng, K. Li and J. Wang, "An Overview of Vehicular Platoon Control Under the Four-Component Framework", *IEEE Intelligent Vehicles Symposium (IV)*, pp. 286–291, Seoul, Korea (South), 2015.

30. Gao, F., S. E. Li, Y. Zheng and D. Kum, "Robust Control of Heterogeneous Vehicular Platoon with Uncertain Dynamics and Communication delay", *IET Intelligent Transport Systems*, Vol. 10, pp. 503–513, 2016.

31. Rajamani, R., *Vehicle Dynamics and Control*, Springer US, Boston, 2012.

32. Zhu, Y. and F. Zhu, "Distributed Adaptive Longitudinal Control for Uncertain Third-Order Vehicle Platoon in a Networked Environment", *IEEE Transactions on Vehicular Technology*, Vol. 67, No. 10, pp. 9183–9197, 2018.

33. Hayat, O., M. Lebrun and E. Domingues, "Powertrain Driveability Evaluation: Analy-

sis and Simplification of Dynamic Models", *SAE Transactions*, Vol. 112, pp. 569–578, 2003.

34. Stankovic, S., M. Stanojevic and D. Siljak, "Decentralized Overlapping Control of a Platoon of Vehicles", *IEEE Transactions on Control Systems Technology*, Vol. 8, pp. 816 – 832, 2000.

35. Jaulin, L., *Mobile Robotics*, Elsevier, London, 2015.

36. Milanés, V., S. E. Shladover, J. Spring, C. Nowakowski, H. Kawazoe and M. Nakamura, "Cooperative Adaptive Cruise Control in Real Traffic Situations", *IEEE Transactions on Intelligent Transportation Systems*, Vol. 15, No. 1, pp. 296–305, 2014.

37. Tejado, I., V. Milanés, J. Villagrá and B. M. Vinagre, "Fractional Network-Based Control for Vehicle Speed Adaptation via Vehicle-to-Infrastructure Communications", *IEEE Transactions on Control Systems Technology*, Vol. 21, No. 3, pp. 780–790, 2013.

38. Guo, X.-G., W.-D. Xu, J.-L. Wang and J. H. Park, "Distributed Neuroadaptive Fault-Tolerant Sliding-Mode Control for 2-D Plane Vehicular Platoon Systems with Spacing Constraints and Unknown Direction Faults", *Automatica*, Vol. 129, p. 109675, 2021.

39. Sacone, S., C. Pasquale, S. Siri and A. Ferrara, "Centralized and Decentralized Schemes for Platoon Control in Freeway Traffic Systems", *60th IEEE Conference on Decision and Control (CDC)*, pp. 2665–2670, Texas, USA, 2021.

40. Pan, Y., C. Yang, L. Pan and H. Yu, "Integral Sliding Mode Control: Performance, Modification, and Improvement", *IEEE Transactions on Industrial Informatics*, Vol. 14, No. 7, pp. 3087–3096, 2018.

41. Karami-Mollaee, A., H. Tirandaz and O. Barambones, "Neural Dynamic Sliding Mode Control of Nonlinear Systems with Both Matched and Mismatched Uncertainties", *Journal of the Franklin Institute*, Vol. 356, No. 8, pp. 4577–4600, 2019.

42. Utkin, V. and J. Shi, “Integral Sliding Mode in Systems Operating Under Uncertainty Conditions”, *Proceedings of 35th IEEE Conference on Decision and Control*, Vol. 4, pp. 4591–4596, Kobe, Japan, 1996.

43. Perruquetti, W. and J. P. Barbot, *Sliding Mode Control in Engineering*, Vol. 11, Marcel Dekker, New York, 2002.

44. Massow, K., I. Radusch and R. Shorten, “A Numerical Study on Constant Spacing Policies for Starting Platoons at Oversaturated Intersections”, *IEEE Access*, Vol. 10, p. 43766–43786, 2022.

45. Seiler, P., A. Pant and K. Hedrick, “Disturbance Propagation in Vehicle Strings”, *IEEE Transactions on Automatic Control*, Vol. 49, No. 10, pp. 1835–1842, 2004.

46. Szabo, F. E., *The Linear Algebra Survival Guide*, Academic Press, Boston, 2015.

47. Bronson, R., G. B. Costa, J. T. Saccoman and D. Gross, *Linear Algebra*, Academic Press, Oxford, 4th edn., 2024.

48. Horn, R. A. and C. R. Johnson, *Matrix Analysis*, Cambridge University Press, Cambridge, 2nd edn., 2012.

49. Butnariu, D., S. Reich and Y. Censor, *Inherently Parallel Algorithms in Feasibility and Optimization and Their Applications*, Vol. 8 of *Studies in Computational Mathematics*, Elsevier, Amsterdam, 2001.

50. Mu, Z., S. Tang, Y. Zhuang and D. Yu, “Attribute-Driven Streaming Edge Partitioning with Reconciliations for Distributed Graph Neural Network Training”, *Neural Networks*, Vol. 165, pp. 987–998, 2023.

51. Ayall, T. A., H. Liu, C. Zhou, A. M. Seid, F. B. Gereme, H. N. Abishu and Y. H. Yacob, “Graph Computing Systems and Partitioning Techniques: A Survey”, *IEEE Access*, Vol. 10, pp. 118523–118550, 2022.

52. Erkan, F., O. Cihan and M. Akar, "Analysis of Distributed Consensus Protocols with Multi-Equilibria Under Time-Delays", *Journal of the Franklin Institute*, Vol. 355, No. 1, pp. 332–360, 2018.

53. Develer, U. and M. Akar, "Cluster Consensus in First and Second-Order Continuous-Time Networks with Input and Communication Delays", *International Journal of Control*, Vol. 94, No. 4, pp. 961–976, 2021.

54. Zahreddine, Z. and E. F. Elshehawey, "On the Stability of a System of Differential Equations with Complex Coefficients", *Indian Journal of Pure and Applied Mathematics*, Vol. 19, pp. 963–972, 1988.

55. Society of Automotive Engineers (SAE), "V2X Communications Message Set Dictionary", *J2735_202309*, SAE International Technical Standard, 2020.